공학박사학위논문

DETERMINATION OF OPTIMIZED HYDRODYNAMIC DESIGN PARAMETERS FOR PHOTOBIOREACTORS USING CFD WITH EXPERIMENTAL PROOF

광생물반응기의 CFD 유체역학적 설계를 위한 매개변수 최적화 및 이의 검증실험

2013 년 8 월

서울대학교 대학원
생태조경·지역시스템공학부 지역시스템공학전공
Jessie Pascual Piog Bitog

DETERMINATION OF OPTIMIZED HYDRODYNAMIC DESIGN PARAMETERS FOR PHOTOBIOREACTORS USING CFD WITH EXPERIMENTAL PROOF

A DISSERTATION

SUBMITTED TO THE DEPARTMENT OF LANDSCAPE ARCHITECTURE AND RURAL SYSTEMS ENGINEERING AND THE COMMITTEE ON GRADUATE STUDIES OF SEOUL NATIONAL UNIVERSITY IN PARTIAL FULFILLMENT OF THE REQUIREMENTS FOR THE DEGREE OF

DOCTOR OF PHILOSOPHY

By

Jessie Pascual Piog Bitog

August 2013

Abstract

Currently, amidst the reality of increasing energy demand and depleting energy sources, finding new alternative energy sources is imperative. The idea of oil extraction from microalgae is again given much attention. It is believed to be the only source which can potentially replace petroleum fuels in the near future. Microalgae are naturally available elsewhere and tapping them as source of energy offers numerous advantages than other oil-rich plants. This includes its carbon dioxide (CO_2) sequestration capability which could play a significant role in decreasing the amount CO_2 in the atmosphere. Microalgae can be cultivated in non-arable lands, which rules out the fear of competing with food and fiber. Microalgae are cultivated in closed photobioreactors (PBRs) where the ideal cell growth requirements are controlled to obtain maximum cell growth. The cells need enough light, carbon dioxide (CO_2), nutrients, etc, for their growth. However, other indirect parameters are also equally important such as the flow hydrodynamics/mixing inside the PBR to ensure equal distribution of CO_2 and cell nutrients. The flow hydrodynamics as well as the method of introducing CO_2 and nutrients into the PBR depends greatly on its geometrical design. In this study, computational fluid dynamics (CFD) was utilized simulate and design a PBR and was followed immediately with a practical evaluation of the designed PBRs to finally conclude and cement the results obtained in the CFD simulation.

In Chapter 2, a comprehensive review on the application of CFD in designing PBRs was conducted which gave profound understanding on microalgae, its production systems such as raceways and PBRs, its main growth requirements

including light, CO_2 and temperature. The various CFD design aspects which considered the light intensity distribution, mixing and gas injection into the reactors were discussed. The CFD approach to correctly simulate the flow hydrodynamics with the proper implementation of the different type of multiphase models and turbulence models were also adequately reviewed. The opportunities of the CFD approach was also discussed where a development of microalgae growth model was proposed which can be integrated in the CFD simulation during the design. Furthermore, the integration of flow hydrodynamics particularly the volume percentages of dead zones, average circulation time and turbulence intensity to be utilized in the analysis in terms of the performance of PBRs and efficient vessel for microalgae production is highly recommended.

In Chapter 4, to establish the reliability of the simulation study, the CFD code and approach was initially validated from particle image velocimetry (PIV) data under various air flow rates and two test regions in the PBR. PIV works by seeding tracer particles which are assumed to faithfully follow the flow dynamics following the principle of Stokes number. The particles are illuminated using a laser so that they become visible for the specialized digital camera which captures multiple frames at high speed. The images of the tracer particles are recorded at least twice with a small time-delay. The displacement of the particle images represents the fluid motion. The flow movements of particles are then being tracked where the velocity and direction of the particles are recorded for computer analysis. In the CFD model, Discrete-phase model of DPM was utilized to simulate the movement of the cells as they travel around, and up and down the PBR. Particle injections can be defined by a text file specifying particle properties, position, and initial velocity.

A circular plane was defined as a source of particles in any part of the computational grid, with a given generation rate expressed in particles per second. The particles are assumed to be passively transported by the hydrodynamic flow and the interaction among cells or with the fluid are not considered. The particles are assumed as spherical and defined by properties such as diameter and density. Comparing the computed average velocity magnitude of the PIV and simulation showed an average error of approximately 6.77% which is generally acceptable.

In engineering perspective, the structural configuration and design of the PBRs have critical role in the flow hydrodynamics inside the reactor which are very significant in providing ideal growth conditions for the microalgae cells. Hence, the flow hydrodynamics inside 30 L PBRs simulating 32 cases were investigated via CFD and presented in Chapter 5. The 32 cases simulated in the study were accounted from four various air flow rates, four nozzle size diameters and two PBR geometry designs. The optimized hydrodynamic evaluation parameters include dead zones, average circulation time and turbulence intensity. Simulation results have revealed the hydrodynamic advantages of the PBRs designed with internal baffle and protruded bottom cone-shaped geometry. This PBR design can eliminate the dead zones at the same time execute better mixing and mass transfer because of its faster average circulation time. This approach of selecting a PBR operating condition and design combining the three hydrodynamics parameters is a first attempt of its kind and no standard value in each parameter is available in literatures. Thus, a criterion on each parameter was set and elimination technique was executed in the 32 simulated cases until some appropriate PBRs suited for microalgae production were selected. Thus, based on the hydrodynamic analysis

inside the PBRs applying the criteria, cases $A_2B_2C_2$ and $A_3B_2C_2$ were chosen. Both cases have the same nozzle size diameter of 10 mm and PBR geometry which are considered design parameters while they only differ in flow rate of 0.10 and 0.15 vvm which is an operating parameter and can be easily adjusted during the actual cultivation of microalgae.

Chapter 6 presents the practical cultivation of microalgae to finally confirm and cement the results obtained in Chapter 5. This was implemented to investigate the growth response of microalgae cells from the numerically investigated 30 L cylindrical bubble column PBRs of 30 L following the recommended PBR design and operating parameters obtained in previous study. However, before the final cultivation of microalgae in the 30 L PBRs, initial laboratory scale experiments were conducted in small size PBRs to determine the effect of temperature and CO_2 on the growth of microalgae. The recommended temperature and CO_2 level obtained in the small scale laboratory tests were supplied in the 30 L culture cultivation. The selected microalgae specie is *Chlorella vulgaris.*

Based on the laboratory scale experiments on temperature and CO_2, temperature range between 20 ~ 35 ^{0}C was found to be more appropriate to the growth of the cells while under 10 % level of CO_2 is also recommended for the specie.

The average fresh cell weight of *Chlorella vulgaris* measured from Experiment 1 in the upgraded PBR is approximately 1.60 as compared to approximately 0.53 g L^{-1}, for the typical PBR. The maximum fresh cell weight in the upgraded PBR can be achieved in 7 days as compared to the typical PBR which is 10 days. The

decrease in time duration in obtaining higher cell concentration using the upgraded PBR is very significant since lesser time for cultivation can result to more production. For instance, in one month duration, batch cultivation of microalgae can be implemented four times in the upgraded PBR while only three batch cultivation can be achieved in the typical PBR. In terms of their specific growth rates, the maximum specific growth rate for the typical PBR is approximately 2.21 day^{-1}, while approximately 2.58 day^{-1} was achieved in the upgraded PBR. Estimating their maximum productivities yields approximately 1.15 g L^{-1} day^{-1} and 3.43 g L^{-1} day^{-1} for the typical PBR and the upgraded PBR, respectively.

The results obtained from Experiment 2 with higher initial cell concentration can lessen the time to achieve maximum cell concentration to about one day. Computing the average fresh cell weight concentration for Experiment 2 gives values of approximately 0.71 and 1.93 g L^{-1} for the typical PBR and the upgraded PBR, respectively. In terms of the specific growth rate, maximum values of 1.28 day^{-1} for the typical PBR is obtained while approximately 1.56 day^{-1} was obtained for the upgraded PBR. Estimating the maximum productivity of the PBRs for Experiment 2, yield productivities of approximately 0.91 g L^{-1} day^{-1} and 3.01 g L^{-1} day^{-1} for the typical PBR and upgraded PBR, respectively. Computing the average maximum productivities for the two successive experiments shows values of approximately 1.03 g L^{-1} day^{-1} and 3.23 g L^{-1} day^{-1} for the typical PBR and upgraded PBR, respectively. This posted an increase of productivity of approximately 314 % in utilizing the upgraded PBR.

Finally, it can be further concluded that the CFD approach have demonstrated its capability in investigating flow hydrodynamics inside the PBRs which can result to better design of efficient and effective PBRs for maximum cultivation of microalgae. The approach can be very promising in doing researches designs of PBRs while reducing significant research time, labor and resources.

Keywords: Computational Fluid Dynamics (CFD), Circulation time, CFD review, Dead zones, Turbulence intensity, Particle image velocimetry (PIV), Microalgae cultivation

Student number: **2007-31072**

Contents

List of Figures

List of Tables

Nomenclature

C_c: slip correction factor

F_x: forces per unit mass, including but not limited to Brownian diffusion.

I: estimated light intensity (μE m^{-2} s^{-1})

I_E: external light intensity on the illuminated wall of PBR (μE m^{-2} s^{-1})

N_o: population size at the beginning of the time interval

N_t: population size at the end of the time interval

T: temperature

V_a: air velocity

V_p: particle velocity

X: cell concentration

d: radial distance from the cell position to the wall surface, m

d_p: particle diameter

g: gravity

i: unit vector in the Cartesian coordinate

k_x: extinction coefficient due to cellular absorption (m^{-1})

k_w: extinction coefficient taking into account the reactor wall attenuation (m^{-1})

r: specific growth rate

t: time

v: kinematic viscosity

x: random umber using the Gaussian distribution

ρ: air density

ρ_p: particle density

μ: viscosity

ζ_{ij}: Kronecker delta function

Δt: the time step

x_p: position vector of the cell

1. General Introduction

Over the past centuries since the industrial revolution, the world has been dependent on fossil fuels such as coal, petroleum and natural gas as source of energy. In US alone, being the largest consumer of energy, fossil fuel supplies 83% of their energy demand (Energy Information Administration, 2010). However, in the last decades, consumption of energy has been greater compared to new discoveries of fossil source fuels. With the rising demand from the first world countries and the continuous industrial and economic development of third world countries, energy consumption and demand has been rapidly increasing. According to a recent report by the US Energy Information Administration (EIA), over the next 20 years US energy demands are predicted to increase by 62% for natural gas, 33% for oil and 45% for electricity. By some estimates, there will be an average of two percent annual growth in global oil demand over the years ahead, along with, conservatively, a three percent natural decline in production from existing reserves.

Fossil fuels are not renewable energy source such that once they are burned and utilized, they cannot be recovered. In the past years, fossil fuels are being depleted significantly prompting energy companies to seek out other energy sources. In addition, the continuous burning of fossil fuels is believed to have significantly contributed to global warming and climate change because they produce significant amount of carbon dioxide into the atmosphere. Alternative and renewable sources of energy are now being continuously explored and developed. These include the energy provided by nature such as hydro, solar, thermal and

wind. Hydro energy is simply energy that is taken from water and converted to electricity. Hydro energy can be obtained by using many methods of capture and process. The most common method of using energy from water is a hydroelectric dam, where water coming down through an area causes turbines to rotate and the energy is captured to run a generator. Power can also be generated from the energy of tidal forces commonly known as wave power, which uses the energy created by waves. Solar energy is energy that is derived from the sun's rays. The light and the heat provided by the sun is "collected" or harnessed by solar panels and then converted into a more useful form of energy. Thermal energy exploits the heat provided by the earth. As such, there are many natural sources of thermal energy on Earth, making it an important component of alternative energy. Energy from wind also is promising, however limited to where wind is significantly available. Wind farms which utilize wind power need no processed fuel to operate. Wind power is free, it is clean, and produces no waste or greenhouse gases.

Other alternative energy sources particularly for biofuel can be derived from oil-rich plants such as corn, canola, soybean, jathropa, coconut, oil palm, etc. Biofuels are produced from living organisms or from metabolic by-products (organic or food waste products). In order to be considered a biofuel, the fuel must contain over 80 percent renewable materials. Biofuels are developed further for biodiesel which are used for diesel engines. Made from agricultural co-products and byproducts such as soybean oil, other natural oils, and greases, it is an advanced biofuel. Biodiesel can be used in any blend with petroleum diesel fuel. Biodiesel is not like vegetable oil alternative fuels. Biodiesel can be used in its

unaltered form in diesel engines. Vegetable oil fuels must be modified and used only in combustion-ignition engines. The biggest feature about biodiesel fuel is that is it environmentally-friendly, which is not found in many traditional fuels. Biodiesel is made from renewable resources which mean it is safe for the environment. It does not produce high emissions like traditional fuels. Biodiesel does not cause harmful effects to the environment that will produce positive effects on our future generations. This makes biodiesel one of the easiest alternative fuels to use. In fact, it is a great option for use on farms in farm equipment.

Historically, the world's farmers produced food, feed and fiber. Today, they are starting to produce fuel as well. Since nearly everything we eat can be converted into automotive fuel, the high price of oil is becoming the support price for farm products. Agriculture's role in the global economy clearly will be strengthened as it faces a vast, virtually unlimited market for automotive fuel. Tropical and subtropical countries that can produce coconut, sugarcane or palm oil will be able to fully exploit their year-round growing conditions, giving them a strong comparative advantage in the world market. With biofuel production spreading, the world price for oil will, in effect, become a support price for farm products. If food and feed crop prices are weak and oil prices are high, commodities will go to fuel producers. This opens the debate whether biofuel produced from agriculture competes with food. With oil prices now high enough to stimulate potentially massive investments in fuel crop production, the world farm economy already struggling to feed 6.5 billion people on earth will face far greater demands.

At present, the most promising sustainable source for biofuel production which attracts enormous attention among scientist, engineers, researchers and oil producers is microalgae. It is believed to be the only source which can potentially replace petroleum fuels in the near future. Microalgae are naturally available elsewhere and tapping them as source of energy offers numerous advantages than other oil-rich plants. This includes its carbon dioxide (CO_2) sequestration capability which could play a significant role in decreasing the amount CO_2 in the atmosphere. Microalgae can be cultivated in non-arable lands, which rules out the fear of competing with food and fiber. Nowadays, there are numerous commercial applications of microalgae not only for biofuel. For example, microalgae can be used to enhance the nutritional value of food and animal feed owing to their chemical composition, they play a crucial role in aquaculture and they can be incorporated into cosmetics. Moreover, they are cultivated as a source of highly valuable molecules. For example, polyunsaturated fatty acid oils are added to infant formulas and nutritional supplements and pigments are important as natural dyes. Stable isotope biochemicals help in structural determination and metabolic studies. Future research should focus on the improvement of production systems for mass production and the genetic modification of strains to obtain high yield. Microalgal products would in that way become even more diversified and economically competitive.

In this study, a comprehensive review about microalgae and the numerical approach of designing reactors where cells are cultivated was conducted. The review gave profound understanding on microalgae, its production systems such as

raceways and PBRs, its main growth requirements including light, CO_2 and temperature. The various CFD design aspects which considered the light intensity distribution, mixing and gas injection into the reactors were discussed. The CFD approach to correctly simulate the flow hydrodynamics with the proper implementation of the different type of multiphase models and turbulence models were also adequately reviewed. The opportunities of the CFD approach was also discussed where a development of microalgae growth model was proposed which can be integrated in the CFD simulation during the design.

The CFD review was followed with validation of the computer code and design approaches using particle image velocimetry (PIV). Validation is very critical in the field of modeling and simulation studies. For instance, in CFD, this is to establish the accuracy of the codes used such as to create credibility and confidence in the results and can be used in making conclusions and decisions. PIV is an optical method to flow visualization in a system under investigation. The method is practically used to obtain instantaneous velocity measurements and related properties of fluids inside a system. Generally, this is done by comparing the simulation results with physical reality by conducting laboratory or field experiments. In this particular study, PIV experiment was initially conducted to obtain data for comparison with simulation results for validation purposes.

After establishing the validity of the CFD code and obtained confidence in the simulation technique, photobioreactors (PBRs) were designed comparing 32 PBR cases based on their hydrodynamic performance. The cylindrical bubble column PBR type design was chosen considering its simplicity in geometry with no

moving parts, suitable heat and mass transfer, less operational cost and requires low energy input in actual cultivation. The 32 simulation cases were comprised from four air flow rates, four bubble size diameter and two PBR geometries. The hydrodynamic investigation parameters include the percentages of dead zones, the average circulation time and turbulence intensity. In the investigation, the approach of assessing the PBR performance combining the three major hydrodynamic parameters is the first of its kind, thus a criteria was set on each parameter where the PBR cases were subjected for evaluation. The cases that passed the set criteria were recommended for actual cultivation of microalgae where the best case was utilized in the actual cultivation of microalgae which was conducted immediately after the CFD simulations.

The practical cultivation of microalgae was focused on determining the biomass concentration of the microalgae cells in the 30 L typical cylindrical bubble design and the recommended PBR from the CFD simulation which is referred here as the upgraded design. The cultivation of microalgae in the PBRs is an ideal approach to finally confirm the results of the numerical simulation technique and finally cement the conclusions drawn during the simulation study.

2. Literature Review

2.1. Microalgae

Microalgae are a new promising source of biodiesel. They are a diverse group of prokaryotic and eukaryotic photosynthetic microorganisms with a simple structure that allows them to grow rapidly (Li *et al*., 2008). In recent reviews in Patil *et al*. (2008) and Chisti (2007), microalgae appeared to be the only source of renewable biodiesel capable of meeting the global demand for transport fuels, with the potential to completely displace the use of fossil fuels (**Table 2-1**). Under optimal growing conditions, some microalgae species can produce and accumulate hydrocarbons up to 30 ~ 70 % of their dry weight, and that the high oil content of some algae species allows them to produce 1000 times as much oil as soybeans grown on the same amount of land (Kong *et al*., 2007). The oil content in microalgae can exceed 80% of the weight of the dry biomass, but commonly achieved oil levels are from 20-50% (Metting, 1996; Spolaore, 2006) (see also **Table 2-2**).

Other benefits from microalgae include their use as a healthy food, as producers of useful compounds (Borowitzka, 1999), biofilters to remove nutrients and other pollutants from wastewaters (Sawayama, 1994) and as indicators for environmental change. They are also commonly used in space technology and as laboratory research systems (Ai *et al*., 2009; Chaumont, 1993). Microalgae are also commercially cultivated for pharmaceuticals, nutraceuticals, cosmetics and aquaculture (Ranjbar *et al*., 2008; Pulz and Gross, 2004; Olaizola, 2003; Molina *et*

al., 1999). Various commercial applications of microalgae and microalgal biotechnology developments have been reviewed by (Spolaore *et al*., 2006; Wen and Chen, 2003; Apt and Behrens, 1999; Radmer and Parker, 1994).

Table 2-1 Comparison of some sources of biodiesel.

Crop	Oil yield (L ha^{-1})
Corn	172
Soybean	446
Canola	1190
Jathropa	1892
Coconut	2689
Oil palm	5950
Microalgae[a]	136,900
Microalgae[b]	58,700

[a] 70% oil (by wt) in biomass, [b] 30% oil (by wt) in biomass

Sources: Singh and Singh (2010); Chisti (2007); Conley (2006)

The production of microalgae is not new; it dates to World War II, when the Germans considered production in open ponds for food supplements (Ugwu, 2008; Borowitzka, 1999). In the 1950s, algae were found to sequester CO_2 in the atmosphere, propelling interest in mass production. Oil extraction from microalgae started during the gas supply scare in the 1970s (Barkley *et al*., 1987). However, further research on mass production and oil extraction were hampered because of high production costs. Currently, amidst the reality of increasing energy demand and depleting energy sources, finding new alternative energy sources is an

imperative and the idea of oil extraction from microalgae is again given much attention. Today, advance microalgae researches both in field and laboratory are underway.

Table 2-2 Oil content of some microalgae.

Microalgae	Oil content (% dry wt)
Botryococcus braunili	25-75
Chlorella sp.	28-32
Crypthecodinium cohnii	20
Cylindrotheca sp.	16-37
Cylindrotheca sp.	23
Dunaliella primolecta	25-33
Isochrysis sp.	>20
Monallanthus salina	20-35
Nannochloris sp.	31-68
Neochloris oleoabundans	35-54
Nitzschia sp.	45-47
Phaeodactylum tricornutum	20-30
Schizochytrium sp.	50-77
Tetraselmis sueica	15-23

Sources: Chisti (2007); Schlagermann *et al*., (2012)

2.2. Optimal factors for microalgae growth

Investigating the growth and multiplication of microalgae cells is very complex. However, the main factors which can contribute to the optimum growth of microalgae are light, CO_2 and temperature which were determined based from many laboratory studies. These optimum factors are hereby discussed.

2.2.1. Light

Since microalgae grow photosynthetically, light intensity is one of the most important limiting factors (Oncel and Sukan, 2008; Oncel and Akpolat, 2006; Kirk, 1994; Kchmond *et al*., 1990). Algal culture systems can be illuminated by artificial light, solar light or both. Naturally illuminated algal culture systems with large illumination surface areas include open ponds, flat-plate and horizontal/serpentine tubular airlift, or inclined tubular PBRs (Chisti, 2007). Flat plate PBRs are generally more efficient at sunlight utilization than tubular PBRs because they have a wider surface area (Tredici and Zittelli, 1988). Several attempts have been made to increase closed-based systems (tanks, hanging plastic bags) to 50-100 liters, but because the light requirement cannot be satisfied, successful biomass development has not been possible (Pulz, 2001). In outdoor cultivation, the ultimate source of light is the sun, which cannot be controlled; therefore, studies on the optimization of light for PBRs are usually done indoors with artificial illumination. Generally, laboratory-scale PBRs are internally or externally artificially illuminated with fluorescent lamps or other light distributors. To successfully use artificial light for photosynthesis, photons with wavelengths between 600-700 nm must be generated.

A comparison of artificial light sources including cool fluorescent, incandescent, halogen, AllnGap II (aluminum indium gallium phosphide with peak wavelength of 643 nm) and light emitting diodes (LEDs) was conducted (Kommareddy and Anderson, 2003). AllnGap II LEDs were found to be the most efficient and economical light source. They emit more than 98% of their light between 600-700 nm. The light intensity requirement is dependent on cell density. Higher cell densities will result in the need for higher light intensities (Fan *et al*., 2007). Every microalgal species has an optimal light requirement, and when this is exceeded, their growth is retarded. Above a certain value, light intensity actually reduces the biomass growth rate. This phenomenon, known as photoinhibition, occurs when microalgae become inhibited at light intensities only slightly greater than the level at which the specific growth rate peaks (Oncel and Akpolat, 2006; Camacho *et al*., 2003; Jansen *et al*., 2003). However, few references are available on photo-adaptation, light inhibition or saturation effects in PBRs. Photoinhibitory processes are time-dependent, and irreversible destruction will occur after few minutes of light stress, with damage exceeding 50% after 10-20 minutes (Pulz, 2001). In tubular PBRs, photoinhibition was observed to occur during the period of peak irradiation, and photosynthetic acidity of the cells recovered after few hours (Molina *et al*., 2001). Elimination of photoinhibition or its shift to higher light intensities would greatly increase the average daily growth rate of algal biomass. An additional unsolved problem is how to avoid photorespiration, which decreases the photosynthetic efficiency (Pulz, 2001). Photorespiration tends to occur when there is a high concentration of oxygen relative to carbon dioxide.

2.2.2. CO_2

Carbon dioxide is the usual carbon source for photosynthetic culture of microalgae. As the carbon is consumed, oxygen is produced by photolysis of water and released into the culture fluid (Molina *et al*., 1999). Since algae live on a high concentration of carbon dioxide, greenhouse gases (GHG), nitrogen dioxide (NO_2) and pollutants in the atmosphere from different sources will be the algal nutrients. Algae production facilities can thus be fed with exhaust gases from combustions of fossil fuels to significantly increase productivity. Several studies has been reported elsewhere utilizing flue gas as carbon source, however, the toxicity of the flue gas components has not been well-documented. In the study by Negoro *et al*., (1991), sulfur and nitrogen oxide (SO_x, NO_x), which were present in flue gas inhibits algal growth. Later, they found out (Negoro *et al*., 1993) that growth productivity of microalgae from flue gas and pure CO_2 was barely influenced by the content of SO_x, NO_x. Similar study by Hauck *et al*. (1996) reported that low level of *NOx*, typically present in scrubbed flue gas did not inhibit the growth of *Chlorella*. The effects of CO_2 concentration on membrane lipid composition, in addition to the effects on photosynthesis was also emphasized in some studies (Tzuzuki *et al*., 1990). The amount of CO_2 needed for growth varies according to microalgal species and PBR type. An airlift bench-type reactor with helical flow promoters was found out to have lower gas requirements for species of *Porphyridium* than the typical bubble and airlift reactors, implying a lower cost in air compression, and in air and CO_2 requirements (Merchuk *et al*., 2000). However, the CO_2 requirement of microalgae as influenced by PBR type still need more further investigations. In

terms of maximum CO_2 tolerance, some species can survive with very high CO_2 concentration, but usually lower CO_2 concentration is required for their maximum growth (**Table 2-3**).

Microalgae have different growth pH requirements too (Kommareddy and Anderson, 2005) and at high pH levels, the availability of CO_2 may become limiting to the growth and photosynthesis of microalgae (Chen and Durbin, 1994). The pH range for most cultured algal species is between 7 and 9, with an optimum range of 8.2 ~ 8.7. Proper pH is accomplished by aerating the culture. In the case of high-density algal cultures, the addition of carbon dioxide corrects for an increased pH, which may reach limiting values of up to pH 9 during algal growth. For *S. dimorphus*, the highest average productivity of 0.54 g dry weight per liter per day was achieved at a pH of 8.5 (Kong *et al*., 2007). The result of their study (Kong *et al*., 2007) also showed the possibility of adding CO_2 to *S. dimorphus* cultures to increase productivity, while any pH reduction produced by addition of CO_2 to cultures of *S. dimorphus* results in lower productivity. Although higher CO_2 concentration can lead to higher biomass productivity, the effect of low pH on the microalgae physiology and the increased possibility of contamination should not be ignored (Chen and Durbin, 1994).

2.2.3. Temperature

Algal growth is also temperature dependent, requiring an optimal value for maximal growth. Temperature is also important for the dissociation of carbon-containing molecules, making the carbon available for photosynthesis

(Kommareddy and Anderson, 2005). Temperature influences respiration and photorespiration more strongly than photosynthesis. However, if CO_2 or light is a limiting factor for photosynthesis, the influence of temperature can be insignificant (Pulz, 2001; Kchmond, 1988; Kchmond *et al*., 1990). The optimal temperature for microalgae cultures is generally between 20 and 24 °C, although this may vary with the composition of the culture medium, the species and strain cultured. Most commonly cultured species of microalgae tolerate temperatures between 16 and 27 °C. Temperatures lower than 16 °C will slow down growth, whereas those higher than 35 °C are lethal for a number of species (Mehlitz, 2009).

Table 2-3 CO_2 tolerance and optimum CO_2 concentration of various microalgae species.

Species	Maximum tolerance of CO_2 concentration	Optimum CO_2 concentration	References
Cyanidium caldarium	100%		Seckbach *et al*., 1971
Scenedesmus sp.	80%	10-20%	Hanagata *et al*., 1992
Chlorococcum littorale	60%		Kodama *et al*., 1993
Synechococcus elongatus	60%		Miyairi, 1997
Euglena gracilis	45%	5%	Nakano *et al*., 1996
Chlorella sp.	40%	10%	Hanagata *et al*., 1992
Eudorina sp.	20%		Hanagata *et al*., 1992
Dunaliella tertiolecta	15%		Nagase *et al*., 1998
Nannochloris sp.	15%		Yoshihara *et al*., 1996
Chlamydomonas sp.	15%		Miura *et al*., 1993
Tetraselmis sp.	14%		Matsumoto *et al*., 1995

Source: Ono and Cuello (2003)

2.3. Large-sized production systems: Raceway ponds and Photobioreactors

The success of mass production of microalgae in large scale depends greatly on the design and performance of the production systems such as ponds and photobioreactors (PBRs). The ponds can be natural or man-made such as raceways. At present, in large scale production systems, raceway ponds are mostly utilized especially for nutraceutical purposes. One strong reason for production in raceways ponds is because of the investment cost where microalgae production requires less production cost and capital equipment than other production vessels such as photobioreactors. The disadvantage comes in quality control since the microalgae are prone to contamination and evaporation because they are exposed to the natural phenomenon. Intensive production in raceway ponds is usually in a shallow circuit typically from 15 cm to 35 cm deep to ensure adequate exposure to sunlight (Darzins *et al*, 2010) The microalgae are cycled continuously around the pond circuit by the action of a paddlewheel which serves as a motive force and keep the algae suspended in the water. The even mixing of inputs across the entire pond can be achieved by slow feeding at a single point as the pond contents move past the feed intake. Likewise, the contents can be harvested evenly across the pond from a single outtake. Algae production in these ponds can be as much as 10 times higher than in extensive ponds. Current installations are lined with plastic or cement, and typically between 0.2 ~ 0.5 ha in size. Larger ponds are envisioned for biofuels production and these ponds may be clay-based (unlined) to reduce capital cost.

Closed system production of microalgae is realized through reactors which are commonly made of transparent materials to effectively expose the microalgae cells

to light. Thus, basically, a PBR is a bioreactor that incorporates some type of light source. Virtually any translucent container could be called a PBR; however the term is more commonly used to define a closed system, as opposed to an open tank or pond. These PBRs have been developed purposely to overcome the contamination and evaporation problems encountered in open raceway ponds. These systems can set-up outdoors for illumination by natural free light or indoors which utilizes artificial light. Generally, PBRs have a large surface area-to-volume ratio geometry (Chisti, 2007) such as tubular designs which are commonly utilized. Large scale productions of microalgae in tubular PBRs are usually realized from a series of usually aligned transparent tubes with the sun's rays to maximize the free energy. In addition, these tubes are generally less than 10 centimeters in diameter to maximize sunlight penetration. The medium broth is circulated through a pump to the tubes, where it is exposed to light photosynthesis, and then back to a reservoir. A portion of the algae is usually harvested after it passes through the solar collection tubes, making continuous algal culture possible.

Considering also economic factors, only PBR systems are now widely recognized for mass production aside from raceway ponds (Chisti, 2007; Molina, 1999; Tredici, 1999; Miron *et al*., 1999; Terry and Raymond, 1985). Growing microalgae in PBRs reduces risk of contamination, improves the reproducibility of cultivation conditions, provides control over hydrodynamics and temperature, and allows appropriate technical design (Pulz, 2001). Because PBR systems are closed, all essential nutrients must be introduced into the system to allow growth and cultivation of the algae. A PBR can be operated in "batch mode", but it is also

possible to introduce a continuous stream of sterilized water containing nutrients, air, and carbon dioxide. As the microalgae grows, excess growing culture overflows and is harvested. Without sufficient care, continuous bioreactors can quickly collapse, but once they are successfully started, they can continue operating for long periods. An advantage of this type of algal culture is that microalgae are maintained in log phase, which generally gives a higher nutrient content than old, senescent algae. The maximum productivity for a bioreactor occurs when the growth culture exchange rate, or time to exchange one volume of liquid, is equal to the doubling time in mass or volume of algae. There are comprehensive comparison of raceway pond system and PBR system that are available in literatures such as Richardson *et al*., 2012; Ugwu and Aoyagi, 2010; Chisti, 2007 while some microalgae large scale production systems is also presented in **Fig. 2-1**.

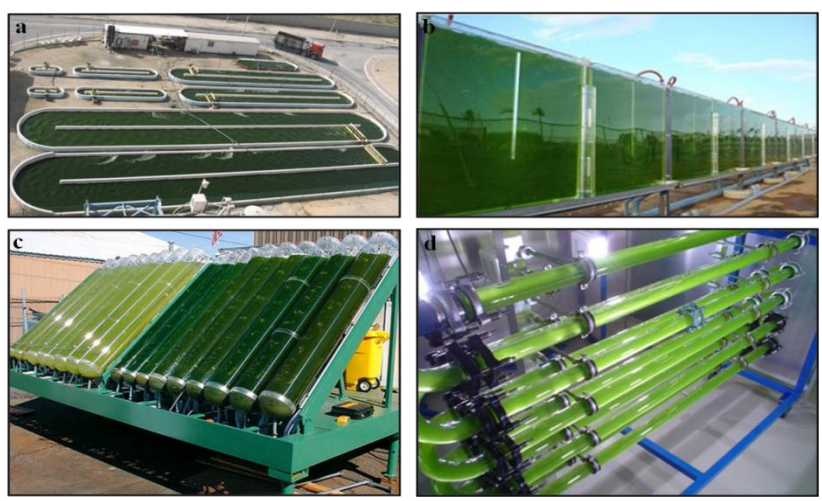

Fig. 2-1 Production systems for microalgae: (a) Raceway pond, (b) Flat-Plate type (c) Inclined tubular type (d) Horizontal/continuous type. Source: Bitog *et al*., 2011

2.4. Important design aspects

In numerical simulation studies, computational fluid dynamics (CFD) technique has been in the forefront in designing photobioreactors (PBRs) where microalgae are cultivated. The advent of CFD in the 1970s and its continuous development have paved the way for the design and development of various PBRs as production systems. The availability of high-tech computers has now allowed detailed analysis of PBRs for microalgal growth, from the simplest level to the most complex. Flow characteristics inside the PBRs which are very critical in the making PBR design can now be completely analyzed and visualized.

However, despite the availability of these PBRs which have been under continuous development for the past decade, only a few can be practically used for mass production. Many limitations still hinder their use, especially during scale-up (Ugwu *et al*., 2008). The scale-up process is still poorly understood because of the complexity and of flow patterns under different sets of design parameters such as diameter, height to diameter ratio, gas sparger type and physical properties of the liquid (Mouze *et al*., 2004; Wild *et al*., 2003; Deckwer, 1992;). PBR development is still one of the major steps that must be undertaken for efficient mass cultivation of algae (Ugwu *et al*., 2008; Chisti, 2007). However, with the advanced CFD technique, the complex flow patterns in relation the PBR designs and operation are now being thoroughly investigated, and solutions to most of the problems were proposed. Discussed below are some design aspects which should be considered especially in scale up designs.

2.4.1. Mixing

Mixing in PBRs is known to considerably enhance biomass productivity (Lou and Al-Dahhan, 2004). Mixing plays a major role in ensuring light intensity distribution, sufficient CO_2 transfer and maintaining uniform pH (Kommareddy and Anderson, 2005). In a study conducted by Lisec (2004), the productivity of *S. dimorphus* in a plate PBR was found to be three times lower than the determined highest productivity of 0.54 g dry weight per liter per day. A possible explanation for the difference between the two studies may be the lower air volume in the plate PBR, and hence poorer mixing regime, in the Lisec's study. In bubble column reactors, the longer time for the air to reside in the medium with smaller bubbles, more mass transfer is expected (Contreras, 1998). Mixing is necessary to prevent algae sedimentation at the same time avoid the cell attachment to the reactor wall. Mixing also ensures that all cells are equally exposed to the light and nutrients and improves gas exchange between the culture medium and the air (Carvalho *et al*., 2006; Kommareddy and Anderson, 2005; Lou and Al-Dahhan, 2004). The latter is of primary importance as the air contains the carbon source for photosynthesis in the form of CO_2. For very dense cultures, the CO_2 originating from the air (containing 0.035 % CO_2) and bubbled through the culture can be limiting for algal growth, and pure carbon dioxide may be supplemented to the air supply (*e.g.* at a rate of 1 % of the volume of air). CO_2 addition furthermore buffers the water against pH changes as a result of the CO_2/HCO_3 balance (Chen and Durbin, 1994).

Poor mixing will permit clumping of cells into aggregates of varying sizes, hence leading to the development of a three-phase system (solid-liquid-gas) inside

the reactor that is prone to decreased mass transfer (Panda, 1989). However, not all algal species can tolerate high agitation for efficient mixing because of their sensitivity to hydrodynamic stresses. High mixing rates may lead to shear-induced injury of cells (Gudin and Chaumont, 1991; Thomas and Gibson, 1990; Panda, 1989) which may also hampers their viability (Carvalho, 2006).

Mixing in bubble column and airlift reactors can be characterized by the axial dispersion coefficient, mixing time, circulation time and Bodenstein number (Miron *et al*., 2004). Analysis of mixing in bubble columns showed that they have shorter mixing times than airlift reactors, although because of efficiency and biomass productivity considerations, airlift reactors are favored (Ranjbar *et al*., 2008; Oncel and Sukan, 2008; Fan *et al*., 2007; Degen *et al*, 2001). This is because the bubbles rising inside the draft tube provide a less turbid zone in the annulus region, thus enabling better exposure to light. In addition, the presence of the draft tube in airlift PBRs results in more effective mixing, because of the internal loop, which enables the culture to circulate through the draft and down through the annulus between the housing column and outside the draft tube (Oncel and Sukan, 2008). Furthermore, airlift reactors have more defined fluid flow and relatively higher gas-liquid mass transfer rates. A bubble column is likely to cause uneven cell density along the length of the reactor, which may induce algal starvation and death (Fan *et al*., 2007).

2.4.2. Light penetration

One of the most important key to successfully scale up PBRs is undoubtedly the light penetration aspect inside the PBR. Illumination inside the PBR influences biomass composition, growth rate, and product formation. Microalgae need light within the photosynthetically active radiation (PAR) to obtain energy by photosynthesis (Fernandes *et al*., 2010). The wavelength of the PAR ranges from 400 to 700 nm, which is equal to visible light (Kommareddy and Anderson, 2003). In dense culture, the gradient of light varies along the radius of the PBR because of light attenuation (Grima *et al*., 1994). The attenuation of light intensity is dependent on its wavelength, cell concentration, geometry of PBR, and the penetration distance of light (Fernandes *et al*., 2010). Therefore, the light intensity at a given point inside the PBR depends on the path length of light, cell concentration, and light absorption by the microalgae (Grima *et al*., 1994). Comparing the light penetration in bubble and airlift PBRs, the light penetration path is wider for bubble columns than airlift PBRs, because of the longer path to the center of the bubble column, and because of the cloud effect caused by chaotic rising bubbles in the column (Oncel and Sukan, 2008).

2.4.3. Gas injection

The introduction of CO_2 supply via bubbles into the PBR should be strongly considered in the design. CO_2 injection refers to the process by which carbon dioxide is artificially introduced into the PBR. Several studies have shown that aeration of carbon dioxide rich gas through a PBR provides CO_2 to the algae and

also aids in deoxygenating of the suspension and provides mixing to increase the cycle frequency thereby limiting light inhibition. However, from the economic point of view, a high aeration rate will lead to higher running costs, so that it is not recommended for the large-scale production of microalgae (Zhang *et al*, 2002). Therefore, several studies have characterized the optimum aeration by carbon dioxide gas for microalgal production in the PBR. Air enriched with 5% or 10% (v/v) CO_2 at rates of 0.025 ~ 1 vvm (volume of air/ medium/time) is found to be cost effective for mass culture (Zhang *et al*, 2002). In flat panel photobioreactors, an optimum aeration rate of 0.05 v/v min^{-1} has been proposed sufficient to improve the mixing and mass transfer (Sierra *et al*, 2008).

2.5. Current PBR designs

Different types of PBRs are available elsewhere (Sato *et al*., 2006; Pulz, 2001; Tredici and Materassi, 1992) and include bubble columns (Oncel and Sukan, 2008; Miron *et al*., 1999), airlift reactors (Oncel and Sukan, 2008; Ranjbar *et al*., 2008; Miron *et al*., 1999), and stirred-tank, tubular (Richmond *et al*., 1993), conical (Contreras *et al*., 1998), and torus PBRs (Pruvost *et al*. (2006). PBRs are generally categorized according to their structure, and for microalgae production, tubular PBRs, flat-plate reactors and vertical column PBRs are the most common. Tubular PBRs are one of the most suitable types for outdoor mass cultures. They usually have large illumination surface area with fairly good biomass productivities and are relatively inexpensive because they are usually constructed of either glass or plastic tubes (Ugwu *et al*., 2008; Pulz, 2001; Richmond *et al*., 1993). Flat-plate PBRs are

generally made of transparent materials for maximum utilization of solar light energy. These PBRs allow good immobilization of algae and a suitable light path, and are readily tempered and easy to clean (Ugwu *et al*., 2008). Vertical column PBRs are compact, inexpensive, and easy to operate. They are promising for the large-scale cultivation of microalgae, and have a high potential for scalability.

In simulation studies, the most common types of PBRs which were thoroughly investigated are bubble column and air-lift reactors. These PBRs are widely used industrially because of their simple construction and operation (Joshi, 2001) and are usually consisting of cylindrical vessels in which gas is sparged into the liquid (Merchuk *et al*., 1994). Air-lift reactors are actually modified bubble column reactors with internal structures which modifies the inside flow characteristics of the PBR. The absence of moving parts and their suitable heat and mass transfer characteristics, along with their inexpensive operational costs from low energy input requirements, make them suitable for the mass production of microalgae. Light availability in these PBRs is influenced by aeration rate, gas holdup, and the liquid velocity (mixing and turbulence) (Miron *et al*., 2000). To obtain sufficient light for bubble column and air-lift PBR, the diameter should not exceed 20 mm or light availability inside the PBR will be severely reduced. In addition, the height of a single device is limited to about 4000 mm for structural reasons and to reduce mutual shading of reactors in a multicolumn facility that would be necessary for any commercial-scale operation (Miron *et al*., 1999). Mixing inside the PBRs is attained through the bubbles released at the sparger, which coalesced immediately forming larger bubbles and rose rapidly along the axis of the columns, setting the

entire liquid into circulation, with upward movement near the cylinder axis and downward movement near the walls (Merchuk *et al*., 1994).

2.6. Computational fluid dynamics (CFD) approach to PBR designs

Among the many models used to predict the hydrodynamics and related characteristics of PBRs and other multiphase flow systems, CFD holds the greatest potential for long term application (Hutmacher and Singh, 2008; Grace and Taghipour, 2004; Leib *et al*., 2001). CFD is a powerful tool used to study fluid flows. This tool uses computers and numerical techniques to solve problems involving the movement of fluids. Using CFD, a computational model that represents a system or device can be built, and by applying fluid flow physics and chemistry to this virtual prototype, a prediction of the fluid dynamics and the related physical phenomena can be determined. The CFD technique numerically solves the Navier-Stokes equations within each cell of the computational domain.

CFD is regarded as an effective tool for complementing the limitations of field and laboratory experiments, and an approach that can be used at minimal cost. CFD can be used to study factors in PBRs that influence the hydrodynamics of flow that greatly influence the liquid currents in the column, such as superficial gas velocity, gas holdup, bubble diameter, column geometry, etc. Because predicting the hydrodynamics of bubble columns in laboratory experiments is difficult, the liquid currents are also hard to predict. However, recent publications have shown that the hydrodynamics of bubble columns can be estimated using CFD simulations (Kommareddy and Anderson, 2004). The application of CFD to PBR design is

becoming more popular, as computers become more capable and affordable, allowing faster computing times and the capability to solve even the most complicated geometries. Over the last decade, numerous papers using CFD in the design of bubble column reactors has been published, with increased interest attributed to: (1) progress in measuring techniques that can be applied to the local hydrodynamics in bubble columns and provide more reliable local measurements for testing the reliability of CFD predictions; (2) increases in computer capacity; (3) improvements in the quality of CFD program systems; (4) improved numerical methods and better choice of turbulence models; and (5) the emergence of bubble column studies as a benchmark of gas-liquid dispersed flows because of flow regimes, deformable gas-liquid interfaces and lack of knowledge about closure terms such as turbulence and bubble-bubble interactions (Wild *et al*., 2003).

2.6.1. Flow Modeling: Turbulence

Turbulence modeling is a key issue in most CFD simulations. In PBRs, the growth rates of microalgae increase initially with increasing turbulence however the growth decreases sharply with further increase of the gas velocity due to cell damage (Merchuk *et al*., 2000). To obtain accurate prediction of hydrodynamics in the PBR, some factors such as bubble size, the grid resolution, and the selection of the turbulence model is very important (Gimbun, 2009). In two phase flows simulations, the *k*-ε turbulence model published by Launder and Spalding (1972) has been widely used (**Tables 2-4, 2-5, 2-6**). This is due to its simplicity and its capability for predicting wall-bounded turbulent flows (Joshi, 2001).

Table 2-4 List of PBRs investigated using CFD in the last decade.

Type of PBR	CFD Code	Focus of the study	Turbulence model	Author
Cylindrical bubble column	FLUENT	Investigation of PBR for microalgae for biodiesel production	*k-ε*	Seo *et al.*, 2012
Flat plate	FLUENT	Study on the destabilization mixing in the PBR	*k-ε*	Su *et al.*, 2010
Pipe type	FLUENT	Development of virtual PBR for microalgae culture considering turbulent flow and flashing light effect	-	Sato *et al.*, 2010
Cylindrical bubble column	FLUENT	Assessment of turbulence models	*k-ε*	Gimbun, 2009
Cylindrical bubble column	FLUENT	Large-sized PBR for microalgae production	*k-ε*	Bitog *et al.*, 2009
Torus reactor	FLUENT	Hydrodynamics in a square-sectioned torus reactor, Mixing time	*k-ω*	Pramparo *et al.*, 2008
Cylindrical bubble column	FLUENT	Comparison of species modeling	-	Yoo *et al.* 2008
Rectangular bubble column	FLUENT	Drag force formulation to describe regime transitions	*k-ε*	Simonnet *et al.*, 2008
Cylindrical bubble column	FLUENT	Continuous phase viscosity, bubble diameter and drag model	-	Santos *et al.*, 2008
Cylindrical bubble column	FLUENT	Use of VOF: Effect of air distributor	*k-ε*	Akhtar *et al.*, 2007
Rectangular bubble column	FLUENT	Radiation distribution in an externally illuminated PBR	RNG *k-ε*	Trujilio *et al.*, 2007
Cylindrical bubble column	FLUENT	Applicability of VOF model, Hydrodynamics of flow	Standard *k-ε*	Akhtar *et al.*, 2007

Table 2-5 List of PBRs investigated using CFD in the last decade (Cont.)

Type of PBR	CFD Code	Focus of the study	Turbulence model	Author
Cylindrical bubble column	FLUENT	Mixing as affected by gas velocity, Effect of Turbulence models	*k-ε*	Rampure *et al*., 2007
Torus shape reactor	FLUENT	Hydrodynamics of flow, Mixing with impeller	*k-ω*	Pruvost *et al*., 2006
Cylindrical bubble column	FLUENT	Design of a gas distributor: 3D CFD simulation of a coupled system consisting of a gas chamber and a bubble column	*k-ε*	Dhotre and Joshi, 2006
Cylindrical bubble column		Prediction of flow pattern using 1D, 2D and 3D *k-ε* models Axial dispersion coefficient	Standard *k-ε*	Ekambara *et al*., 2005
Cylindrical bubble column	FLUENT	Gas-liquid-solid flow modeling	*k-ε*	Glover and Generalis, 2004
Draft tube airlift reactor	FLUENT	Pressure drop to measure gas hold-up, Vertical velocity	-	Blazey *et al*., 2004
Rectangular flat walled column	FLUENT	Hydrodynamics of flow, Mixing characteristics	-	Kommareddy and Anderson, 2004
Cylindrical bubble column	FLUENT	Bubble size distribution, Axial liquid velocity, Gas holdup	-	Mouza *et al*., 2004
Jet-loop reactor	FLUENT	Hydrodynamics of flow, Three phase system (gas-liquid-solid)	Standard *k-ε*	Szafran and Kmiec, 2004
Airlift reactor	CFX 4.2	Hydrodynamics of flow	Standard *k-ε*	Baten *et al*., 2003
Fluidized bed	Modified K-FIX	Hydrodynamics of flow with binary mixtures	-	Huilin et al., 2003

Table 2-6 List of PBRs investigated using CFD in the last decade (Cont.)

Type of PBR	CFD Code	Focus of the study	Turbulence model	Author
Plate type	FLUENT	Hydrodynamics of flow and improvement of the PBR	RNG *k-ε*	Perner *et al.* 2003
Rectangular and Cylindrical bubble columns	FLUENT	Comparison among modeling approaches, 2D v/s 3D, order of discretization, turbulence closure	Standard *k-ε*, Prandtl	Bertola, 2003
Cylindrical bubble column	CFX 4.2, 4.4	Scaling up with highly viscous liquid phase	Standard *k-ε*	Krishna and Baten, 2002
Cylindrical bubble column	CFX 4.3	Influence of superficial gas velocity, solid loading and geometry on liquid flow velocities and hold-up distributions	Standard *k-ε*	Michele and Hempel 2002
Cylindrical bubble column	FLUENT	Simulate transient fluid dynamics and mixing in a shallow PBR	Standard *k-ε*	Ranade and Tayalia 2001
Cylindrical bubble column	CVD-2	Hydrodynamics of bubble rising in a liquid medium at high pressures	-	Li *et al*. 2000
Cylindrical bubble column	CFX 4.2, 4.4	Three-phase Eulerian simulation in churn turbulent regime	Standard *k-ε*	Krishna *et al*. 2000
Cylindrical bubble column	FLUENT	Simulation of a two-phase flow	ASMM	Glover *et al*., 2000
Rectangular bubble column	STABilized	Effect of aspect ratio of bubble column on flow pattern	-	Delnoij *et al*., 1999
Rectangular bubble column	CFX 4.2	The influence of turbulence modeling (Turbulent and Laminar)	Standard *k-ε*	Pfeger *et al*. 1999
Cylindrical bubble column	FLUENT	Validation of a transient, 2D simulations	RNG *k-ε*	Sanyal *et al*., 1999

There are three different options available for turbulence modeling of multiphase flow in FLUENT namely the mixture *k*-ε, dispersed *k*-ε and two-phase *k*-ε models (Fluent manual, 2006). All three turbulence models used the same model constants but have different equations to account for the turbulence viscosity (Gimbun, 2009). The appropriate use of these models is hereby presented as discussed by Gimbun (2009). The mixture model is applicable when phases separate, for stratified (or nearly stratified) multiphase flows, and when the density ratio between phases is close to 1. In these cases, using mixture properties and mixture velocities is sufficient to capture important features of the turbulent flow. Dispersed *k*-ε model is suitable when the secondary phase is dilute and the primary phase is clearly continuous, the dispersed *k*-ε turbulence model is used and solves the standard *k*-ε equations for the primary phase. The most general turbulence model for multiphase flows solves a set of *k* and ε transport equations for each phase. This turbulence model is the appropriate choice when the turbulence transfer among the phases plays a dominant role *i.e*. high gas void fraction.

An assessment of the turbulence models in bubble column PBR was conducted by Gimbun (2009) and found out that the selection of an appropriate turbulence model for gas-liquid modeling is highly dependent on the void fraction (gas hold-up) of the dispersed phase. When the void fraction of the dispersed phase is high (up to 30% gas hold-up), the two-phase turbulence model seems to be more appropriate. More elaborated turbulence model such as the large eddy simulation (LES) had also been employed recently to model the two-phase flow in the bubble column (Dhotre *et al*., 2007). However, the modeling of turbulence in multiphase

flows is an extremely complex issue because of the large number of terms that have to be modeled in the momentum equation (Szafran and Kmiec, 2004).

In a study by Pfleger *et al*. (1999), the focus was on the influence of turbulence modeling. Laminar and turbulent simulations were carried out and results show a qualitative correct picture of overall fluid circulation (**Fig. 2-2**). A standard *k*-*ε* was used to describe turbulence occurring in the continuous fluid in a bubble column PBR. Results show that a turbulent model has to be considered to gain correct results. The laminar model shows a chaotic behavior and not the harmonic oscillations observed in experiments. A correctly formed velocity profile was found with the turbulent description of the liquid phase. The turbulent result fits very well with the experiment in the upper and medium height. A comparison on axial velocity of *k*-ε models to experimental data was also plotted by Szafran and Kmiec (2004) in a jet-loop reactor and result have shown that enhanced *k*-ε models did not bring better accuracy (**Fig. 2-3**) but led to extended computation time. Velocity profile for a standard of *k*-ε model is closer to experimental data, but differences between the models are insignificant in comparison to the total calculation error. Standard *k*-ε model also achieved the fastest solution convergence and stability.

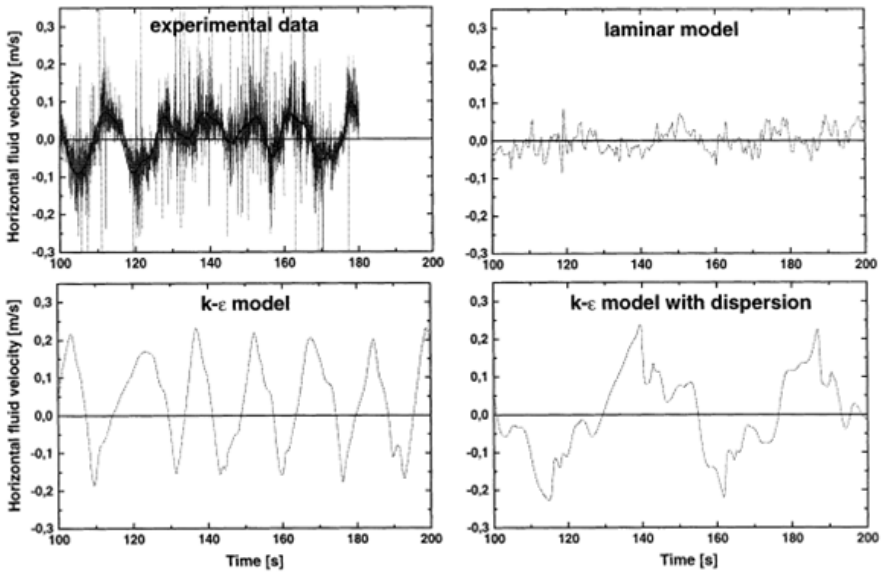

Fig. 2-2 Time series of the horizontal fluid velocity at the center point of bubble column. Source: Pfleger *et al*. (1999).

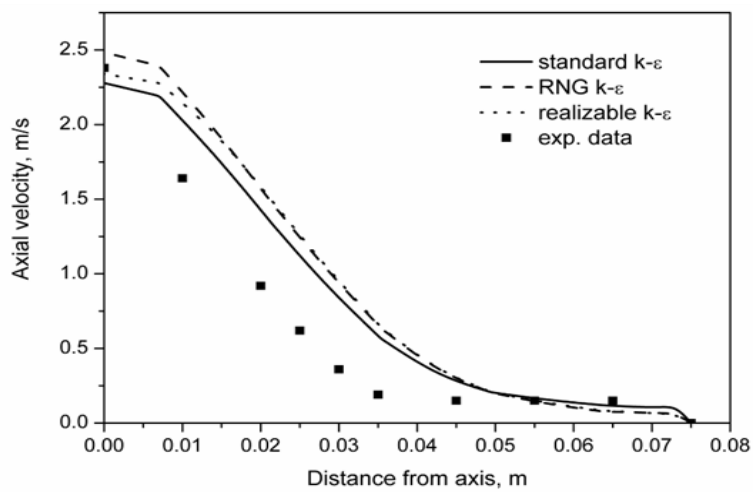

Fig. 2-3 Comparison of predicted water axial velocity profiles in draft tube at the distance of 125 mm from the outlet of ejector, achieved for different turbulence models, with experimental data. Source: Szafran and Kmiec (2004)

2.6.2. Multiphase modeling

Simulation of bubble inside the PBR can be realized through multiphase modeling where species transport models can be applied. Among the available multiphase simulation approaches for hydrodynamic studies, the Eulerian-Eulerian and the Lagrangian-Eulerian multiphase models have been popularly used (Bakker, 2002). In the Eulerian-Eulerian approach, there are three models of multiphase flow: the volume of fluid (VOF), the mixture model and the Euler model while the Lagrangian-Eulerian multiphase models is usually implemented with the Disrete-phase model (DPM) which is used to obtain real distribution of solid phase and the fluid phase is treated as a continuum, while the dispersed solid phase is solved by tracking a large number of particles through the flow field (Kozic *et al*., 2011). The species transport in multiphase models solves the conservation equations describing convection, diffusion, and reaction sources for each component species. Multiple simultaneous chemical reactions can be modeled, with reactions occurring in the bulk phase (volumetric reactions) and/or on wall or particle surfaces, and in the porous region. The most common species transport models and their capabilities are hereby discussed.

2.6.2.1. Eulerian-Eulerian

The Eulerian-Eulerian multiphase model averages the Navier-Stokes equations over the volume, including arbitrary particles plus a continuous phase. It solves the continuity, mass and momentum equations for fluid and solid phases, and tracks the volume fraction (Fluent manual, 2006). It uses only a single pressure field for

all phases, so the pressure field is the same regardless of whether the phase is continuous or dispersed. The interaction between the mean flows of phases is modeled through the interaction term, which includes a drag force, and virtual mass effect, when acceleration of secondary phase relative to the primary and additional lift forces exists. This model is appropriate for modeling multiphase flows involving gas-liquid or liquid-liquid flows. The Eulerian-Eulerian approach considers both the continuous and dispersed phases in an Eulerian representation, creating the need for mass and momentum balances for each phase (Bertola *et al*., 2003). For example, droplets or bubbles in the secondary phase are dispersed in the primary or continuous phase. The phases mix or separate and the secondary phase volume fraction can vary between zero and 100%. Practical applications of the Eulerian-Eulerian model include evaporation, aeration boilers, and separators, but inappropriate for modeling situations where an accurate description of the interface boundary is important, such as in stratified free-surface flows. In bubble column PBRs, The Eulerian-Eulerian approach treats the bubble cloud as a continuous medium with properties analogus to those of a fluid (Bertola *et al*., 2003). More details on the governing equations for Eulerian-Eulerian multiphase model can be easily found in literatures (Yoo *et al*., 2009, 2008; Santos, 2007; Szafran and Kmiec, 2004; Krishna *et al*., 2000).

2.6.2.2. Volume of Fluid (VOF)

Especially in bubble columns PBRs, VOF is one of the most well known techniques. Many studies predicted the dynamic behavior of a single bubble using

other approaches, but cannot accurately model the behavior of a bubble swarm or continuous chain in a bubble column where VOF can (Akhtar *et al*., 2007). In addition, the bubble-bubble interaction and higher level of turbulence, which becomes more important with continuous chain of bubbles where the inter-phase forces models based on single bubble studies, do not provide good results (Akhtar *et al*., 2007). VOF is designed to track the position of the interface between two or more immiscible fluids. This method has been shown to be more flexible and efficient than other methods for treating complicated free boundary configurations especially for volume tracking in which the motion of all phases is modeled by solving a single set of transport equations with appropriate jump boundary condition at the interface (Delnoij *et al*., 1997; Krishna *et al*., 1999; Hirt and Nichols, 1981). The VOF approach which is use to simulate bubble motion is based on the Navier-Stokes equations which are given for the mixture phases. The continuity equation as well as the single momentum equation is solved throughout the domain and shared by all the phases (Fluent Manual, 2006). Tracking is accomplished by solving a phase continuity equation, with abrupt changes in the resulting volume fraction indicating the interface location. A mixture fluid momentum equation is solved using mixture material properties, so that the mixture fluid material properties will show a jump across the interface. Turbulence and energy equations are also solved for the mixture fluid. Surface tension, mixtures of species and wall adhesion effects can be taken into account, and phases can be compressible. Especially in a column of fluid, VOF simulation technique can be a powerful tool for studying the rise velocity of single air bubbles, as well as the inline interaction of pairs of spherical cap bubbles (Akhtar *et al*., 2007; Krishna

and Baten, 2001). Other advantages of VOF methods are that bubble breakup and coalescence are handled implicitly (Lorstad and Fuchs, 2004). The only drawback of VOF is the so-called artificial (or numerical) coalescence of gas bubbles, which occurs when their mutual distances are less than the size of the computational cell. This also makes the approach memory intensive for simulation of dispersed multiphase flows in large equipment (Ranade, 2002). More detailed information on VOF model can be found in Yoo *et al*. (2009) and Krishna and Baten (2001).

2.6.2.3. Lagrangian-Eulerian

In the Eulerian-Eulerian approach both the fluid/gas and the particles are treated as continuum and continuum equations which are solved for both phases with an appropriate interaction. In the Lagrangian-Eulerian approach, the fluid/gas is also treated as continuum, but the particulate phase is treated as single particles, where particle trajectories, representing a stream of particles, are calculated as a result of forces acting on them. In the first step, the flow field is calculated from the balance equations of the quasi-homogeneous gas–liquid dispersion where the mean density varies with the local gas hold-up. In the second step, the local gas hold-up determined by tracking all individual bubbles of the system in the actual flow field and both the steps are repeated until convergence is obtained. According to Joshi (2001), using Lagrangian-Eulerian formulation especially for bubble column PBRs gives some advantages since each individual bubble is modeled for its flow through the column. This allows access to bubble dynamic characteristics including bubble trajectory and a direct consideration of additional effects related to bubble–bubble

and bubble–liquid interaction (Akhtar *et al*., 2007). Mass transfer without and the chemical reaction, bubble coalescence and re-dispersion can be added directly to the model. A second advantage is that there is no numerical diffusion introduced in the dispersed phase as the bubble trace can be calculated accurately within a given volume element (Joshi, 2001). However, in this approach, the gas bubbles are assumed to be spherical, which limits its application to the bubble columns with small bubbles in the homogeneous regime (Akhtar *et al*., 2007). In the heterogeneous regime, the consideration of large, deformable bubble becomes important in order to simulate different aspects of the large bubbles, such as bubble breakage and coalescence (Li *et al*., 2000). The Lagrangian-Eulerian approach is more realistic but the track of a sufficient number of particles, required for accurate modeling, demands high computational memory and speed (Delnoij *et al*., 1997). Also, the movement of bubbles due to turbulent dispersion makes the Lagrangian-Eulerian formulation more computation intensive (Joshi, 2001).

2.6.2.4. Discrete-Phase model (DPM)

The application of DPM to systems under investigation assumes that the volumetric fraction of the discrete phase is small and models particles as a point of mass with associated negligible volume as compared to continuous phase which require nominally a particle volume fraction of less than 12 %. In DPM, the individual particles are injected into a continuous phase where the system itself has a well-defined entrances and exits. The particles are only accelerated by forces based on interaction with the continuous phase, such as bouyancy and drag. The

trajectory of the particles which can be understood as bubbles, droplets, small solid structures, etc. can be associated to the flow effects considering the instantaneous or average fluctuations of the continuous phase velocity. Also, the particles do not exert any influence on the generation or dissipation in the continuous phase.

DPM was implemented by Pereira *et al*., 2010 in an annular flow investigation. Their study focused on the field of viscoplastic fluid flows in annular spaces based on analysis of the profiles of pressure drop, entrance length, axial and tangential velocities, and on the flow path prediction. Accordingly, these variables are usually considered relevant for an understanding of well drilling mudflow and the particles transported by it. Their results specifically the velocity profiles gave better understanding of the flow conditions, enabling one to identify preferentially axial, tangential or mixed flows. The evaluations conducted help shed further light on the flow field, expanding the application of velocity profiles to the entrainment of suspended particles through the annular space. Wu *et al*., (2011) attempted to enhance further the application of DPM in a gas-solid fluidized bed by proposing an improved coupling method to ensure mass conservation. In enforcing the mass balance for the continuous phase in such algorithms using the single phase flow solvers, any heterogeneity in the particle concentration field (caused by clustering of particles) creates non-zero source terms. Their study have demonstrated that if enforcing the mass balance is not handled properly, it can create large numerical errors of up to 10% and any oscillation in the flow field manifests itself in a similar error in the mass conservation. Thus, by using the conservative form of the equations in integral formulation, the coupling between the DPM and CFD models

ensures mass conservation on the global scale in the entire domain, even in the presence of local heterogeneities in the flow field. The method also offers a consistent implementation of mass flow boundaries at the inlet. Numerical results have also shown the superiority of the new coupling method over their previous study in conserving mass and handling transport processes in fluidized beds.

A thorough investigation was conducted Seo *et al*., in 2012 where the multi-phase models were considered to simulate fluid flow of the culture medium formed by CO_2 bubble movement. The theoretical characteristics of each multi-phase model were analyzed, and the models were simulated using a simple, two-dimensional structure of 1 m x 1 m PBR. Half of the PBR using a single bubble injector with 0.1 m diameter at the center of the bottom surface was filled with culture medium and the other half was filled with air. The computed contours of the air phase after 30 s from the start of bubble injection by 0.3 m s^{-1} according to multi-phase models was shown in **Fig. 2-4.** Accordingly, their results presented that the VOF model was appropriate among the multi-phase models supported by FLUENT®. VOF model have been also used for similar researches conducted by Li *et al*. (2000), Akhtar *et al* (2007), etc. However, such results cannot be conclusive especially in simulating bubble column PBRs considering some reasons such as: 1) The CFD simulation models was conducted in a very simple structure of 1 m x 1 m which is not the actual case in PBRs; 2) The simulation was done in 2D where in it has some limitations especially in the turbulence models. For instance, in an investigation by Irani and Khodagholi (2011), it was shown that a 2D turbulent model is not capable of reproducing the dynamic characteristics of the

flow in a bubble column, due to the fact, that the column walls dampens the turbulence intensity which results in a decrease of the effective viscosity inside the reactor. Their results obtained with the 3D version of the k-ε turbulence model are on the contrary and in surprisingly good qualitative and acceptable quantitative agreement with their experimental results.

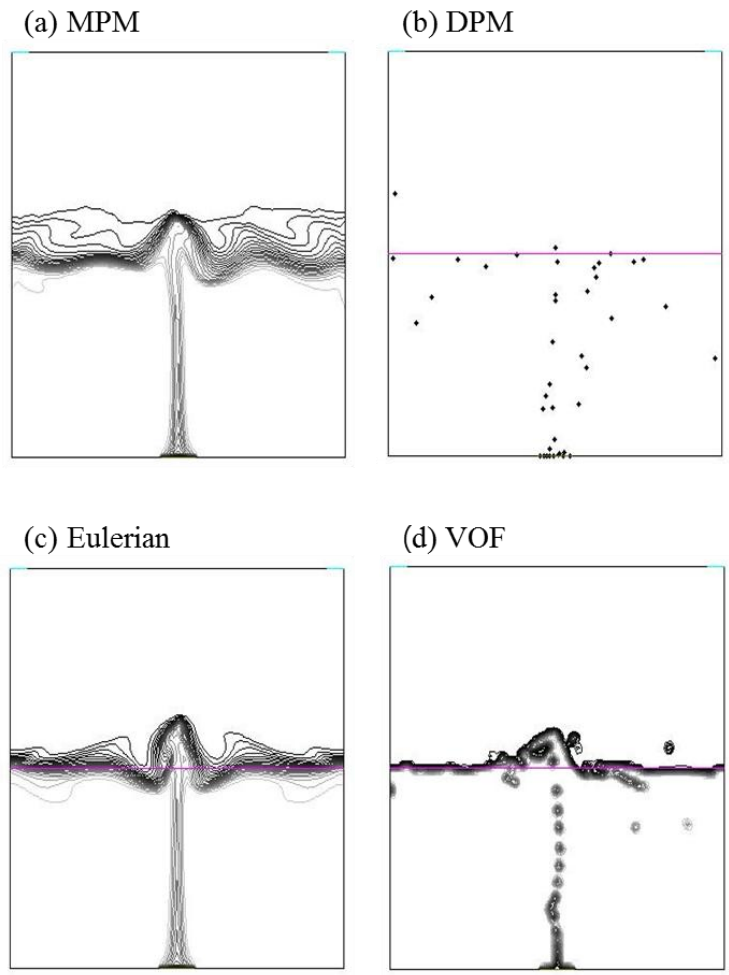

Fig. 2-4 CFD computed contours of the air phase after 30 s from the start of bubble injection by 0.3 m s^{-1} according to multi-phase models. Source: Seo *et al*. (2012)

2.6.3. Numerical issues on different representation of multiphase/turbulence models

In the simulation process, the challenge still exists in most multiphase reactive flow systems both numerical technique and physical understanding of multiphase interactions. However, some progress has been made for multiphase cold flow systems and few reactive flow systems via CFD modeling (Jiang *et al*., 2002). Although the tools for applying single-phase flow CFD are already widely available, the application of multiphase CFD is still complicated due to the difficulty in describing the variety of interactions in these systems (Zhang *et al*., 2004). For example, there is currently no agreement on the governing equation and closure model. In addition, the proposed constitutive models for inter-phase momentum transfer are partially empirical correlations (van Wachem *et al*., 2001).

Joshi (2001) discussed some important characteristic of a multiphase flow which is the existence of an interface separating the phases and the associated discontinuities of properties across the phase interface. The various transfer mechanisms between phases and between a two-phase mixture and a surrounding wall strongly depend upon the two-phase flow regime. The two-phase flows are generally classified into three flow regimes - separated flows, transitional and dispersed flows. Transport phenomena in dispersed phase flows depend upon the collective dynamics of bubbles interacting with each other and with the surrounding continuous phase.

In terms of turbulence models, it is not always clear from the literatures why

some previous researchers have been able get a good prediction of the gas hold-up and liquid velocity profile using the dispersed *k*-ε model at high void fraction (Gimbun, 2009). Most studies were assumed to be reliable since reasonable agreements with experimental data were obtained. However, this alone will not be enough to justify a given single-grid calculation, especially if adjustable parameters are involved (Celik, 1993). In a study by Chen *et al.* (2005), they demonstrated a technique where the input bubble size might be tweaked to get a better fit to the experimental data. However, according to Gibun (2009) this is not an acceptable solution because a good model should be able to predict the two-phase flow field without any tuning and hence becoming fully predictive.

2.6.4. CFD modeling of PBRs

CFD technique automatically accounts for column geometry and scale effects (Baten *et al.*, 2003). However, the success of the CFD simulation strategy is dependent on the proper modeling of the momentum exchange and drag coefficients between the gas and liquid phases. Although the air-water system has several drag correlations, no general guidelines are available for estimating the drag coefficient for systems other than air-water systems (Krishna and Baten, 2002). Numerous CFD studies have been conducted elsewhere for different types of PBRs. The specific focus and some recommendations for PBR designs and CFD model improvement are presented here. Summary lists of these studies were already presented in **Tables 2-4, 2-5 and 2-6**. Most CFD studies investigated the hydrodynamics of bubble column type PBR using FLUENT software, a powerful

and flexible general-purpose computational fluid dynamics (CFD) package.

Simulation of a two-phase flow for an experimental airlift reactor was conducted (Blazey *et al*., 2004). Comparisons were made between vertical velocity and gas hold-up from a series of simulations where the superficial gas velocity in the riser was varied. In airlift reactors, Blazey *et al*. (2004) proposed the implementation of complex, multiple gas/discrete phase model equations to accurately model the motion of gas and liquid. For a highly viscous liquid such as tellus oil, the gas holdup was decreased as the diameter of the bubble column increased (Krishna and Baten, 2002), indicating the strong influence of column diameter on the gas holdup and bubble swarm velocity. The scale effect becomes stronger as superficial gas velocities increase. The applicability of CFD in designing spargers for shallow bubble column reactors has been investigated by Ranade and Tayalia (2001). The flow generated by gas through two different spargers in a bubble column with a height to diameter ratio of 2, by employing a two-fluid model to simulate dispersed gas-liquid flow was simulated. The study extends the application of CFD to screening different sparger designs.

Thakre and Joshi (1999) presented a simulation for flow in bubble column reactors, focusing on specifying drag force and radial lift force on the basis of drift flux constants of the drift flux model as earlier proposed by Zuber and Findlay (1969). The drift flux constants accounts for the hold- up profile and the bubble rise velocity in the reactor. The study clearly exhibits a profile of the slip velocity where maximum values were determined at the center, and decreases towards the wall. However, the slip velocity value (the difference in velocities between liquids

and solids or gases and liquids in the vertical flow of two-phase mixtures through a reactor because of the slip between the two phases) cannot be predicted for an unknown gas-liquid system. Explanations for the enhancement in the slip velocity in the heterogeneous regime were provided.

The hydrodynamics of airlift reactors was investigated by Baten *et al*. (2003) where experimental results and CFD simulations were thoroughly compared. The authors accounted for interactions between bubbles and liquid by means of a momentum exchange, or drag coefficient that was based on correlations from the literature. The axisymmetric two-dimensional grids were assumed to be valid since results from experiments and simulation showed good agreement. The assumption of two-dimensional axisymmetry led to radial profiles of velocity that have a more parabolic character than fully three-dimensional simulations. Accordingly, the CFD model has the potential to be applied as a tool for scale-up.

The data of flow velocities should be totally independent of the number of grid cells. The choice of grid layout and density, especially in the near-wall region, is very important in numerical simulations (Rampure *et al*., 2007; Szafran and Kmiec, 2004). A structured and unstructured mesh design conducted by Szafran and Kmiec (2002) in a Jet-loop reactor was symmetrically designed to reduce the computational times and the required system resources. The first mesh is full structured with quadrilateral cells in core and near wall region while the second mesh is unstructured, composed of triangular cells in the core region and quadrilateral cells in the near-wall region. The simulation result showed that the unstructured mesh reduces discrepancies on the axis of symmetry caused by the

axisymmetric solver and is more accurate. Similar approach was used where an unstructured grid design was also adopted by Rampure *et al*. (2007) and Blazey *et al*., (2004) in a cylindrical bubble column and airlift reactor, respectively. It was also very important to capture gradients near the wall, where flow is expected to be parallel to the cylindrical wall. To consider the said condition, the "O"-type grids near the wall was used and to minimize skewness, hexahedral computational cells were created. Rampure *et al*. (2007) also investigated influence of the number of computational cells (9000-52000) (**Fig. 2-5**). The investigation revealed that the radial profile of the local gas holdup with 9000 cells predicted a horizontal profile, whereas for higher grid resolution, parabolic profiles were obtained showing good agreement with experimental data. In terms of time-averaged axial liquid velocity, using 9000 cells were lower than those obtained with higher number of computational cells and experimental data.

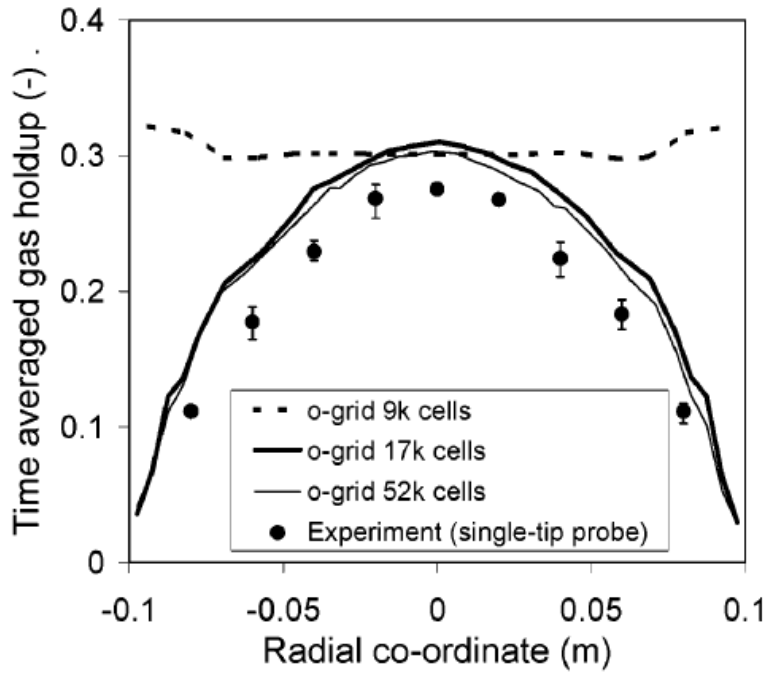

Fig. 2-5 Effect of grid size on time-averaged gas holdup and axial liquid velocity at $U_g = 0.10$ ms^{-1} predicted at a height of 0.65 m. Source: Rampure *et al*. (2007)

As of this time only a few papers have attempted to simulate a multi-fluid (three-phase) system. In the first attempt to three-phase system, Krishna *et al*. (2000) simulated a three-phase model in a bubble column reactor as liquid, "small" bubbles and "large" bubbles by Eulerian-Eulerian description (**Fig. 2-6**). Interactions between both bubble populations and the liquid were analyzed for momentum exchange, or drag coefficients, which differed for the small and large bubbles. However, the study is limited since the interaction between the large and small bubble phases was ignored. Good contacting between phases in multiphase reactors is essential to promote inter-phase transport of species and energy

(Sundaresan, 2000). The strong influence of scale on the hydrodynamics inside the bubble column was emphasized, stressing the need for further investigations in tandem with light distribution within the reactor.

Furthermore, the results of the study of Szafran and Kmiec (2004) disputed the results of Krishna *et al*. (2000) by finding a significant computational error on the axis of symmetry in the two-axisymmetric solver. However, the error can be reduced to acceptable values if unstructured instead of structured mesh are used. The prediction errors for the water circulation rate ratio for a gas-liquid system gave an acceptable engineering calculation of about 4% for the two-phase system, and about 15% for the three-phase system. In addition, the simulations conducted by Szafran and Kmiec (2004) did not precisely predict the gas hold-up that was addressed by Michele and Hempel (2002) through a detailed measurement of local dispersed phase holdups in a pilot-sized bubble column, operated at high superficial gas velocities and solid holdups. This study considered the influence of superficial gas velocity, solid loading and sparger geometry on measured and computed liquid flow velocities and holdup distributions. The CFD calculations by Michele and Hempel (2002) are very significant since it proved the importance of correctly modeling the direct interactions of dispersed gas and solid phases in a three-phase flow.

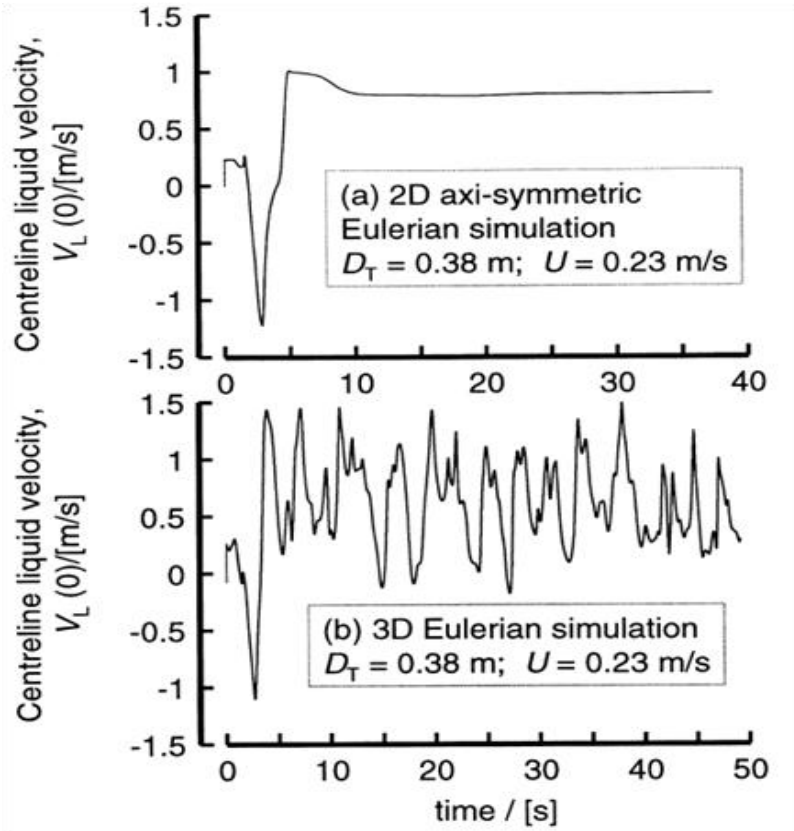

Fig. 2-6 2D and 3D CFD Eulerian-Eulerian simulations of a 0.38 m diameter column with air-water system operating at a superficial gas velocity of 0.23 m s^{-1}. Obviously, the 3D simulation showed chaotic behavior (U: superficial gas velocity, m s^{-1}; D_T: column diameter, m). Source: Krishna *et al*. (2000)

2.6.5. Specific focus of CFD studies on PBR

2.6.5.1. Mixing studies

Perner-Nochta and Posten (2007) investigated a tubular PBR where static mixers are used for efficient mixing of liquid and also gases with liquid. However,

the author's choice of using *k*-ε turbulence model only approximated the real and neglecting the flow eddies which could actually resolved realistically by using the more complex CFD such as Large Eddy Simulations or even Direct Numerical Simulation. The authors also neglected the role of bubbles in the mixing process because they simulated only single-phase flow. If bubble size is being considered, it is correctly assumed that the small bubbles are well transported with the main flow, whereas bigger bubbles cause additional turbulence behind them. A numerical investigation of hydrodynamics and mixing conditions in a PBR focusing on the influence of PBR geometry on the growth of microalgae was conducted by Pruvost *et al*. (2006). A torus-shaped PBR was designed to enable light control, while providing efficient mixing via an impeller, particularly along the culture light gradient. A high degree of mixing was observed, showing the potential of this innovative geometry for cultivation of photosynthetic microorganisms, and for designing lab-scale processes for conducting modeling experiments under well-controlled conditions of light and flow. Pramparo *et al*. (2008) further investigated the torus PBR, focusing on only a square-section, and using batch and continuous conditions. Mixing time was found out to be independent of the Reynolds number when the impeller rotation speed was greater than 1200 rpm (Re > 5800). Thus, a fully turbulent regime could be obtained in the PBR from the Reynolds number values for N = 1200 rpm. Nonetheless, the torus PBR is less attractive for scale-up because its geometry limits the production volume after scale-up.

The hydrodynamics of bubble column reactors at high gas velocity was

discussed thoroughly by Rampure *et al*. (2007), comparing CFD simulations to actual experiments. Important conclusion was drawn such as "multiple snapshots" approach allows significant savings in computing resources without jeopardizing the accuracy of the model especially when simulating mixing time. The multiple snapshot approach stores flow fields after specific time intervals. Such stored, flow-field snapshots are used to solve only the tracer mass-fraction equation for the interval snapshots. At the beginning of each new interval, the tracer concentration distribution within the column is stored and used for further solution using the next flow-field snapshot. Ekambara *et al*. (2005) also predicted the flow patterns in bubble column reactors employing the k-ε turbulence model for one-dimensional (1D), two-dimensional (2D) and three-dimensional (3D) models. All simulation showed good agreement with experimental data for axial and fractional gas holdup profiles, except for eddy diffusivity, for which only the 3D predictions closely agreed with the experimental data. For the axial dispersion coefficient, which characterizes mixing efficiency, only the 3D model showed excellent agreement with the experimental values. They reasoned that convection currents became restricted for the 1D and 2D models, and that the Residence Time Distribution (RTD) became correspondingly narrower, thus resulting in lower values for the dispersion coefficient. RTD is a probability distribution function that describes the amount of time a fluid element could spend inside a reactor which is used to characterize the mixing and flow conditions within a reactors.

2.6.5.2. Light simulation studies

Despite several simulation studies on bubble column reactors, analysis of light penetration in PBRs has been limited, even though the light availability within the PBR is the most important factor controlling the algae's growth. **Fig. 2-7** shows a schematic diagram of the exponential decay of illuminance in an externally illuminated PBR. According to Merchuk and Wu (2003), the PBR is divided into three zones with different growth rates in each zone. The first zone extends from the illuminated wall to the point where light energy intake just balances the energy needed for growth at the maximum rate (I_1). The second zone ends at the point where the light energy intake just balances the energy needed for maintenance (I_2), and the third zone is where growth is negative because of the limited availability of light. However, the schematic presentation becomes more complicated if photoinhibition is considered, since this may lead to a decrease in growth rate in the first zone, near the light source (dotted line) (Merchuk and Wu 2003). Nevertheless, modeling of light inside the PBR does not need some complex algorithm and a simple user defined (UDF) coding can be implemented. Moreover, estimating the light intensity in PBRs can also be achieved during the post-processing of data which can be obtained after the simulation.

Simulations of variation in light intensity in PBRs have been conducted by Perner-Nochta and Posten (2007). This investigation focused on the temporal and spatial aspects of light patterns that may affect the photosynthetic reaction. Particle trajectories representing the path of algal cells were analyzed to obtain light fluctuations on single cell. The simulations showed the potential of reviewing

radial flow in a tubular PBR using a static mixer, and the usefulness of CFD and trajectory analysis for scale-down and scale-up. The radiation distribution in a new, immobilized, catalyst bubble column PBR with external illumination has been analyzed by Trujillio *et al*. (2007). The results indicated that gas bubbling considerably increases the incident radiation in the gas-liquid mixture, enhancing the radiative flux and the absorbed radiation on a titania-coated plate. The CFD results paved the way for the optimization of a solar photocatalytic reactor for the degradation of organic pollutants. Perner *et al*. (2003) numerically optimized a plate PBR in which improvement of the reactor and plate geometry was performed based on the reduction of pressure loss (reduction by 70%), as well as the light intake capability of the reactor. The study also strongly pointed out that the flow geometry can reduce deposition and affects insufficiently mixed zones. The investigation showed that bent pipes with large radius of curvature and circular cross area are preferable to rectangular channels.

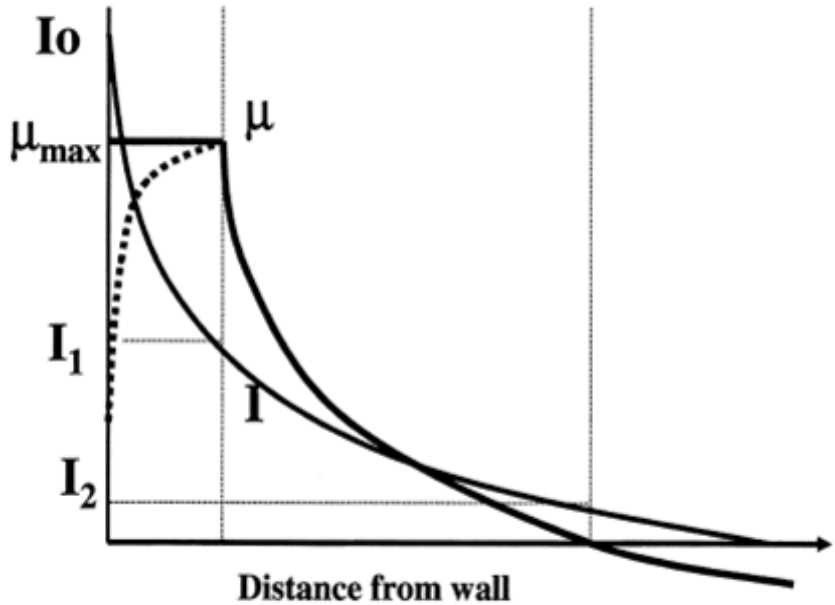

Fig. 2-7 Illumination and local growth as a function of distance from the illuminated wall (I: Illuminance, or photon flux density, μE m^{-2} s^{-1}; I_0: light intensity at the surface, μE m^{-2} s^{-1}; I_1: Illuminance balancing the energy needed for growth at the maximum rate, μE m^{-2} s^{-1}; I_2: Illuminance balancing the energy needed for maintenance, μE m^{-2} s^{-1}; μ: Specific growth rate, h^{-1}).

Source: Merchuk and Wu (2003)

2.6.5.3. Species modeling studies

The Eulerian-Eulerian model in a gas-liquid-solid phase simulation of a bubble column operating in the churn-turbulent regime and focusing on scale up was investigated (Krishna *et al*., 2000). Two types of approaches were compared: (a) a simulation model assuming axi-symmetry and (b) a complete three-dimensional

model for the cylindrical columns. The results of the simulation of Krishna *et al*., (2000) showed that a chaotic behavior occur in the three-dimensional simulation (**Fig. 2-8**). The two-dimensional simulations assuming axi-symmetry were found to be of sufficient accuracy for estimating the average gas hold-ups in the dispersion and circulating liquid velocities.

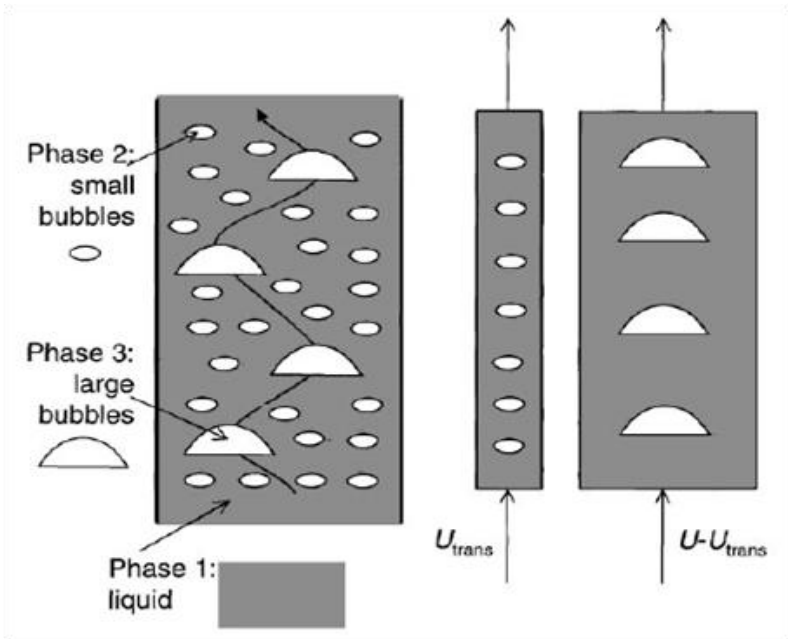

Fig. 2-8 Three-phase model for bubble column operating in the churn turbulent regime. In the turbulent flow regime, it was assumed that two distinct bubble classes exist, "small" and "large" bubbles (U: superficial gas velocity, m s^{-1}; U_{trans}: superficial gas velocity at the regime transition point for air-water, m s^{-1}).

Source: Krishna *et al*. (2000)

Bertola *et al*., (2003) analyzed the ability of different models based on the Eulerian-Eulerian approach to predict gas-liquid systems operating under different conditions. Their study focused to describe both the time-dependent motion of the bubble plume and time averaged flow pattern in the bubble column PBR. The authors performed simulations in 2D to compare *Prandtl's mixing length* and *k*-ε closures. However, both models failed to capture the unsteady condition of the systems due to high value of turbulent viscosity predicted in small systems.

Akhtar *et al*. (2007) and Li *et al*. (2002) both exploited the VOF approach to investigate the hydrodynamics of a continuous chain bubble rising through a liquid, and a bubble rising in liquid medium at high pressure, respectively. The former investigation studied the effect of operating and design parameters on the bubble size distribution and bubble rise trajectory for an air-water system, while the latter focused on simulating the rise behavior of a single bubble at elevated pressures in a bubble column. The simulation results of Akhtar *et al*. (2007) indicated the formation of bubbles at a low superficial gas velocity and relatively large bubbles at higher velocities (**Fig. 2-9**). The increase in the hole-size of the distributor showed similar behavior. Analysis of bubble trajectories for different superficial velocities and distributors demonstrated that small bubbles formed at low superficial gas velocity exhibited an oscillatory behavior. These findings support the simulation results of Li *et al*. (2000) in which pressure was found to affect bubble size (**Fig. 2-10**). The simulation results indicated that as the pressure increases, the maximum stable bubble size decreases. Both simulation studies were thoroughly verified by experimental findings.

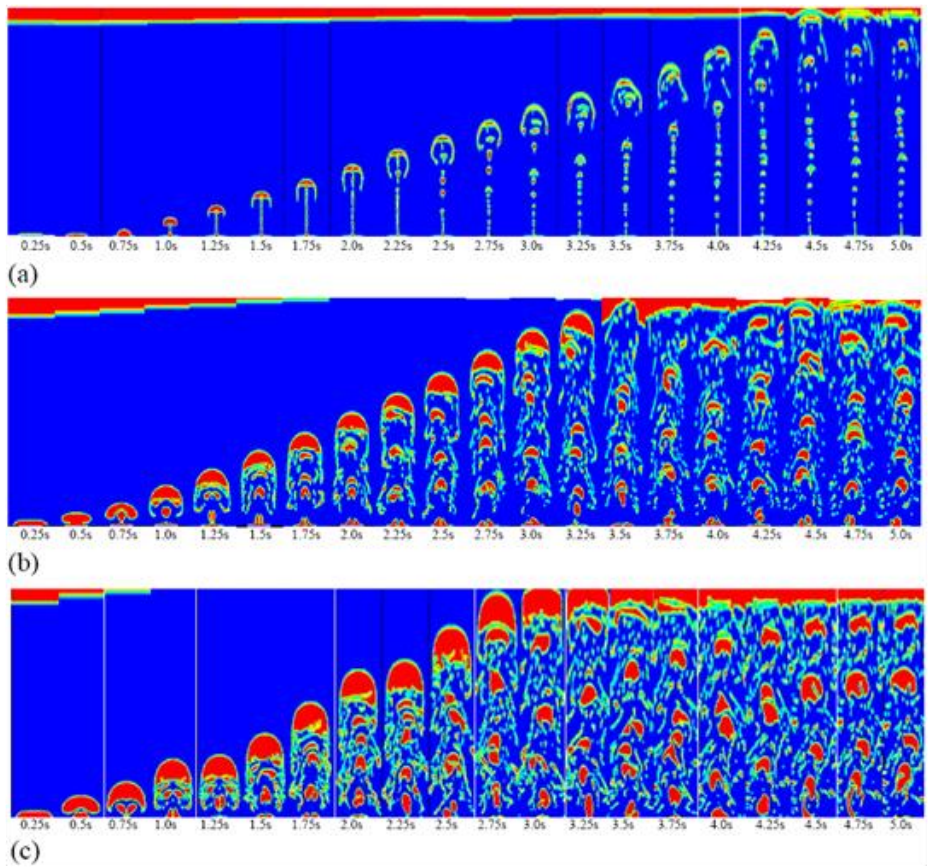

Fig. 2-9 Two-dimensional effect of gas superficial velocity on bubble size distribution. Simulated using VOF method (Column width: 20 cm; H: 100 cm, Hole size: 10 cm). (a) U_g: 1 cm s^{-1}; (b) U_g: 5 cm s^{-1}; (c) U_g: 10 cm s^{-1}).

Source: Akhtar *et al*. (2007).

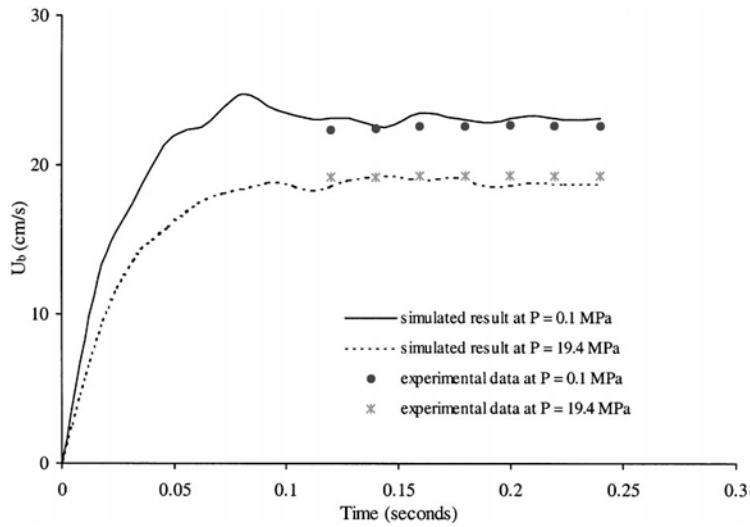

Fig. 2-10 Comparisons of simulated and experimental rise velocities under different pressures (U_b: is the bubble rise velocity, cm s^{-1}). Source: Li *et al*. (2000)

2.6.6. Challenges in PBR design

Designing PBRs still remains a big challenge and significant research undertakings related on these are being carried elsewhere. However, up to this date, a successfully scaled up PBRs up for mass production of microalgae are still limited. The most important factors which should be strongly considered in the design such as light penetration and distribution, mixing and gas distribution inside the PBRs are closely interrelated which makes the designing more complex. The penetration and distribution of light inside the PBR is affected by the mixing characteristics which are also influenced by the gas injection method.

2.6.6.1. CFD design for light distribution

One of the main challenges in the design and construction of PRRs is to provide high illuminated surface-area-to-volume ratio. In order to attain high productivity, the volume of the non-illuminated parts of the reactor should be minimized and to ensure a high efficiency of light use by the culture, the design must provide for the uniform illumination of the culture surface and the fast mass transfer of CO_2 and O_2. In PBRs, turbulent flow conditions and light gradients also frequently occur. Thus, algal cells cultivated in such reactors experience fluctuations in light intensity (Perner-Nochta and Posten, 2007) which is influenced by the mixing characteristics inside the PBR (Seo *et al*., 2010). Therefore, discussion on the influence of mixing on light distribution is also presented here.

An example case was presented by Perner-Nochta and Posten (2007) of a tubular photobioreactor where static mixers are used for the efficient mixing of liquid and also of gases with liquid. They demonstrated that motionless helical mixing elements improve the radial tubular flow, increasing both frequency and regularity of the motion ensuring light distribution for the cells inside the PBR. Su *et al*. (2010) attempted to use a destabilizing structure applied in a flat plate PBR and the flow field and particle trajectory were simulated to optimize the structural parameters of the PBR. The results showed that the vertical velocity along the light path was produced in the condition of destabilization, which helps to achieve homogenous mixing of medium needed for microalgae growth. The fluid in the flow field waved regularly, which made the algae cell transmitted between light and dark area inside the PBRR and enhance the efficiency of photosynthesis. This

destabilizing structure had a great potential to be used in the PBR design.

2.6.6.2. CFD design for gas distribution

Introduction of CO_2 gas through bubble at the bottom of PBRs has been the common method for gas distribution. The rising bubbles have an important role in the liquid mixing and mass transfer (Akhtar *et al*., 2007). Great progress has been made in modeling the hydrodynamics of bubbly flow especially in bubble column (Lain *et al*., 2001) and airlift PBRs (Huang *et al*., 2010). However, the prediction of mass transfer and mixing of chemical species in bubbly flow is still a great challenge, mainly because the interfacial transfer rates in a bubble swarm do not follow the laws of interfacial transfer valid for isolated bubbles in general (Ayed *et al*., 2007). Nevertheless, these models are derived from a specific situation with diversified geometric forms. It is very important and necessary to validate these models and find ones that can describe the inter-phase mass transfer accurately and be used for a wide range of operating conditions, geometries and fluids (Huang *et al*., 2010). Mass transfer rates in a bioreactor are largely affected by the fluid properties, liquid and gas velocity, and by the geometry and type of PBR (Velarde *et al*., 2010). Mass transfer is frequently assessed by the volumetric mass transfer coefficient. In practical terms, prediction and optimization of mass transfer by the mass transfer coefficient seeks maximal mass transfer with minimal energy input (Chisti, 1989).

A study by Sanyal *et al*. (1999) validated a transient, two-dimensional axisymmetric simulation of a laboratory-scale cylindrical bubble column, run under

bubbly flow and churn turbulent conditions. The simulation results suggest that simple, two-dimensional axisymmetric distributions can be used to obtain reasonable engineering calculations for the overall flow pattern and gas holdup distributions. However, a fully transient, three-dimensional model maybe used to capture the transient flow structures in a bubble column is still strongly recommended, which are in general not axisymmetric and have a significant azimuthal component. Dhotre and Joshi (2007) attempted to simulate the flow pattern on the upstream and downstream of a distributor and its effect on performance of a bubble column PBR. They proposed some procedures for connecting the gas chamber to bubble column PBR. Results of their study revealed that the effect of inlet nozzle size and its location with respect to the distributor were very important. The flow pattern within the gas chamber has been comprehensively analyzed and the velocities through all the holes have been estimated for assessing the uniformity of the gas distribution. It was found that the chamber configuration has an effect on the uniformity of gas distribution particularly in the sparger region of bubble column reactors. Furthermore, the uniformity of gas distribution was found to increase with an increase in the distributor pressure drop and a decrease in the inlet kinetic head of the gas.

Simonnet *et al*., (2008) through a CFD simulation investigated the importance of the drag force formulation to describe regime transitions in a bubble column PBR. Results of their study found out that accounting bubble-bubble interactions through drag coefficient which depends on the local void fraction have allowed predicting the onset of the regime transitions. Their study also has shown that the

use of the drag correlation allows reproducing some typical characteristics of the different regimes (velocity profiles becoming parabolic in the transition regime, typical transient phenomena, accumulation of large bubbles in the column centre in the transition and heterogeneous regimes).

2.6.6.3. Opportunities for CFD approach

CFD has established itself as a viable technique for performing research and solving engineering problems, and when used correctly, can give accurate results for many fairly complex problems (Celik, 1993). In the design of PBRs, the engineering principles regarding light distribution, mixing, hydrodynamics and gas distribution have already been set up and available for use in developing various geometries qualified for scale up. A commercial scale up of the PBR should be a primary design criterion and should always be the main goal.

Although relationship between hydrodynamics and mass transfer has been extensively investigated and correlated in bioreactors for heterotrophic cultures, only a few studies on these aspects are available in phototrophic cultures (Ugwu, 2008). Hydrodynamics and mass transfer characteristics that are applicable in photobioreactors include; the overall mass transfer coefficient, mixing, liquid velocity, gas bubble velocity and gas holdup. The overall mass transfer coefficient is the most commonly used parameters for assessing the performance of photobioreactors which can be predicted using CFD. The term is generally used to describe the overall volumetric mass transfer coefficient in photobioreactors. The volumetric mass transfer coefficient of photobioreactors is dependent on various

factors such as agitation rate, the type of sparger, surfactants/antifoam agents and temperature. However, these factors can be thoroughly investigated using CFD technique which saves lot of time and effort including cost as compared to actual constructing several PBRs for the study.

In terms of the turbulence models, the *k*-ε model has been popularly use, but it should be recognized that bubbles can also affect the characteristics of flow which can be accounted through the turbulent kinetic energy or by inserting additional turbulence factor caused by the bubbles. This theory has not yet been investigated but should be considered in future simulation studies.

The major growth factors for microalgae are mentioned in the earlier part of the paper; however, the growth of microalgae was not taken into account in the simulation studies. This can be explored in the near future where the growth of microalgae is modeled inside the PBR through the growth equation models. The growth models can be connected to the main module of CFD via the user defined functions (UDF) of the software. However, the developed growth equation models available in literatures were limited only to one or two growth factors and the ranges of the growth factors were also narrow, for example, the temperature ranges is from 20 ~ 35 ^{o}C and light intensity ranges from 300 ~ 400 μE m^{-2} s^{-1}. Therefore, an integrated growth model equation taken into account wider ranges of the main growth factors must be developed first (Bitog *et al.*, 2009). The very first task should be to grow the microalgae in laboratory scale where the effect of the major growth factors as well as their interaction effect will be accounted. This could be very challenging to conduct, however, very critical in developing an integrated

growth model equation. The equation can also be utilized to evaluate the efficiency of various designed PBRs.

Validating the solution of future CFD studies can be done via reliable experimental results provided experimental uncertainty must be established. However, it should be clearly understood first that the prospect of CFD related studies aims to predict the outcome of a physical event for which experimental data is not available. Although no standard method for evaluating numerical uncertainty in currently available by the CFD community, numerous methods and techniques are available to CFD users to accomplish this task. Guidelines on this matter can be found in Celik (1993) and Roache *et al.* (1986).

3. General Objectives

The overall goal of this research was to investigate the flow hydrodynamics in 30 L PBRs using computational fluid dynamics. The optimized hydrodynamics factors were utilized to analyze which PBR designs are appropriate for microalgae production. The focus of the investigation is on bubble column PBRs which is chosen because of its simple design with no moving parts but with suitable heat and mass transfer. The study aimed to recommend the most appropriate operating parameter and inner structure configuration of the PBR for efficient microalgae mass production. To obtain these objectives, studies were implemented with their specific goals as follows:

In Chapter 3, a CFD review aimed to obtain significant understanding about microalgae, its environmental growth requirements and the growth vessels such as the PBRs where microalgae are cultivated. The review also targeted to conduct a comprehensive survey on the numerical simulation approaches and analysis in designing PBRs.

In Chapter 4, the objective was to validate the CFD code and simulation technique using Particle Image Velocimetry or simply PIV. This is very critical since the modeling approach is carefully investigated and the result should be consistent with the results obtained in real or actual phenomenon.

The application of CFD in designing PBRs based from the flow hydrodynamics such as volume percentages of dead zones, average circulation time

and turbulence intensity were explored and combined to evaluate the performance of bubble column PBRs was the specific goal in Chapter 5. There were 32 simulated cases of PBR designs which were evaluated in terms of the integrated flow hydrodynamics. To obtain the accurate flow characteristics in the PBR, the elaborate simulation modeling using CFD technology was performed. To determine the average circulation time, DPM model was performed and the discrete random walk tracking approach was utilized. To determine the appropriate operating parameters in the PBRs, the air flow rate and nozzle size were varied from 0.05, 0.10, 0.15 and 0.20 vvm and 5, 10, and 15 and 20 cm, respectively. For the PBR structure, with and without internal baffle was considered. The objective is to determine which operating parameter and PBR design among the PBR simulation cases is suitable for microalgae production. The PBR model from the varied air flow rates, nozzle size diameters and PBR geometries resulted to 4 x 4 x 2 = 32 simulation cases.

The objective of Chapter 6 in conducting the practical cultivation of microalgae cells in the designed PBRs is to finally confirm the simulation results obtained in Chapter 5. This will also cement the conclusion drawn from the previous chapter with the hydrodynamic investigation of the PBRs. The practical cultivation of microalgae was conducted in two sets of succeeding experiments in a 30 L PBR where the biomass concentration and specific growth rate obtained from a typical PBR design and the proposed PBR which was decided based on the results obtained in Chapter 5 was compared. The general flowchart of the study is presented in **Fig. 3-1**.

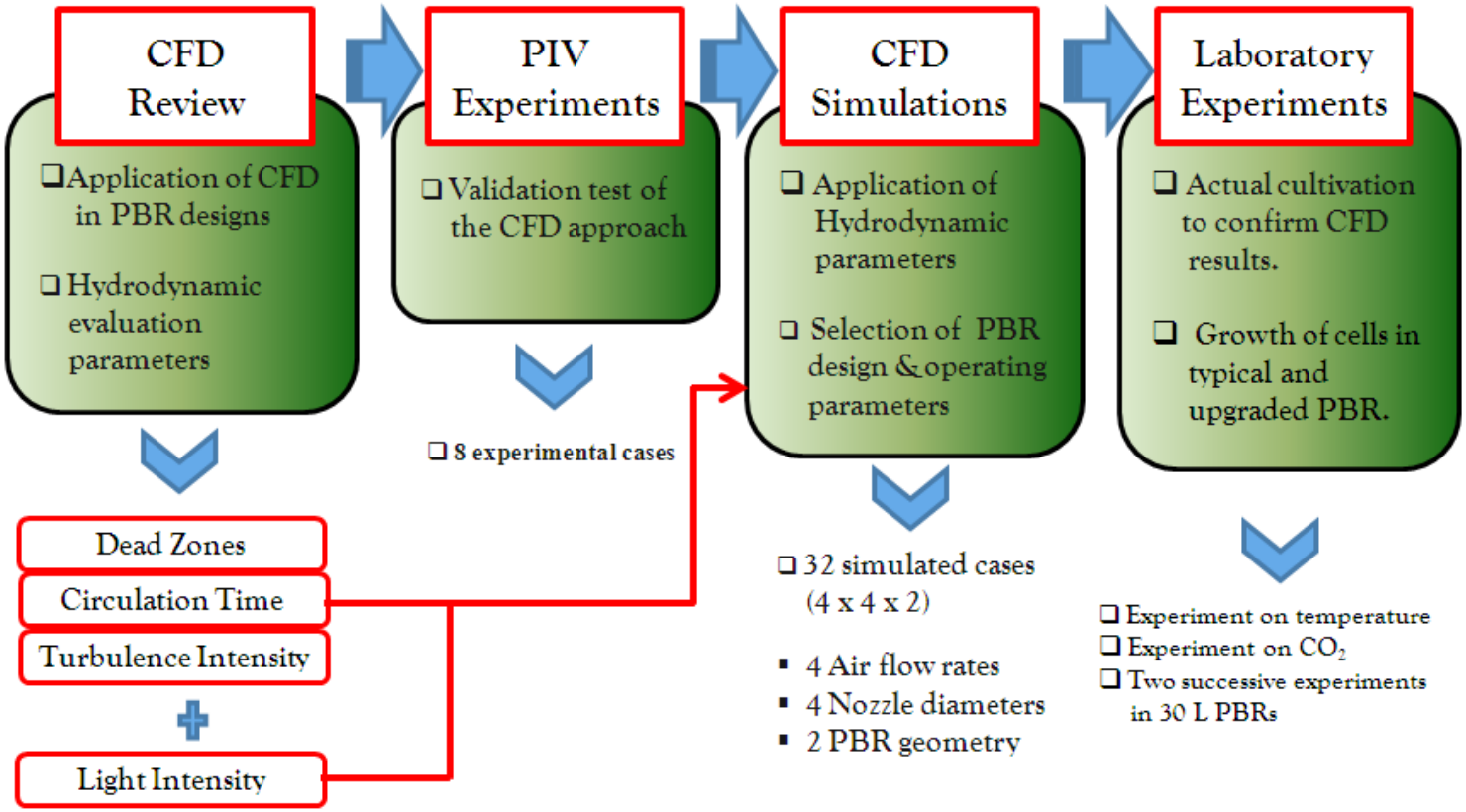

Fig. 3-1. Flow chart of the study where PIV test, CFD simulation and laboratory experiments were successively conducted.

4. Validation of CFD simulations using Particle Image Velocimetry (PIV) data

4.1. Introduction

PIV is an optical method to flow visualization in a system under investigation. The method is practically used to obtain instantaneous velocity measurements and related properties of fluids inside a system. PIV works by seeding tracer particles which are assumed to faithfully follow the flow dynamics following the principle of Stokes number. The particles are illuminated using a laser so that they become visible for the specialized digital camera which captures multiple frames at high speed. The images of the tracer particles are recorded at least twice with a small time-delay. The displacement of the particle images represents the fluid motion. The flow movements of particles are then being tracked where the velocity and direction of the particles are recorded for computer analysis. A schematic diagram of a PIV system is shown in **Fig. 4-1**.

The seeding particles are an inherently critical component of the PIV system. Depending on the fluid under investigation, the particles must be able to match the fluid properties reasonably well. Otherwise they will not follow the flow satisfactorily enough for the PIV analysis to be considered accurate. While the actual particle choice is dependent on the nature of the fluid, generally for macro PIV investigations they are glass beads, polystyrene, aluminum flakes or oil droplets (if the fluid under investigation is a gas). Refractive index for the seeding

particles should be different from the fluid which they are seeding, so that the laser sheet incident on the fluid flow will reflect the particles towards the camera. The particles are typically of a diameter on the order of 10 to 100 micrometers. As for sizing, the particles should be small enough so that response time of the particles to the motion of the fluid is reasonably short to accurately follow the flow, yet large enough to scatter a significant quantity of the incident laser light. For some experiments involving combustion, seeding particle size may be smaller, on the order of 1 micrometer, to avoid the quenching effect that the inert particles may have on flames. Due to the small size of the particles, the particle motion is dominated by stokes drag and settling or rising affects. Approximating the particles as spherical particles of very low Reynolds number, then the ability of the particles to follow the fluid's flow is directly proportional to the difference in density between the particles and the fluid and directly proportional to the square of the particles' diameters. The scattered light from the particles is dominated by Mie scattering and so it is also proportional to the square of the particles' diameters. Thus the particle size needs to be balanced to scatter enough light to accurately visualize all particles within the laser sheet plane but small enough to accurately follow the flow. The seeding mechanism needs to also be designed so as to seed the flow to a sufficient degree without overly disturbing the flow.

To perform PIV analysis on the flow, two exposures of laser light are required upon the camera from the flow. Originally, with the inability of cameras to capture multiple frames at high speeds, both exposures were captured on the same frame and this single frame was used to determine the flow. A process called

autocorrelation was used for this analysis. However, as a result of autocorrelation the direction of the flow becomes unclear, as it is not clear which particle spots are from the first pulse and which are from the second pulse. Faster digital cameras using CCD or CMOS chips were developed since then that can capture two frames at high speed with a few hundred ns difference between the frames. This has allowed each exposure to be isolated on its own frame for more accurate cross-correlation analysis. The limitation of typical cameras is that this fast speed is limited to a pair of shots. This is because each pair of shots must be transferred to the computer before another pair of shots can be taken. Typical cameras can only take a pair of shots at a much slower speed. High speed CCD or CMOS cameras are available but are much more expensive. Additional details of PIV principle and procedures can be found in many published books and literatures such as Adrian and Westerweel (2010), Brossard *et al*. (2009), Schroder and Willert (2008), and Westerweel (1997).

To this date, PIV has been applied to a wide range of flow problems, varying from the flow over an aircraft wing in a wind tunnel to vortex formation in prosthetic heart valves. 3-Dimensional techniques have been sought to analyze turbulent flow and jets, for instance, Lehr and Bolcs (2000) used the system to thoroughly investigate the periodic unsteady flow around an isolated compressor blade. The PIV system was able to deliver instantaneous flow field information. In addition, the system yielded the mean velocity field and turbulence quantities of the flow by statistical treatment of the instantaneous data sets they have obtained.

Shinji *et al*. (2006) have also utilized PIV in order to clarify characteristics of

spatial flow structures and wind pressures above a roof of a cube. The time-averaged separation bubble on the roof had flat shape with gradual curvature. They have carried out a wind tunnel experiment in two types of turbulent boundary layers and the flow was measured by PIV system. Simultaneous multi-pressure measurements on the surface were also performed. With the obtained PIV they have found out that when intensity of turbulence of the approaching flow was large, strong local negative pressure was generated and a flat conical vortex was formed in the former edge corner. The spatial structure of the flow was different from that or the time-averaged flow. Several papers can be found in literature where PIV application was strongly implemented such as Kazunori *et al*., (2006); Yan *et al*. (2005); Naoya *et al*. (2000); Hideki *et al*. (1999); and Lecuona *et al*. (1998).

In addition, the use of PIV has become increasingly significant especially in simulation studies where PIV plays a very important role of validating the computer code used in the modeling approach. In a study by Medvitz *et al*., (2009), PIV was used to validate their CFD technique in assessing the hydrodynamic performance of a positive displacement left ventricular assist device. The computational model uses implicit large eddy simulation direct resolution of the chamber compression and modeled valve closure to reproduce the in vitro results. The computations are validated through comparisons with experimental PIV data. Qualitative comparisons of flow patterns, velocity fields, and wall-shear rates demonstrate a high level of agreement between the computations and experiments. Quantitatively, the PIV and CFD show similar probed velocity histories, closely

matching jet velocities and comparable wall-strain rates.

Methodologies of validating CFD simulations were conducted by Sheng *et al*., (1998) in a stirred tank used in chemical process industry. From the PIV data, the mean velocity, turbulent kinetic energy, Reynolds stress and dissipation rate fields were extracted and by introducing several tools to quantify the similarities and differences between two-dimensional fields, CFD predictions of the flow filed were validated against the PIV data. In addition, they have utilized the PIV data setting up the boundary conditions in their model. Similar study was conducted by Shigeya *et al*. (2005) where they further strengthen the use of PIV as a validation tool for CFD. They have thoroughly used PIV experimental data to investigate the CFD code especially for unsteady state simulations. For instance, two examples of PIV data compared with corresponding CFD data, that is, leading edge separation vortices of a cranked arrow wing and a tip vortex of a rectangular wing, are presented in order to evaluate the capability of PIV as a CFD validation tool. As a result, the detailed velocity field data via PIV are proved to be useful in the evaluations of different turbulence models and algorithms in CFD analyses. Also, important issues to be carefully considered for getting successful results in the CFD validation using PIV were discussed, such as differences in spatial/temporal resolutions and data point locations.

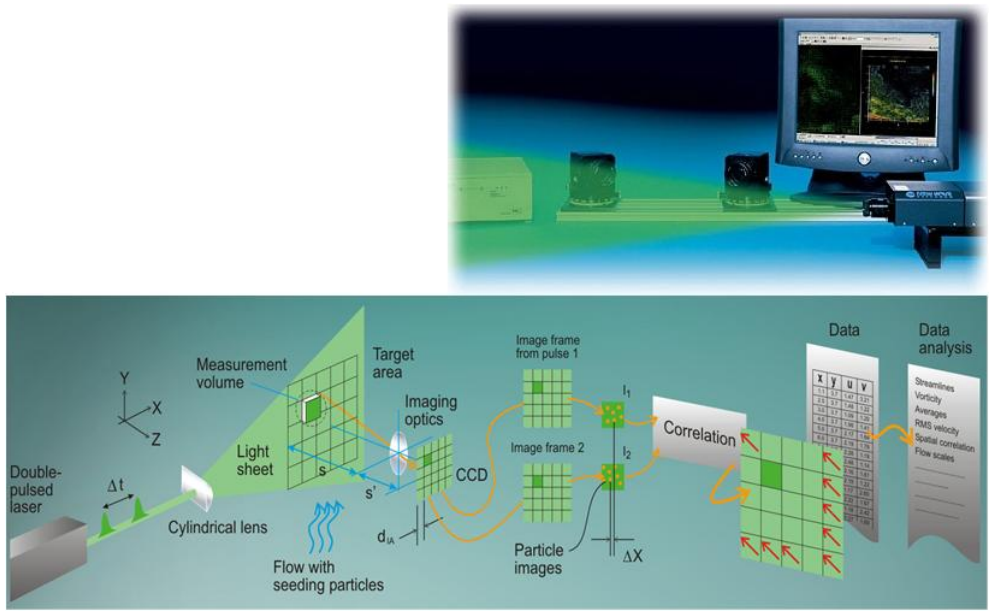

Fig. 4-1 Schematic diagram of a PIV system. Source: http://images.google.com/

4.2. Materials and methods

4.2.1. Particle image velocimetry (PIV)

Validation is very critical in the field of modeling and simulation studies. For instance, in CFD, this is to establish the accuracy of the codes used such as to create credibility and confidence in the results and can be used in making conclusions and decisions. Generally, this is done by comparing the simulation results with physical reality by conducting laboratory or field experiments. In this particular study, PIV experiment was initially conducted to obtain data for comparison with simulation results for validation purposes.

The bubble column PBR used in the PIV test was a typical design type and was

made of 5 mm transparent acrylic panel with an inner diameter of 185 mm. The actual height is 1400 mm. Therefore, for a culturing capacity of 30 L, the water level is approximately 1050 mm. An injection hole with a nozzle diameter of 10 mm was punched at the center bottom of the PBR where air can be easily introduced. The PBR was vertically supported with square frames with movable and adjustable wheels. Air pump was connected to the bottom of the PBR via host connected to the nozzle that was directly connected to the injection hole. The air flow rate was controlled with a regulator and a flow meter attached to the air pump.

The validation of the CFD code to be implemented in the modeling and simulation of the PBRs was realized through comparison of average flow velocities computed from the PIV data and CFD simulation modeling. Aside from visual comparison of the flow between the PIV and simulation results, their computed average velocity magnitudes were quantitatively compared. Four air flow rates of 0.05, 0.10, 0.15 and 2.0 vvm which corresponds to 0.32, 0.64, 0.95 and 1.27 m s^{-1}, respectively were tested in the PIV experiment in two regions in the PBR. Two regions were considered since the set up of the PIV in terms of its resolution during the test is limited in height of approximately 450 mm. Thus, the lower part of the PBR was designated as Region 1 while the upper portion was designated as Region 2. This totaled to 8 experimental conditions. PIV data were obtained from every set flow rate after approximately 5 minutes where the flow was observed to be stable and the flow characteristics inside the PBR can be assumed to be solely affected by the flow rate. The high speed camera (Nikon AF Nikkor 50mm f/1.8D, Japan) was used to take images in every 0.1s in 3s thus capturing 300 images in each test case.

Presented in **Fig. 4-2** is the actual PBR used in the PIV test. The regions where the instant velocities of particles inside the PBR were captured and considered in the PIV data analysis were also shown. A snapshot of one of the PIV experiments being conducted is shown in **Fig. 4-3**. The obtained PIV data were post processed using available commercial computer softwares such as Ensight 3G and Tecplot.

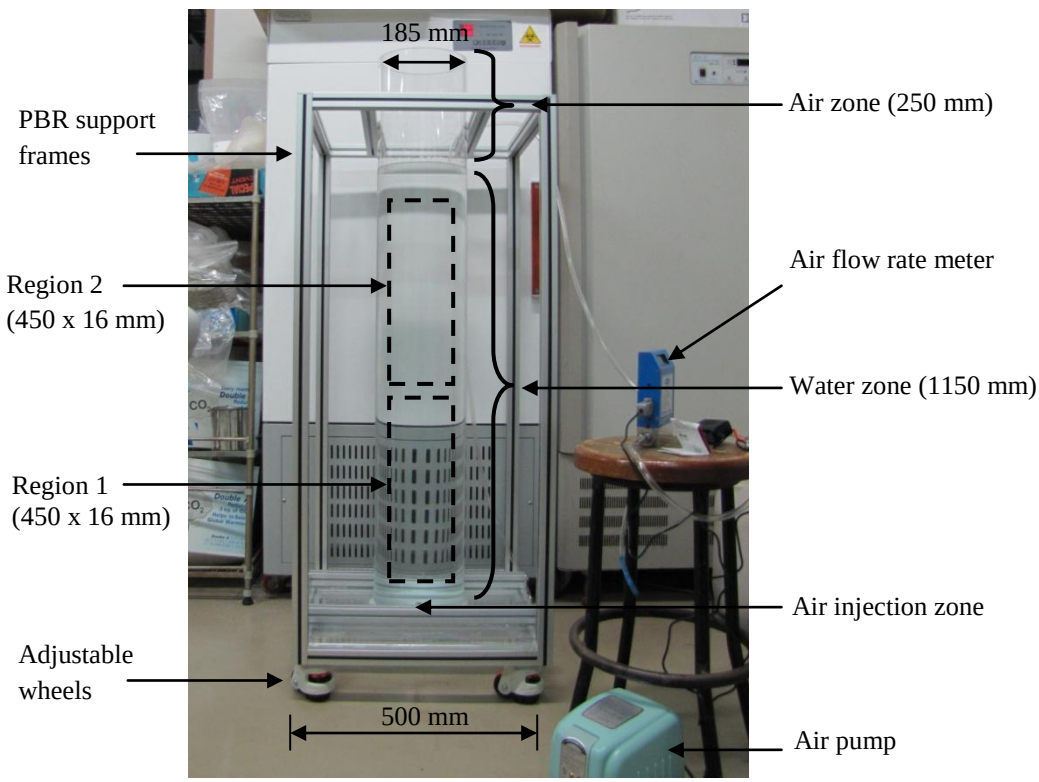

Fig. 4-2 The actual view of the PBR used in the PIV experiment.

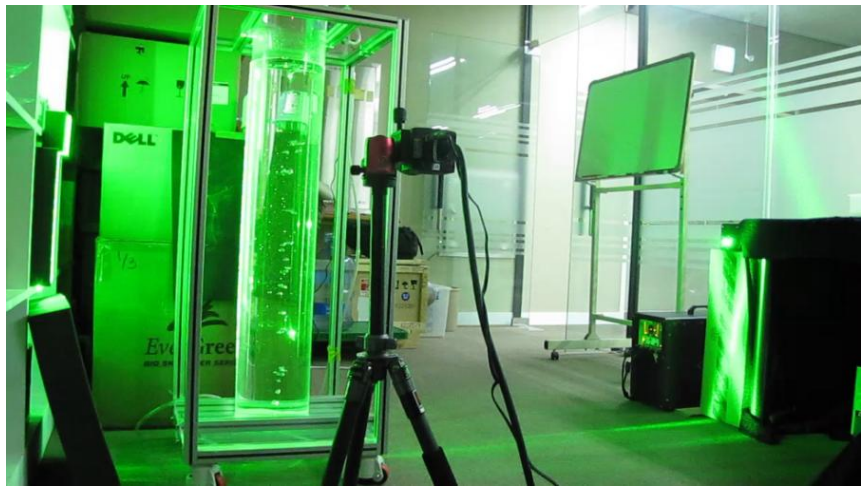

Fig. 4-3 A snapshot photo taken during the actual PIV experiment.

4.2.2. Computational fluid dynamics (CFD)

The geometry of the 30 L PBR was pre-processed using Gambit software (ver. 2.2, Lebanon, N.H, Fluent, Inc.). The PBR was partitioned into three zones as air, water and injection zones. The actual height is 1400 mm. Therefore, for a culturing capacity of 30L, the water zone is approximately 1050 mm. The nozzle diameter at the injection zone is approximately 5 mm. The total number of the unstructured mesh cells of the whole computational domain was 500,428. Evaluating the mesh quality using the equiangle skewness value, it ranged from 0.25 ~ 0.50 which is considered good (Fluent manual, 2006; Baker, 2002).

The Fluent program (ver. 6.2, Lebanon, N.H., Fluent, Inc.) was utilized as the main module and solver to perform the CFD calculation. Presented in **Table 4-1** are information on the data and values utilized in the boundary conditions of the

simulation model to validate the CFD code and technique applied modeling. The multiphase model implemented was Lagrangian-Eulerian model following previous simulation studies such as Li *et al*., 2000; Joshi, 2001; Akhtar *et al*., 2007. According to Joshi (2001), using Lagrangian-Eulerian formulation especially for bubble column PBRs gives some advantages since each individual bubble is modeled for its flow through the column. The RNG *k-ε* turbulence model was employed with dispersed characteristics which has been already used in similar PBR simulations such as Sanyal *et al*., 1999; Perner *et al.* 2003; Trujilio *et al*. 2007. To realize bubble rising, the bubble size diameter was pegged at 0.005 m which is the same with the minimum mesh grid size implemented in the mesh design. Air was introduced at the inlet boundary condition based on the cases simulated as shown in **Table 4-2**.

Table 4-1 Data and variables implemented in the in the CFD simulation of the 30 L PBR to validate CFD code.

Characteristics	Values
Total mesh number	500, 428
Solver	Pressure based (implicit)
Multiphase model	Lagrangian-Eulerian
Phases	Water (primary), Air (secondary)
Specified operating density	1.225 kg m^{-3}
Turbulence	RNG k-ε turbulence model (dispersed)
Near-wall treatment	Standard wall functions
Discretization	Second order upwind
Conditions	Unsteady state
Bubble size	0.005 m
Time interval	0.01s
Solver	Pressure based (implicit)

Table 4-2 Air inlet velocity implemented in the CFD simulation of the 30 L PBR.

PIV test case	Area considered in the PIV Analysis	Air flow rate, vvm	Inlet velocity implemented in the simulation, m s^{-1}
1	Region 1	0.05	1.27
2	Region 1	0.10	2.55
3	Region 1	0.15	3.82
4	Region 1	0.20	5.09
5	Region 2	0.05	1.27
6	Region 2	0.10	2.55
7	Region 2	0.15	3.82
8	Region 2	0.20	5.09

4.3. Results and discussion

4.3.1. Mesh grid interval size

Pre-processing of the model is very crucial part particularly in simulation studies to obtain reliable results. These requires experience and skills on how to create the geometry of the model and make good decision on what mesh type and mesh size to be used, etc. The geometry of the bubble column PBR is not complex thus only the mesh type and size should be appropriately decided. Presented in **Fig. 4-4** is the top view of the PBR according to mesh interval size from 0.001 ~ 0.011 m which were simulated to decide what mesh size should be employed. Obviously, the mesh type implemented was tetrahedron. The total number of mesh employing varied mesh interval sizes of 0.001, 0.003, 0.005, 0.007, 0.009 and 0.011 m and the estimated time for simulation is presented in **Table 4-3**. The quality of the meshes was evaluated via the equiangle skewness value and in all mesh interval sizes, the values are below 0.50 which are evaluated with good quality (Bakker, 2002, Fluent Manual, 2006).

Simulation results have shown that the mesh grid interval size have significant effect on the computed average velocity magnitude. Mesh grid interval sizes particularly 0.007, 0.009 and 0.011 m displayed higher percentage difference to velocity magnitude compared to PIV while mesh grid sizes 0.001, 0.003 and 0.005 m displayed lower values below 10 % and can be comparable with the PIV result (**Fig. 4-5**). The result could suggest that either of these mesh grid interval sizes can be chosen to be implemented in the succeeding simulations. The smaller the mesh

grid size, the longer time is required to complete the simulation. However, this can be easily solved by employing parallel computing system which can significantly lessen the simulation time. The percentage difference of average velocity magnitude compared to PIV at mesh grid interval sizes of 0.001, 0.003 and 0.005 m considering all air flow were approximately 5.28, 5.81 and 6.78 %, respectively. Therefore, without sacrificing the quality of the simulation results and also significantly minimizing the simulation time, a mesh grid size of 0.005 m was wisely chosen. Furthermore, this is almost in congruence with the results obtained by Seo *et al.*, (2012) where a mesh size of 0.004 m was selected to simulate bubble flow in a 2 L PBR.

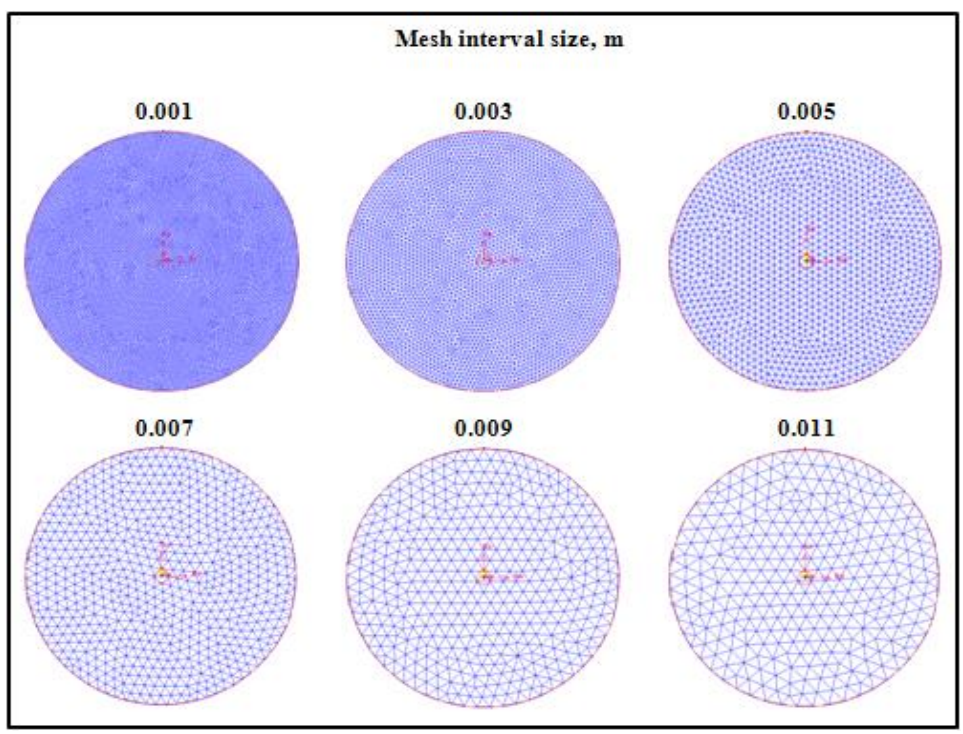

Fig. 4-4. Top view of the PBR according to the employed mesh interval size.

Table 4-3 Total mesh nodes at varied mesh size interval and the estimated time for simulation.

Mesh size interval, m	Total # of mesh nodes	Approximate simulation time, hrs
0.001	3,465,247	336
0.003	1,825,403	225
0.005	622,500	140
0.007	226,077	115
0.009	111,061	100
0.011	64,071	90

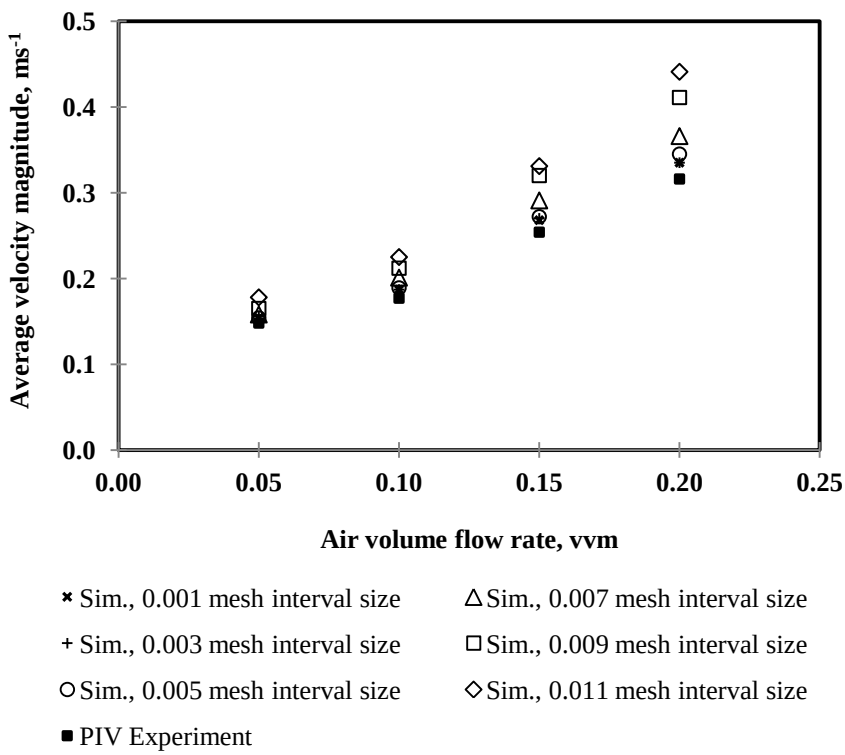

Fig. 4-5 Average velocity magnitude obtained from simulation compared to PIV at varied air flow rates.

4.3.2. Visualization of fluid flow

Flow visualization from the PIV tests is possible which can be analyzed in relation to the hydrodynamic parameters such as mixing or dead zones inside the PBR. Dead zones are regions where the fluid velocity is too low and can be assumed that the plug flow is experienced in that region. The flow is also visualized to investigate if a uniform flow distribution is achieved which is very important for microalgae cells particularly in their light absorption.

The movement of fluid inside the PBR caused by the injection of air at the bottom part of the PBR can be clearly visualized by the naked eye during the conduct of the experiments. The formation of bubbles, their flow characteristics as the bubble rise in the PBR as well as when they disintegrate can be easily observed. More so, as the air flow rate was increased, more bubbles were being introduced and more turbulence inside the PBR can be visibly observed. More detailed observation has also shown that the velocity of the fluid have registered higher values in sections where bubbles are rising. The larger are the bubbles; higher velocity values are being observed and computed. This is clearly shown in **Fig. 4-6** where a series of PIV snap shot was taken in one of the experimental cases. The flow of the bubbles inside the PBR shows a chaotic behavior which makes the validation from this data almost impossible. Thus, the average flow velocity data obtained from the total 300 snap shots in each case was used. This observation can also show the regions where good mixing and higher turbulence can possibly happen. Thus in the PBR, the regions where bubbles are expected to be rising experience better mixing and turbulence which is usually at the inner section of the

PBR while poor mixing can be suspected in the wall and near wall sections.

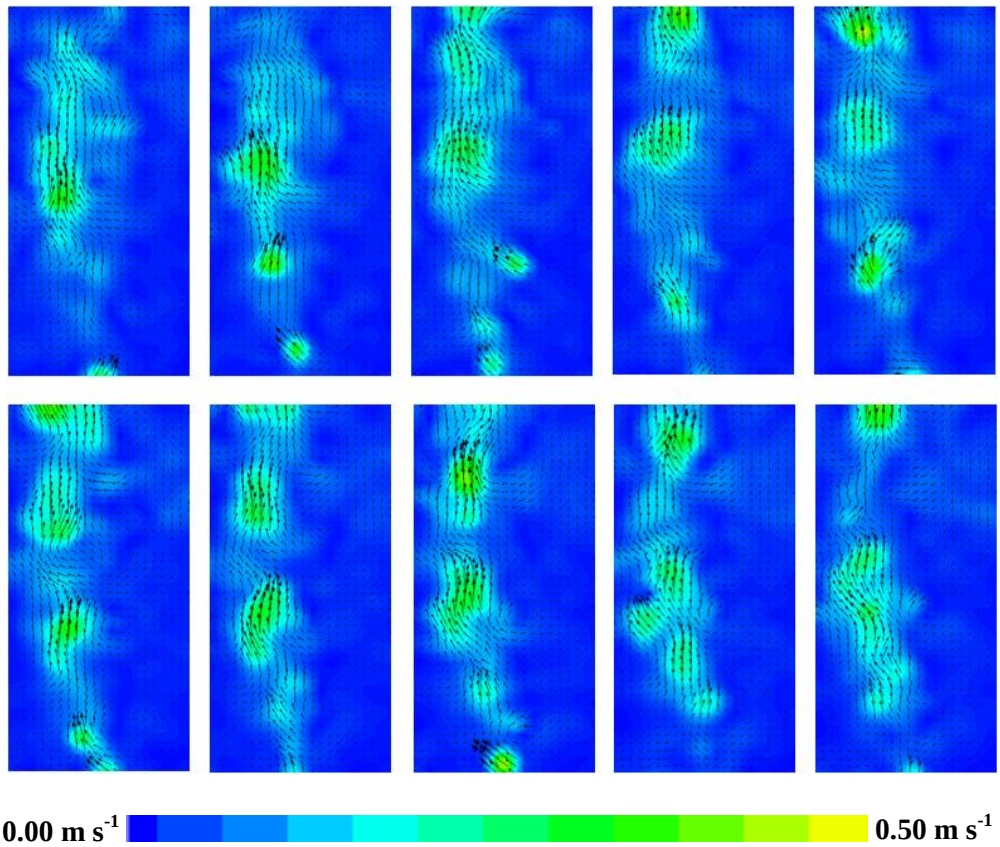

Fig. 4-6 Fluid flow visualization inside the PBR obtained in one of the PIV test cases which showed chaotic behavior with regards to the flow of bubbles.

4.3.3. Validation of the CFD model

In this study, the average velocity magnitude obtained from PIV and simulation data were visually and quantitatively compared (**Figs. 4-7 and 4-8; Table 4-4**). In **Fig. 4-7**, the PIV results was the average velocity magnitude obtained from 300

captured images in each test case which were post processed using Ensight 3G and Tecplot softwares. As shown in **Table 4-4**, the computed velocity magnitude obtained from CFD at 0.001, 0.003 and 0.005 mesh grid sizes is comparable to the computed average velocity magnitude obtained in PIV as highlighted in dotted square shape. The computed percentage differences of overall average velocity magnitude compared to PIV were approximately 5.31, 5.84, 6.77, 12.67, 21.83 and 29.31 % for 0.001, 0.003, 0.005, 0.007, 0.009 and 0.011 mesh grid interval sizes, respectively. Since air flow rate is the main catalyst of flow characteristics in the PBR, it is expected that as the air flow rate is increased, the average velocity magnitude will also increase. Furthermore, the percentage differences in velocity magnitude compared to PIV is observed to be increasing at higher flow rates. However, the percentage differences cannot be solely attributed to the flow rate but also to the mesh grid size used in the model as earlier discussed.

Presented in **Fig. 4.8** is percentage comparison of CFD computed average velocity magnitude according to mesh grid size to PIV at varied air flow rates. The percentage comparison obtained when the mesh grid size 0.007, 0.009 and 0.011 drastically decreased while mesh grid size of 0.005, 0.003 and 0.001 have displayed comparable values to PIV which is estimated at approximately 95 %. The difference is almost acceptable among simulation experts. Therefore, either of these 3 mesh grid sizes can be wisely chosen to be utilized in the succeeding simulation. However, considering calculation time in the simulation, and without sacrificing the accuracy of the result, a mesh grid size of 0.005 is a wiser choice. Furthermore, the percentage differences of the average velocity magnitude between

the PIV data and simulation result at varied air flow rates of 0.05, 0.10, 0.15 and 0.20 vvm using 0.005 mesh grid size are as follows: 4.05, 6.78, 7.09 and 9.18 % for. The percentage difference falls also below 10 % where it is also generally considered acceptable in computer modeling studies.

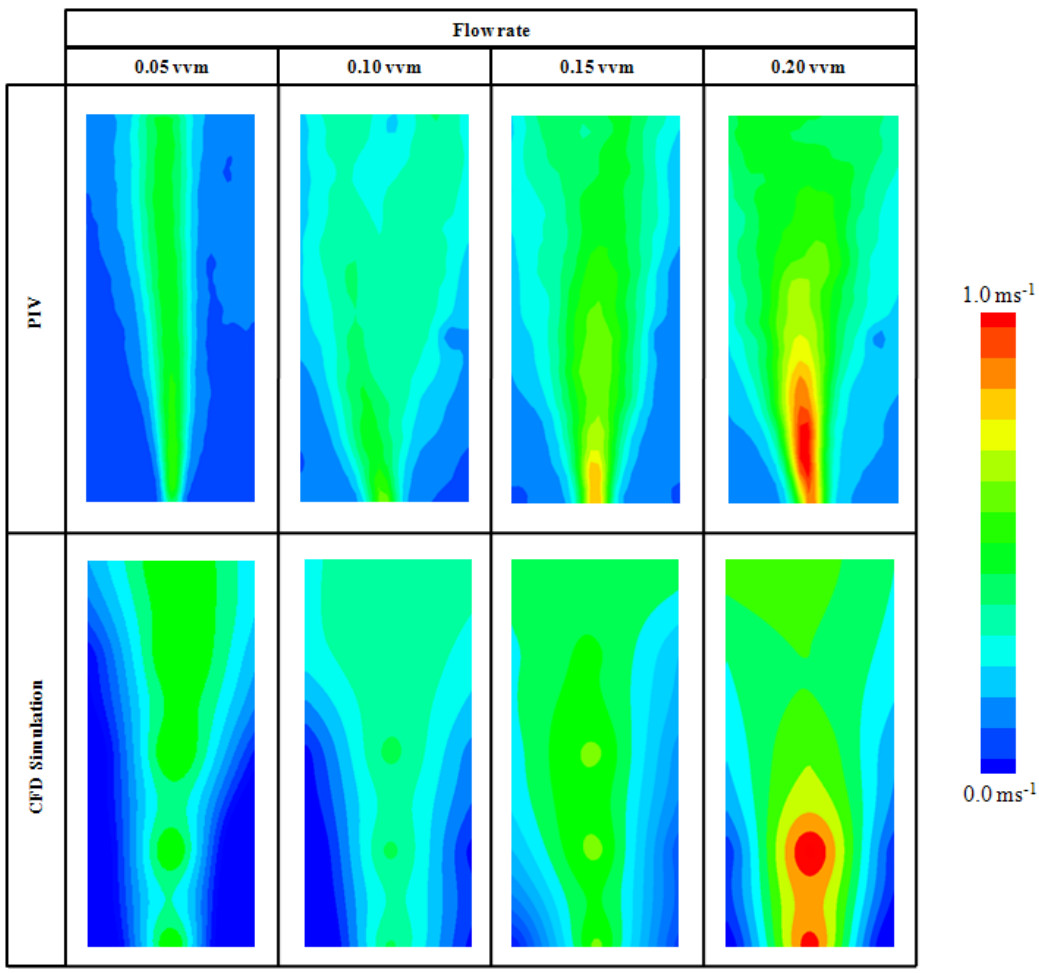

Fig. 4-7 Visual comparison of average velocity magnitude compared to PIV data at 0.005 mesh grid size interval.

Table 4-4 Comparison of average velocity magnitude computed from PIV and CFD simulation.

Flow rate, vvm	Computed average velocity, m s^{-1}						
	PIV	Simulation, Mesh interval size					
		0.001	0.003	0.005	0.007	0.009	0.011
0.05	0.154	0.157	0.159	0.159	0.173	0.178	0.181
0.10	0.185	0.188	0.189	0.190	0.206	0.216	0.226
0.15	0.257	0.268	0.275	0.278	0.294	0.325	0.336
0.20	0.325	0.331	0.334	0.348	0.366	0.415	0.448

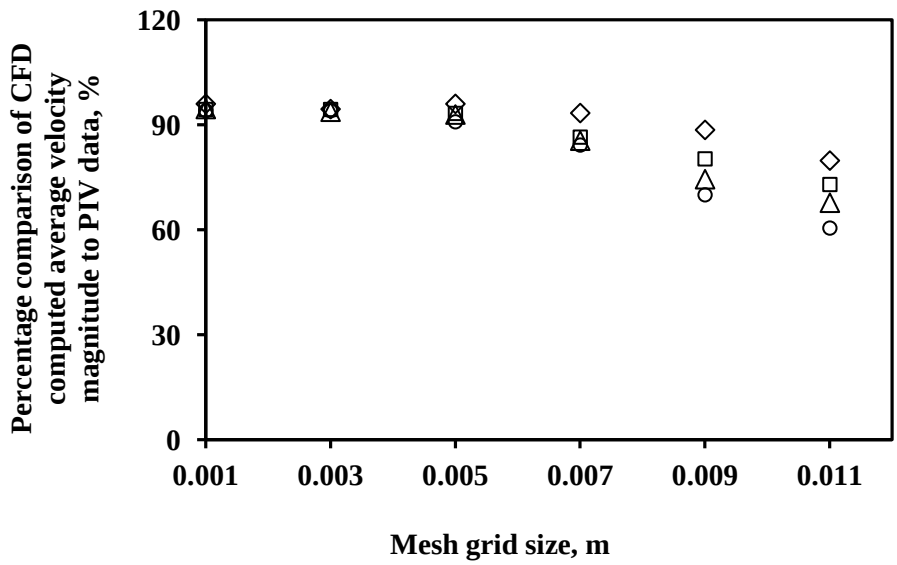

Fig. 4-8 Percentage comparison of CFD computed average velocity magnitude according to mesh grid size to PIV at varied air flow rates (Air flow rates, vvm: ◊ - 0.05, □ – 0.10, Δ - 0.15, ○- 0.20).

4.4. Conclusions

In this study, PIV was utilized to validate the CFD code used in simulation modeling of a 30 L PBR. There were 8 PIV test cases data which were accounted from 4 air flow rates and two experimental regions where PIV data were extracted. Based on the PIV extracted data which were post-processed using Ensight 3D and Tecplot computer softwares, the average velocity magnitude were obtained in all the cases. The computed average velocity magnitudes from each PIV case were compared quantitatively to the computed average velocity magnitude obtained in the simulation. The overall average velocity obtained from simulation varies based on the air flow rate and the mesh grid size that was implemented. Utilizing mesh grid sizes of 0.007, 0.009 and 0.011 in the simulation have shown higher computed average velocity magnitudes. However, using mesh grid sizes of 0.005, 0.003 and 0.001 have shown comparable results and similar with the computed PIV results. The percentage comparison of computed CFD average velocity magnitude to computed PIV for the three mesh sizes is estimated at approximately 95 % which is generally acceptable among modeling experts. Thus, either of the three mesh sizes can be selected and implemented in succeeding CFD simulations. However, considering calculation time but not sacrificing the simulation accuracy, 0.005 mesh grid size is preferable. Using a 0.005 mesh grid size, the percentage difference of PIV data and simulation results considering the four air flow rates used in the PIV test is within the acceptable simulation error which is not more than 10%. In addition, PIV technique has further demonstrated its applicability in validating simulation approaches such as CFD.

5. Numerical investigation and design of PBRs from three hydrodynamic evaluation parameters and light

5.1. Introduction

Bubble column photobioreactors (PBRs) which are efficient in growing photosynthetic cells have been receiving enormous attention in the past decade. These PBRs offers many advantages such as simplicity in the design with no moving parts, easy to construct and operate (Bitog *et al*., 2011). They have suitable heat and mass transfer characteristics and require less operational cost because of low energy input requirements. In engineering perspective, the structural configuration and design of the PBRs have critical role in the flow hydrodynamics which is also important in providing ideal growth conditions for the cells. Thus, hydrodynamics of bubble column PBRs of various geometries has been investigated both in the laboratory as well as through simulation studies (**Tables 5-1 and 5-2**). However, the current PBR designs still need to resolve many hydrodynamic issues within the PBR especially for the process of scaling-up. Many equally important factors should be considered such as light penetration and distribution, gas injection and mixing, the cell specie and the cells response to shear stress (Bitog *et al*., 2011, Michels *et al*., 2010, Perez *et al*., 2006). In culturing high density cells in PBRs, the main criteria are good mixing, mass transfer and light utilization (Chiu *et al*., 2009). These factors are closely interrelated such that the penetration and diffusion of light inside the PBRs is affected by the mixing

characteristics which are strongly influenced by the gas injection method (Bitog *et al*., 2011).

Mixing or movement of fluid inside the PBRs is one of the most important factors to be considered in PBR design. In bubble column PBRs, flow hydrodynamics is realized through bubbles which are usually introduced at the bottom section at the same time provides more time for mass transfer and CO_2 supply. The reactant gas itself provides the stirring action that is required to conduct gas-liquid and gas-liquid-solid interactions and reaction (Rampure *et al*., 2007). According to Barbosa et al., (2003) the movement of cells from the dark zone to the light zone of the PBRs is very important for the cells to experience light/dark cycles which was found to increase the cells productivity. Mixing characteristics especially for column PBRs are attained through the introduction of bubbles. Higher superficial gas velocity generated by air bubbles in PBRs would result to better mixing but would also increase the shear forces which have been long suspected to cause cell death.

Tramper *et al*. (1986) have distinguished three regions where the cells are likely to experience too much stress which may cause the death of cells. High shear stresses are suspected to occur at the sparger where the bubbles are formed, in the path where the bubbles rise, and at the surface where bubbles break-up (Tramper *et al*., 1986). Overcoming shear stress of microalgae cultures in sparged PBRs has been the focus of the study by Barbosa *et al*. (2003) and found out that bubble formation at the sparger was the main cause of cell death. Suzuki *et al*. (1995) reported an increase in death rate of microalgal cells for superficial gas velocity

values above 1.7 cm s^{-1}. However, a study conducted by Barbosa et al. (2003) has shown otherwise. They found out that superficial velocity up to 7.6 cm s^{-1} has no effect on growth of microalgae cell *D. tertiolecta* and the viability is above 94%. Higher superficial velocity was obtained for *C. reinhardtii* where a value of 8.4 cm s^{-1} was determined. The recommended superficial velocity in photobioreactors varies with microalgae specie as shown in **Table 5-3.** Thus an optimum superficial velocity which would create high degree of turbulence allowing a fast circulation of the cells at the same time not harmful to their growth should be desired.

Light cannot be considered as a common substrate for microalgae insofar as it involves two antagonist phenomena: on one hand, a high amount of photonic energy is required to ensure microalgae growth conditions, but on the other hand, the increase of the biomass concentration in the reactor decreases the light penetration depth in the culture due to cell self-shading (Loubiere *et al*., 2009). Thus, the use of light in the culture is the major constraint in PBRs, which makes their scale-up difficult and often limits the production of concentrated biomass with high quality and productivity. This makes light penetration in PBR design very crucial because illumination inside the PBR also influences the mass composition, growth rate, and product formation (Bitog *et al*., 2011). In dense culture, the gradient of light intensity is dependent on its wavelength, cell concentration, geometry of the PBR, and the penetration light distance (Fernandes *et al*., 2010). Therefore, the light intensity at a given point inside the PBR depends on the path length of light, cell concentration, and light absorption by the microalgae (Grima *et al*., 1994). Some data suggest that a single vertical tubular photobioreactor (bubble

column or airlift designs) cannot exceed about 20 cm in diameter or light availability will be severely reduced (Miron *et al*., 1999). In addition, the height of a single device is limited to about 40 cm for structural reasons and to reduce mutual shading of rectors in multi-column facility that would be necessary for any commercial scale operation (Miron *et al*., 1999).

Various reports have shown different growth of algae when cultivated in different growing conditions and the geometry of the PBR cannot be ignored. It is probably one of the critical factors to consider especially when scaling up is desired. In a study by Zusuki *et al*. (1995), they found a linear correlation between the specific death rate and the inverse of culture height. However, no explanation has been provided. Camacho *et al*. (2000) reported the inverse behavior: an increase in culture height caused an increase in death rate. The authors related the effect of fluid height to cell attachment of bubbles: a greater height of rise means that more cells can be captured by the rising bubbles and carried to the surface where cells die as the bubbles rupture. However, Barbosa *et al*. (2003) disputed the claim by stressing that bubble bursting is not the only factor and might not even be the most important factor leading to cell death. The authors have shown that the sparger site has a major effect on cell damage and the gas entrance velocity should be considered as a possible indication of cell death. However, more work is still needed to be done in order to clarify the influence of this parameter on cell death and its scalability as a reactor-design and scale-up tool for different microalgae strains (Barbosa *et al*., 2003).

Increasing the culture height also may cause longer cycle time which can even

decrease in photosynthetic efficiency (Janseen *et al*., 2001). In addition, fast circulation times have shown to give rise to considerable higher photosynthetic efficiency (Matthijs *et al*., 1996). Thus, the required growing conditions of photosynthetic cells in the height of bubble column PBRs are limited in scale. The PBR diameter is also limited to some extent, for instance, to ensure light penetration inside the PBR, the diameter should not exceed 20 cm or light availability will be severely reduced (Miron *et al*., 1999). However, until now, no standard PBR geometry or working volume is recommended in terms of mass production of photosynthetic cells such as algae. In addition, the fluid hydrodynamics inside the PBR is strongly influence by the geometry of the structure which directly affects the irradiance intensity and mixing conditions inside the PBRs, thus structure optimization is not only necessary, but also very critical (Yu *et al*., 2009).

Recently, numerical simulation approach has been applied elsewhere in investigating reactor designs which were always guided by the purpose of the production facility, the cell strain and product of interest. This method employed computational techniques to simulate large variety of engineering and physical systems. Specifically, the simulation approach attempts to imitate the hydrodynamic behavior of a system and predict the sequences of events that control that behavior (Oran and Boris, 2001). In PBR design and analysis, numerical simulation approach in studying fluid flow inside PBRs is now widely recognized among design engineers as an effective tool in predicting the complex inherent phenomena inside PBRs especially in cases where utilization of the

experimental approach is restricted by technical constraints (Bitog *et al*., 2011).

The flow hydrodynamics inside the PBR plays a very critical role in terms providing ideal growth environment for cells. The flow affects the gas holdup and volumetric mass transfer in the PBRs which are equally important to achieve sufficient CO_2 and nutrients for the cells. This becomes complex because the flow is affected by several factors such as the PBR size and design, gas flow velocity, etc. Numerical simulation studies have already attempted to investigate one or more of these factors. For instance, the gas hold-ups and volumetric mass transfer coefficients on a phenomenological model for bubble breakup and coalescence in column reactors were investigated by Shimizu *et al*., (2000) using CFD. They proposed a compartment model to describe the bubble movements. Their simulation study do not provide a complete description of bubble behaviors, however, it gives significant insights of the phenomena in bubble column reactors. A similar study was conducted by Baten and Krishna (2002) where CFD was utilized to investigate bubble characteristics inside a bubble column PBR under homogenous and heterogeneous regimes. Their results have revealed that in the heterogeneous flow regimes, the large bubbles are found to concentrate in the central core of the bubble column, while the small bubbles are distributed throughout the column. The small bubble holdup is also found to be constant in the heterogeneous flow regime. A follow-up study was conducted by Baten *et al*., (2003) where the hydrodynamics of internal air-lift reactors was investigated and experimental results versus CFD simulations were compared. They have developed a scaling up model from the results however only applicable in air-lift reactors. In

their scaled-up model, there was a significant reduction in the gas holdup due to significantly higher liquid recirculation. However, the authors stressed the need for experimental verification especially when scaling up is involved. Yamashita and Suzuki (2006) studied gas holdup inside the PBR which is a very important parameter for design and scale up of bubble columns PBRs. Their CFD investigation showed that gas holdup depends on many factors such as gas and liquid velocity, physical property of gas and liquid, type and arrangement of gas spargers, gas inlet height and inclination of bubble columns. Drag force on bubbles in bubble swarms was investigated by Roghair *et al.*, (2009) and focused their study on the effect of the presence of neighboring bubbles on the drag as a function of the void fraction. They found out that the normalized drag coefficient increases for higher void fractions. Furthermore, their study recommended that the effects of preferential horizontal alignment on averaged drag experienced by the bubbles should be taken into account explicitly in drag closure correlations.

These research results provided profound understanding of the complex flow characteristics in the PBRs. However, despite these research attempts, simulation results which can be applied in designing a PBR suited for mass production of microalgae is still limited. In this study, numerical simulation using CFD technique was implemented to investigate hydrodynamics characteristics in cylindrical bubble column 30 L PBRs. The CFD code and simulation approaches were initially conducted using PIV and discussed in Chapter 4 and the results were also utilized in improving the succeeding simulation models. The flow hydrodynamics as affected by various air flow rates, various nozzle size diameters and the effect of

additional internal baffle were thoroughly investigated. The hydrodynamic measuring parameters used in the investigation of PBRs were the volume percentage of dead zones, average circulation time and turbulence intensity. The three hydrodynamic parameters combined with the estimated light were used to select the appropriate PBRs for actual cultivation of microalgae. The recommended operating parameters such as air flow rate and nozzle size diameter that is appropriate for the 30 L PBR was determined. The effect of PBR design parameter by adding internal baffle with modified PBR bottom geometry in terms of hydrodynamic the parameters was also thoroughly quantified.

Table 5-1 A summary list of typical bubble column PBRs.

Type	Culture volume	Focus of the study	Reference /Year
Cylindrical column Rectangular column	20L	Comparison of Multi-phase models, Validation of CFD code from PIV data	Seo *et al*., 2012
Cylindrical column	21 L	Mass transfer and shear, Mathematical model to improve reactor design and performance	Bannari *et al*., 2011
Cylindrical column with centric tube and porous centric tube	4 L	Laboratory study on flow patterning high-density cultures of microalgae and carbon dioxide removal	Chui *et al*., 2009
Square type column	10 L, W: 15, D: 15, H: 45	Eulerian-Eulerian modeling of flow, mass transfer and chemical reaction	Zhang *et al*., 2009
Rectangular column	15 L, W: 25, D:15, H: 40	Optimization of inner structure parameters	Yu *et al*., 2009
Cylindrical column with centric tube	20 L	Local characteristics of hydrodynamics in the reactor	Lou and Al-Dahhan, 2008
Rectangular column	8L, W: 4, D: 20, H: 100	Simulation on drag force formulation	Simonet *et al*., 2008
Rectangular column	12 L, W: 20, D: 5 H: 120	Modeling of two-phase flow using class method of population balance	Bannari *et al*., 2008

(L: liters, R: radius, W: width, D: depth, H: height, unit dimension are in cm)

Table 5-2 A summary list of typical bubble column PBRs (Cont.).

Type	Culture volume	Focus of the study	Reference /Year
Cylindrical column	30 L, R: 10, H: 100	Application of volume of fluid (VOF) model and study on the effect of air distributor and validated with laboratory experiment on superficial gas velocity	Akhtar *et al*., 2007
Cylindrical column	63 L, R: 10, H: 200	CFD and Laboratory study on the effect of high gas velocity	Rampure *et al*., 2007
Cylindrical column	60L, R: 9.6, H: 205	Mixing as a new approach to characterize dispersion coefficients	Rubio *et al*., 2004
Cylindrical column	35 L, R: 7.5, H: 200	CFD analysis of flow validated with laboratory experiment	Baten *et al*., 2003
Cylindrical column	13 L, R: 6.5, H: 100	Simulation of algal growth	Wu and Merchuk, 2002
Cylindrical column	24 L, R: 8, H: 120	Validation of a transient, two-dimensional axisymmetric simulation	Sanyal *et al*., 1999
Rectangular column	4.5 L, W: 20, D: 5, H: 45	Simulation using Eulerian-Eulerian modeling approach	Pfleger *et al*., 1999
Square type column	26 L, W: 17.5, D: 17.5, H: 84	Effect of the aspect ratio on of the bubble column on flow pattern	Delnoij *et al*., 1999

(L: liters, R: radius, W: width, D: depth, H: height, unit dimension are in cm)

Table 5-3 Recommended superficial velocity of some microalgae specie.

Specie	Maximum superficial velocity ($cm\ s^{-1}$)	Reference
Anabaena variabilis	2.0	Yoon *et al*., 2008
Haematococcus pluvalis	0.04	Powtongsook *et al*., 2006
C. reinhardtii	8.4	Barbosa *et al*., 2003
D. tertiolecta	7.6	Barbosa *et al*., 2003
Phaeodactylum tricornutum	5.0	Camacho *et al*., 2001
Phorphyridium sp.	0.54~0.82	Merchuk *et al*., 2000
Dunaleilla tertiolecta	1.7	Zusuki *et al*., 1995

5.2. Materials and methods

5.2.1. Computational fluid dynamics

The application of computational fluid dynamics (CFD) in the design photobioreactors has been rapidly advancing and was thoroughly reviewed in Chapter 2. Direct measurements are probably the best way to understand the behavior of flow and pollutant load but they cannot be made before the PBR has been built. Computational fluid dynamics (CFD) offers an alternative way to give the design engineer predictions about this behavior. CFD is now regarded as a

powerful tool to study and analyze fluid flows. This tool uses computers and numerical techniques to solve problems involving the movement of fluids. Using CFD, a computational model that represents a system or a device can be built, and by applying fluid flow physics and chemistry to this virtual prototype, a prediction of the fluid dynamics and the related physical phenomena can be determined (Bitog *et al*., 2011). Bubble column and air-lift PBRs have been simulated and analyzed in terms of flow characteristics, energy and mass transfer, light penetration and distribution, etc using CFD technique. The continuous developments of CFD and the availability of more powerful and affordable personal computers have paved the way for modeling and designing PBRs based on their purpose. This has been observed in the past decade where rapid increases in simulation studies on PBRs were conducted.

The practice of designing PBRs using CFD gave in-depth understanding of the hydrodynamics/flow pattern in the PBRs which the key for design and scale up. In our review paper (Bitog *et al*., 2011), the power of CFD as a tool in predicting complex inherent phenomena in the PBRs, especially in those cases where utilization of experimental approach is restricted by technical constraints have been presented. Today, CFD is now widely accepted as a powerful technique in the design of PBRs; however, its application is still on the process of development to consider all complex factors involved in the growth of microalgae inside the PBRs. More details on the application of CFD for modeling and designing PBRs for microalgae production can be found in Bitog *et al*., (2011).

Validation is very critical in field of modeling and simulation studies. For

instance, in CFD, this is to establish the accuracy of the codes used such as to create credibility and confidence in the results and can be used in making conclusions and decisions. Generally, this is done by comparing the simulation results with physical reality by conducting laboratory or field experiments. In this particular study, PIV experiment was already conducted and discussed earlier in Chapter 4.

After establishing the validity of the CFD code being implemented, simulations of the PBR with and without baffle at varied nozzle diameters of 5, 10, 15 and 20 mm and air flow rates of 0.05 0.1, 0.15 and 0.2 vvm were conducted. The evaluation parameters employed to evaluate the hydrodynamic performance of the PBRs were the volume percentages of dead zones, average circulation time and turbulence intensity. The simulation results were carefully analyzed on the concept of providing a good hydrodynamic environment for the microalgae cells to grow. Based on the hydrodynamic parameters used to evaluate the PBRs, a PBR simulation case was chosen with the appropriate flow rate and nozzle size diameter and utilized in the actual cultivation of microalgae.

The 30 L cylindrical bubble column PBRs were designed using Gambit software (ver. 2.2, Lebanon, N.H., Fluent, Inc.), a pre-processing tool perfectly suited for the Fluent program. The calculations were performed by Fluent program (ver. 6.2, Lebanon, N.H., Fluent, Inc.) and also post-processes the results. The Eulerian-Lagrangian multiphase model was utilized in the study. This model has been widely used especially for modeling gas-liquid or liquid-liquid flows. Furthermore, it is applicable even for wide range of volume fractions and

turbulence model is automatically included. More detail information on multiphase models are available elsewhere in the literature. The data and values employed in the simulation are presented in **Table 5-4**. The RNG *k-ε* turbulence model was employed with dispersed characteristics. The RNG-based *k-ε* turbulence model is derived from the instantaneous Navier-Stokes equations, using a mathematical technique called ``renormalization group" (RNG) methods. The analytical derivation results in a model with constants different from those in the standard *k-ε* model, and additional terms and functions in the transport equations for *k* and *ε*. (Fluent manual, 2006). A more comprehensive description of RNG theory and its application to turbulence can be found in Choudhury (1993). This turbulence model has been used in similar PBR simulations such as Sanyal *et al*., 1999; Perner *et al.* 2003; Akhtar *et al*. (2007); Trujilio *et al*. (2007). To realize bubble rising, the bubble size diameter was pegged at 0.005 m which is the same with the minimum mesh grid size implemented in the mesh design.

The main factors investigated in the PBR design were as follows: 1) Air flow rate with 4 sub-factors, 2) Nozzle size diameter with 4 sub-factors and 3) PBR geometries with 2 sub-factors. This totaled to 4 x 4 x 2 = 32 simulation cases. The air flow rates considered were 0.05, 0.10, 0.15 and 0.20 vvm while the nozzle diameters were 5, 10, 15 and 20 mm. In implementing the simulation of the PBRs, the air inlet velocity was varied according to the simulation cases based particularly from the air flow rates and nozzle size diameters as presented in **Table 5-5**. The 2 sub-factors of PBR geometry is comprised of with and without internal baffle. In addition with the PBRs with internal baffle, the bottom part geometry was also

designed to be protruding with a vertical cone-shaped structure. The PBR design models without baffle and PBR with baffle and protruded bottom design is presented in **Fig. 5-1**.

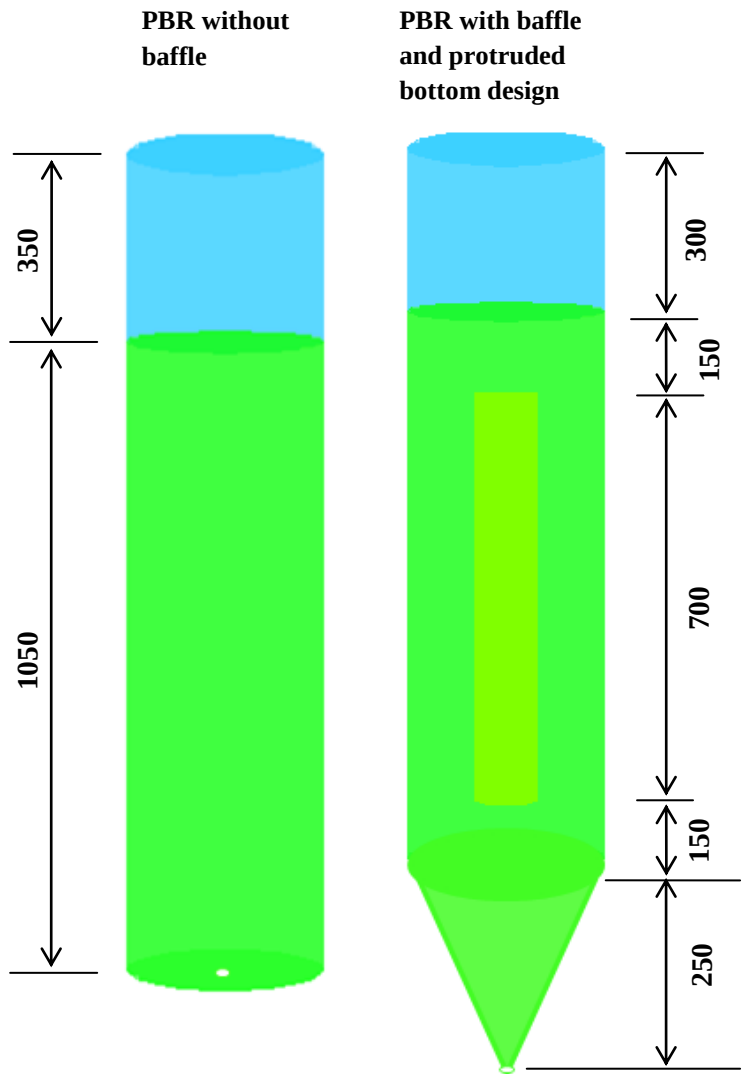

Fig. 5-1 The 30 L PBR design models investigated in the study in terms of their flow hydrodynamics (Dimensions in mm).

Table 5-4 Data and variables implemented in the simulations.

Pre-processing (Gambit software)	PBR without baffle	Inner diameter	185 mm
		Height of water zone	1150 mm
		Height of air zone	250 mm
		Total number of mesh	500428
	PBR with baffle	Inner diameter	185 mm
		Height of water zone	1032 mm
		Height of air zone	218 mm
		Height of injection zone (cone-shaped)	250 mm
		Total number of mesh	622500
Main Module (Fluent program)		Solver	Pressure based (implicit)
		Multiphase model	Eulerian-Lagrangian
		Phases	Water (primary), Air (secondary)
		Specified operating density	1.225 kg m^{-3}
		Turbulence	RNG k-ε turbulence model (dispersed)
		Near-wall treatment	Standard wall functions
		Discretization	Second order upwind
		Conditions	Unsteady state
		Bubble size	0.005 m
		Time interval	0.01s

Table 5-5 Air inlet velocity implemented in the simulation of the PBRs.

Air flow rate, vvm	**Inlet velocity implemented in the simulation, m s^{-1}** (based from air flow rate and nozzle size diameter)			
	5 mm nozzle	**10 mm nozzle**	**15 mm nozzle**	**20 mm nozzle**
0.05	1.27	0.32	0.14	0.08
0.10	2.55	0.64	0.28	0.16
0.15	3.82	0.95	0.42	0.24
0.20	5.09	1.27	0.57	0.32

5.2.2. Hydrodynamic parameters used to evaluate the PBRs

The PBRs were evaluated in terms of the volume percentages of dead zones, average circulation time and the turbulence intensity. Dead zones as defined by Yu *et al.* (2009) are the zones in which liquid velocity is below 1.0×10^{-3} m s^{-1}. The percentages of dead zones in the PBR were quantified comparing the 32 simulation cases. The regions where there exist some dead zones could provide information and suggest some measures to be done to eliminate these zones. The presence of dead zones caused settling of cells which would result to cell deterioration, anaerobic decomposition and the quality of the product (Suh and Lee, 2003).

The average circulation time refers in this study is the average travel time it takes for the particles to travel from the bottom of the PBR to the water-air interface and back. The average circulation can be determined by introducing particle cells at the bottom of the PBRs and monitored to determine their locations as they move vertically to the water-air interface and back. The cells were appropriately assumed to be mass-less and volume-less particle and treated as passive particulate tracer in the continuous phase, because the size of the microalgae is very small, i.e about 0×10^{-5} to 0×10^{-6} m (Sato *et al*., 2010). In this manner, Sato *et al.* (2010) pointed out that the cells are transported even for small eddies in the spatial scale smaller than the mesh. Therefore, to account this phenomenon, a random walk tracking model was implemented (Fluent Manual, 2006). Considering bubble column PBRs where air, CO_2 and other nutrient are usually introduced at the bottom, a faster travel time would be preferable to maximize mass transfer rate. If in case enough nutrition is supplied to the PBRs,

both the CO_2 fixation rate and O_2 evolution rate will only depend mainly on the gas bubble travel time and the gas liquid mass transfer rate (Fan *et al*., 2007). Furthermore, faster circulation can imply shorter cycle time and thus can result to faster mixing. This can also result to higher photosynthetic efficiency (Janseen *et al*., 2001; Matthijs *et al*., 1996).

Basically, turbulence intensity measures the ratio of the root-mean-square of the velocity fluctuations to the mean free stream velocity. Turbulence has been proven to be advantageous to cells because it causes continuous shift in the relative position of the cells with respect to the photic zones which relates to the flashing light effect (Terry 1986). However, too much turbulence can be very detrimental to cells which can result not only into restrictions to the algal growth and metabolic activity but up to cell death. The three main zones inside the PBR where shear stress to cells occur leading to their death due to very high turbulence as identified by Tramper *et al*. (1986) were investigated in terms of their turbulence. These zones were previously investigated by Camacho (2000), Barbosa *et al*. (2003) and Zhong and Yuan (2009) through laboratory experiments. The results obtained by Camacho (2000) found out that more cell deaths happen at the water-air interface zones. Zhong and Yuan (2009) also reported that similar results with Camacho (2000), however, this was earlier disputed by Barbosa *et al*. (2003) who found out that mostly cell death takes place at the injection zone, but, the effect of bubble size on cell death has never been related to bubble formation at the sparger. Such conflicting results from previous studies will be investigated from the CFD results obtained in all the simulated cases.

5.2.3. The Discrete-Phase model (DPM)

The quantitative data used to investigate the hydrodynamic parameters inside the PBRs particularly using dead zones and turbulence intensity can be obtained after post-processing the simulation results. However, to obtain quantitative data to for circulation times, additional model must be included in the simulation such as the Discrete-Phase model (DPM).

FLUENT DPM is one of the commercial software packages available for CFD. It contains the broad physical modeling capabilities needed to model flow, turbulence, heat transfer, and reactions for industrial applications including bubble column reactors. As discussed by Robinson *et al*. (2007), DPM uses the Lagrangian solution technique to predict the trajectory of discrete phase particles. The particle trajectory equation can either be solved with the momentum and energy equation for the continuum flow (coupled) or after the momentum and energy have converged (uncoupled). The coupled option allows particles to interact with the flow fluid and affect the flow solution.

The particle tracking explores capability of CFD programs to predict trajectories of dispersed phase particles (the particles must have the same properties, e.g. density, as the continuous phase). The trajectories and residence times are integrated on the basis of known velocity field of continuous phase (Lagrangian method). This approach is straightforward in laminar (convective) flows, on contrary to turbulent flows, where random fluctuations of velocities must be superposed to the mean velocity of continuous phase (discrete or continuous

random walk models). The particle trajectories are calculated by integrating the force balance equation shown in Eq. (5-1) (Fluent Inc, 2006).

$$\frac{dV_p}{dt} = \frac{18\mu}{d_p^2 \rho_p C_c}\left(V - V_p\right) + \frac{g_x\left(\rho_p - \rho\right)}{\rho_p} + F_x \qquad (5\text{-}1)$$

The sedimentation deposition efficiency is governed by the first and second terms on the right-hand side of Eq. (5-1), which are, respectively, Stokes drag force per unit mass and buoyancy force per unit mass. The buoyancy force accounts for the difference between the fluid density and the particle density. Diffusion deposition efficiency is governed by Brownian motion treated as random external forces, modeled as a Gaussian white noise process with amplitudes defined in Eq. (5-2). The equation was derived in Li and Ahmadi (1992) for turbulent channel flows as presented by Robinson *et al*. (2007). Deposition is determined by summing up the "trapped" fate particles. Particles are considered trapped when their center of mass (center point) touches the wall. Fluent also reports the number of incomplete, aborted, evaporated, or unable to be tracked particles. In most circumstances, these numbers can be minimized by adjusting various input parameters (Robinson *et al*. 2007).

$$F_{x,diff} = \xi_{ij} \sqrt{\frac{21.6\nu\sigma T}{\Delta t \pi \rho d_p^2 \left(\frac{\rho_p}{\rho}\right)^2 C_c}} \qquad (5\text{-}2)$$

The boundary conditions to be set up for the particles can be simulated when a particle strikes a boundary face as follows (Fluent manual, 2006): 1. The particle

may be reflected via an elastic or inelastic condition; 2. The particle may escape through the boundary where the particle is lost from the calculation at the point where it impacts the boundary; 3. The particle may be trapped at the wall and Nonvolatile material is lost from the calculation at the point of impact with the boundary then volatile material present in the particle or droplet is released to the vapor phase at this point; 4. The particle may pass through an internal boundary zone, such as radiator or porous jump; 5. The particle may slide along the wall, depending on particle properties and impact angle. Another option is also available which can be implemented to model the particle behavior when hitting a boundary using a user-defined function of the Fluent program.

There are two different models for turbulent dispersion of particles: the stochastic tracking model and the particle cloud model. Dispersion of particles in a turbulent flow is due to turbulent fluctuations. This turbulent dispersion is very important to be included in the model to provide a degree of physical realism even if it added some computational expense. Furthermore, from a numerical standpoint, including turbulent dispersion enhances stability by smoothing out source terms and eliminating local spikes in the coupling between the discrete phase and the gas phase. The DPM model has associated with it a finite number of injections for any mass loading that will be introduced into the simulation model. Therefore, each individual injection do not represent an individual particle but an individual mass loading, divided equally amongst N number of tracks. If turbulent dispersion was not included in the model, at a given individual injection that has associated with it some finite mass loading, every single particle that is represented by that finite

injection or finite loading follows the exact same path which is not physically realistic. In a turbulent flow if particles are injected from the same position with the same initial conditions, it is expected that the cells would take different paths. However, this will not be realized if turbulent dispersion is not included. This explains the importance of considering turbulent dispersion in the model because it gives a level of physical realism and because it allows smoothing out or distributing the sources in a more realistic manner which is also easier for the solver to deal with. Therefore, instead of having all the mass follow in a single path, more injections or tracts is encouraged where the mass follows a slightly different path that can allow source terms to be distributed.

FLUENT DPM was utilized to simulate the movement of the cells as they travel around, and up and down the PBR. Particle injections can be defined by a text file specifying particle properties, position, and initial velocity. Particles should not be injected in the first element within the flow field because of occasional issues with the grid resolution n in the first plane of elements that can interfere with particle injection. Additionally, it is recommended that particles not be injected any closer than one element from walls to avoid artifactual immediate deposition (Robinson *et al*., 2007). During the simulation, assuming that the cells do not multiply in number in a 10 minutes time, using a 0.001 time step size, the number of time step is therefore pegged at 600,000.

To quantify the circulation time in the PBRs, the movement of the cell inside the PBR should be known. The cells can be appropriately assumed to be mass-less and volume-less particle and can be treated as passive particulate tracer in the

continuous phase, because the size of the microalgae is very small, about 0 x 10^{-5} to 0 x 10^{-6} m (Sato *et al*., 2010). As earlier discussed by Sato *et al*., (2010), the cells are transported even for small eddies in the spatial scale smaller than the mesh. Therefore, to account this phenomenon, a random walk model was adopted in this study where the position of the cell can be calculated using Eq. (5-3) also proposed by Sato et al. (2010).

$$x_p^{n+1} = x_p^n + U_p \Delta t + i\sqrt{2 v_t \Delta t x} \qquad (5\text{-}3)$$

When the cells hit the wall boundaries of the PBRs, the particle is expected to rebound (**Fig. 5-2**) with a change in its momentum as defined by the coefficient of restitution presented in Eq. (5-4) where V_n is the particle velocity normal to the wall and the subscript 1 and 2 refer to before and after collision, respectively. Similarly, the tangential coefficient of restitution, e_t, defines the amount of momentum in the direction tangential to the wall that is retained by the particle. A normal or tangential coefficient of restitution equal to 1 was employed in this study which implies that the particle retained all of its normal or tangential momentum after the rebound (an elastic collision). The normal coefficient of restitution defines the amount of momentum in the direction normal to the wall that is retained by the particle after the collision with the boundary.

$$\text{Coefficient of restitution} = \frac{V_{2,n}}{V_{1,n}} \qquad (5\text{-}4)$$

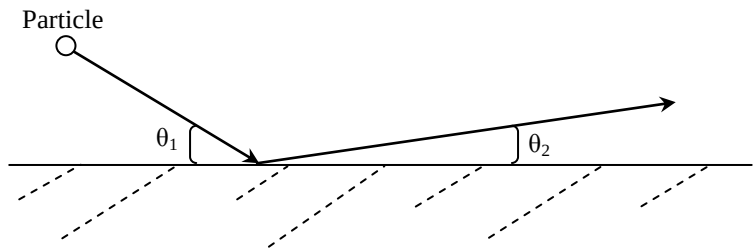

Fig. 5-2 Schematic diagram of the characteristics of CFD simulated particles as they hit a certain boundary inside the PBR.

5.2.4. Predicting light intensity in the PBRs

Light intensity inside the PBRs cannot be ignored being one of the major growth factors which can be estimated based from the distance of the injected particles to the walls. Assuming a uniform supply of light into the PBRs, an estimate of the illumination experience of an algal cell can be determined from Lambert-Beer Law (Eq. 5-5) proposed earlier by Lou and Al-Dahhan (2003). The model assumes that external light intensity is uniform along the cylindrical walls of the PBR. Therefore, at a given radial distance from the wall, the light intensities received by the cell particles can be estimated. Aside from the hydrodynamic evaluation parameters to evaluate the 32 investigated cases, cases with estimated high light intensity is desirable.

$$I = I_E \exp\left[-(k_x . X + k_w)d\right] \qquad (5\text{-}5)$$

5.3. Results and discussion

5.3.1. Realizing PBR design

Creating the PBR geometry using the Gambit software (ver. 2.2, Lebanon, N.H., Fluent, Inc.) especially for the typical bubble column design can be immediately realized because of its simple design which is just a single vertical column. However, the PBR structure with internal baffle and protruded bottom cone-shaped geometry is somewhat challenging. Especially for the meshing part in the bottom geometry wherein several approaches were attempted to realize acceptable mesh quality when checked using equiangle skewness value and should be in ranged from 0.25 ~ 0.50 the same with the typical bubble column which is considered good (Fluent manual, 2006; Baker, 2002). The mesh design geometry of the PBRs were realized by dividing the PBR to 4 sub-parts such as: 1) the injection zone or the protruded geometry, 2) the internal baffle, 3) the main column which is now become hollow because the internal baffle is not included, and 4) the upper part which comprises the air zone. This approach can allow comfortable meshing and acceptable mesh quality can be achieved. In the end, the mesh geometry of PBR with internal baffle and protruded bottom cone-shaped design was realized with pyramid and mostly hexahedron meshes. Presented in **Fig. 5-3** is the mesh design of the PBR with internal baffle and protruded cone-shaped bottom geometry.

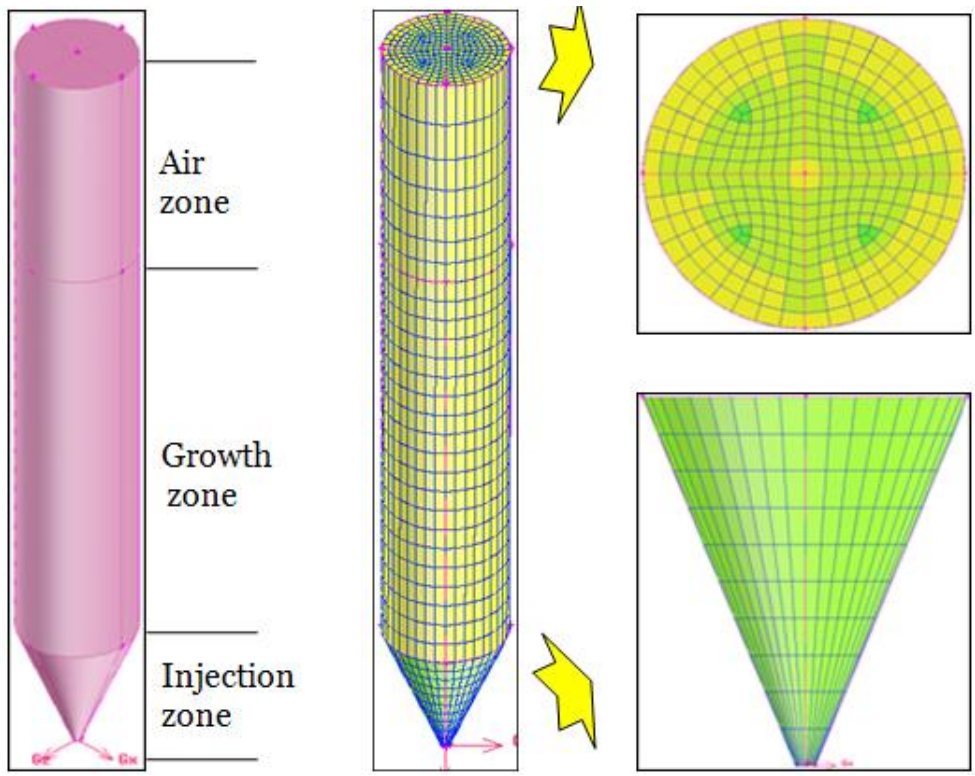

Fig. 5-3 The mesh design of the 30L PBR with internal baffle and protruded bottom cone-shaped geometry pre-processed using Gambit software.

5.3.2. Percentage of dead zones inside the PBRs

The quantitative results of the volume percentage of dead zones from the 32 simulated CFD multiphase models were presented in **Table 5-6**. In terms of the percentages of dead zones inside the PBRs, the case with the smallest volume percentage was observed in case $A_4B_1C_2$ with 2.87 % while the highest was observed in case $A_1B_4C_1$ with 42.51 %. The effect of baffle and cone-shaped geometry can be easily recognized to decrease the percentages of dead zones in the

PBRs. Regardless of air flow rate and nozzle size diameter, the average percentage of dead zones of PBRs without baffle and the PBRs with internal baffle is estimated to be 17.25 and 11.35 %, respectively while the highest reduction of the percentage of dead zones from the PBRs without baffle to PBRs with internal baffle is approximately 10 %. Considering also the effect of air flow rate only regardless of nozzle size diameter and PBR geometry, the percentages of dead zones were observed to be decreasing from 22.44, 14.21, 11.35 and 9.20 % at air flow rates of 0.05, 0.10, 0.15 and 0.20 vvm. However, if the effect of nozzle size diameter is considered, an increasing trend is observed with percentage of dead zones was estimated to be 4.55, 9.13, 18.02 and 25.45 % when the nozzle diameter is increased from 5, 10, 15 and 20 cm, respectively. The various results obtained in all the simulated cases have suggested that the factors of air flow rates, nozzle size diameters and PBR geometry have significant effect on the volume percentages of dead zones within the PBR. Particularly for air flow rate and nozzle diameter, where the inlet velocity was based in computing the air velocity and was used as boundary condition in the inlet velocity field, a decreasing trend on the volume percentages of dead zones is observed following the power-law ($y = 5.3652x^{-0.695}$) with R^2 value of 0.9451 as shown in **Fig. 5-4**. The graph was extracted from the volume percentages of dead zones in cases of PBRs with internal baffle only. However, similar trend is also observed for cases of PBRs without internal baffle.

Furthermore, simulation results have revealed that most of the dead zones are located at the bottom part and near the walls particularly for the PBRs without internal baffle while for the PBRs with baffle and cone-shaped bottom design, the

dead zones can be seen at the outer surface of the inner baffle, however, minimal. This strongly suggests that the cone-shaped bottom of the upgraded PBR have eliminated the dead zones particularly at the bottom and injection regions of the PBRs.

Table 5-6 Volume percentages of dead zones of the 32 CFD simulated cases.

Case	Volume percentage of dead zones, %	Case	Volume percentage of dead zones, %
$\mathbf{A_1B_1C_1}$	8.21	$\mathbf{A_3B_1C_1}$	6.61
$\mathbf{A_1B_1C_2}$	3.66	$\mathbf{A_3B_1C_2}$	3.12
$\mathbf{A_1B_2C_1}$	18.86	$\mathbf{A_3B_2C_1}$	6.31
$\mathbf{A_1B_2C_2}$	11.41	$\mathbf{A_3B_2C_2}$	4.18
$\mathbf{A_1B_3C_1}$	34.58	$\mathbf{A_3B_3C_1}$	14.88
$\mathbf{A_1B_3C_2}$	26.61	$\mathbf{A_3B_3C_2}$	9.51
$\mathbf{A_1B_4C_1}$	42.51	$\mathbf{A_3B_4C_1}$	26.66
$\mathbf{A_1B_4C_2}$	33.67	$\mathbf{A_3B_4C_2}$	18.85
$\mathbf{A_2B_1C_1}$	7.08	$\mathbf{A_4B_1C_1}$	5.24
$\mathbf{A_2B_1C_2}$	3.12	$\mathbf{A_4B_1C_2}$	2.87
$\mathbf{A_2B_2C_1}$	11.01	$\mathbf{A_4B_2C_1}$	9.51
$\mathbf{A_2B_2C_2}$	4.87	$\mathbf{A_4B_2C_2}$	4.65
$\mathbf{A_2B_3C_1}$	22.21	$\mathbf{A_4B_3C_1}$	13.67
$\mathbf{A_2B_3C_2}$	14.61	$\mathbf{A_4B_3C_2}$	8.11
$\mathbf{A_2B_4C_1}$	29.81	$\mathbf{A_4B_4C_1}$	20.08
$\mathbf{A_2B_4C_2}$	20.67	$\mathbf{A_4B_4C_2}$	11.66

A: Air flow rates of 0.05, 0.10, 0.15 and 0.20 vvm which corresponds to A_1, A_2, A_3 and A_4, respectively.
B: Nozzle size diameter of 5, 10, 15 and 20 mm which corresponds to B_1, B_2, B_3 and B_4, respectively.
C: PBR geometry design without baffle and with baffle which corresponds to C_1 and C_2, respectively.

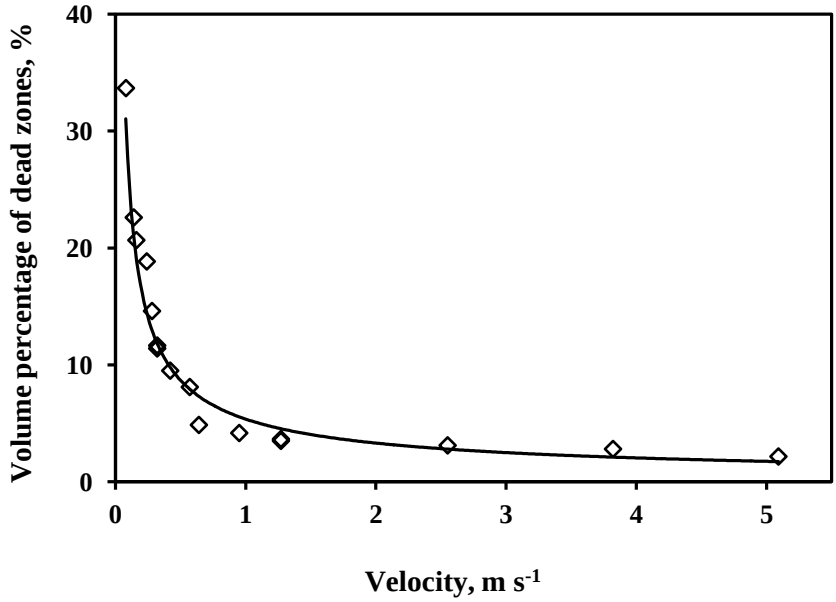

Fig. 5-4 Effect of inlet velocity used as boundary condition in the simulation in terms of the volume percentage of dead zones inside the PBRs with internal baffle.

5.3.3. Average circulation time in the PBRs

The average circulation time for the particles to travel from the bottom of the PBR to the water-air interface and back is also summarized (**Table 5-7)**. These were obtained by introducing particle cells at the bottom of the PBRs and were monitored to determine their locations as they move vertically from the bottom of the PBR to the water-air interface and back. The shortest average circulation time comparing all the simulated cases was observed in case $A_4B_1C_2$ with approximately 8.05 s. This case has also the lowest percentages of dead zones as earlier observed. The longest circulation was observed in case $A_1B_4C_1$ with approximately 26.89 s. As a representative example, the movement of the cell particles inside the PBR of

the case with the shortest average circulation time ($A_4B_1C_2$) is shown in **Fig. 5-5**.

General observation revealed that the value of average circulation time is directly influenced by the set flow rate similar to the observations made in the volume percentages of dead zones. This trend is presented in **Fig. 5-6**. As set flow rate is increased, the distribution of the computed average circulation time tends to decrease following a power-law equation ($y = 10.195x^{-0.259}$) with R^2 value of 0.7428. Further analysis of the results have revealed that with the same flow rate and nozzle size diameter, the average circulation time of PBRs with baffle is always lower by an average of about 5.5 s when compared with the PBRs without baffle. Regardless of nozzle size diameter and PBR geometry, the average circulation time were estimated at 19.10, 15.63, 14.60 and 13.70 s for 0.05, 0.10, 0.15 and 0.20 vvm. This shows that except for the air flow rate of 0.05 vvm, the average circulation time obtained at air flow rates of 0.10, 0.15 and 0.20 vvm are almost comparable. At varied nozzle size diameter regardless of the geometry and air flow rates, the average circulation time was 11.52, 13.63, 17.81 and 20.07 s, for a nozzle size diameter of 5, 10, 15 and 20 mm, respectively. This can imply that nozzle size diameter plays a significant role in terms of circulation times in the PBRs. This is expected since the air velocity input value used in the simulation depends on the nozzle size diameter. This therefore could suggest that selecting a nozzle diameter can be decided based on the average circulation time. The suggestion also can indirectly support the earlier findings of Meier *et al*., (1999) and Zhong and Yuan (2009) that nozzle diameter have cause minimal effect in terms of death of cells which they found out in actual laboratory experiments.

Table 5-7 Average circulation time computed in each the 32 CFD simulated cases.

Case	Average circulation time, s	Case	Average circulation time, s
$\mathbf{A_1B_1C_1}$	14.88	$\mathbf{A_3B_1C_1}$	14.05
$\mathbf{A_1B_1C_2}$	9.21	$\mathbf{A_3B_1C_2}$	8.41
$\mathbf{A_1B_2C_1}$	19.57	$\mathbf{A_3B_2C_1}$	15.55
$\mathbf{A_1B_2C_2}$	13.81	$\mathbf{A_3B_2C_2}$	9.51
$\mathbf{A_1B_3C_1}$	25.66	$\mathbf{A_3B_3C_1}$	18.51
$\mathbf{A_1B_3C_2}$	20.01	$\mathbf{A_3B_3C_2}$	13.67
$\mathbf{A_1B_4C_1}$	26.89	$\mathbf{A_3B_4C_1}$	21.41
$\mathbf{A_1B_4C_2}$	22.81	$\mathbf{A_3B_4C_2}$	15.66
$\mathbf{A_2B_1C_1}$	15.65	$\mathbf{A_4B_1C_1}$	13.84
$\mathbf{A_2B_1C_2}$	9.08	$\mathbf{A_4B_1C_2}$	8.05
$\mathbf{A_2B_2C_1}$	16.21	$\mathbf{A_4B_2C_1}$	15.01
$\mathbf{A_2B_2C_2}$	10.08	$\mathbf{A_4B_2C_2}$	9.29
$\mathbf{A_2B_3C_1}$	20.51	$\mathbf{A_4B_3C_1}$	17.22
$\mathbf{A_2B_3C_2}$	14.48	$\mathbf{A_4B_3C_2}$	12.41
$\mathbf{A_2B_4C_1}$	22.31	$\mathbf{A_4B_4C_1}$	19.88
$\mathbf{A_2B_4C_2}$	17.71	$\mathbf{A_4B_4C_2}$	13.91

A: Air flow rates of 0.05, 0.10, 0.15 and 0.20 vvm which corresponds to A_1, A_2, A_3 and A_4, respectively.
B: Nozzle size diameter of 5, 10, 15 and 20 mm which corresponds to B_1, B_2, B_3 and B_4, respectively.
C: PBR geometry design without baffle and with baffle which corresponds to C_1 and C_2, respectively.

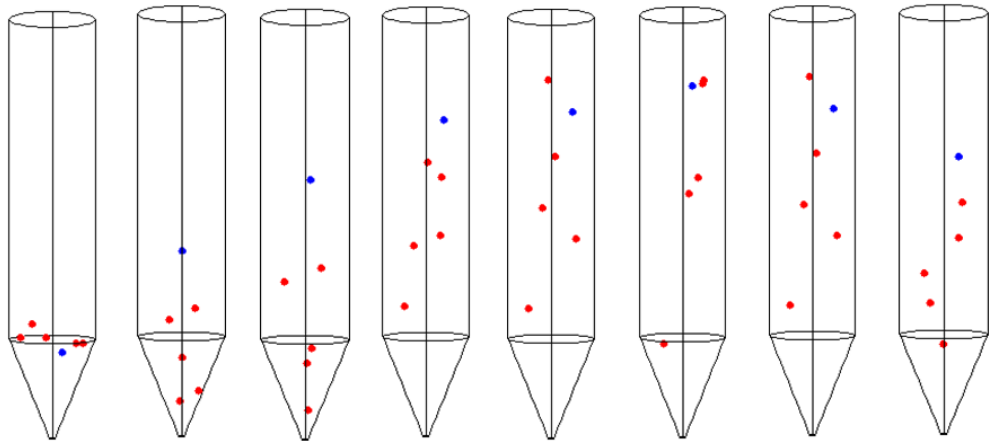

Fig. 5-5 Movement of some particle cells inside the PBR for case ($A_1B_4C_1$) which showed the shortest average circulation time as a representative example of the results obtained in CFD simulation.

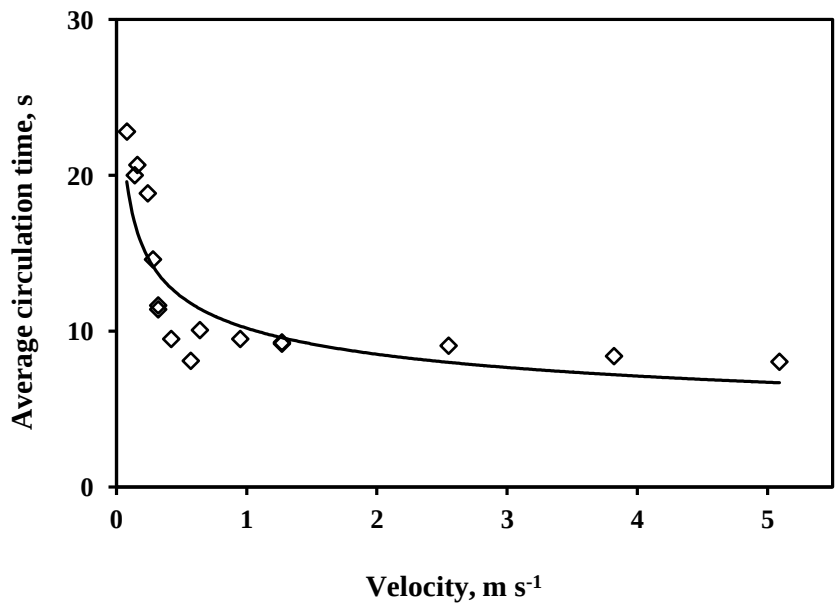

Fig. 5-6 Effect of inlet velocity used as boundary condition in the simulation in the terms of the computed average circulation time.

5.3.4. Turbulence intensity in the PBRs

The three regions where shear forces are generated and usually suspected for cell death were thoroughly investigated and compared in terms of turbulence intensity. These regions were particularly evaluated at 20 mm above the injection zone, at the vertical path where the bubble rises and at 20 mm below the water-air interface. Such locations were previously recommended by Tramper *et al*. (1986). In fluent program, the turbulence is characterized as high, moderate and low turbulence when the turbulent intensity is ≥10 %, ≥ 1 % ≤ 10 % and ≤ 1 %, respectively (Fluent manual, 2006). The quantitative results as presented **Tables 5-8 and 5-9** have shown that higher turbulent intensities can be found in the water-air interface where bubbles break-up. This is followed by the injection zone then the bubble rising region. The highest turbulence was found at the water-air interface in case $A_4B_3C_1$ with 18.21 %. Furthermore, results revealed that high turbulence intensity is always registered in the simulation cases when the nozzle size diameter is 15 and 20 mm regardless of the PBRs with or without internal baffle. This can be reasoned out that because of wider nozzle size diameter, bubble formations are also larger and as these bubbles travel and break up at the water-air interface, higher turbulence is created. Interestingly, with wider nozzle size diameter of 15 and 20 mm, the set air flow rate is lower compared to 5 and 10 mm and if the flow rate has significant effect on turbulence, the value obtained in 5 and 10 mm should be higher. However, the results showed otherwise. Thus, the bubble size which being formed when air is introduced to the PBRs are wisely suspected to cause higher turbulence during break up. This was also observed in the investigation conducted

by Yu *et al*. (2009) where they utilized turbulence as one of the parameter to optimize the inner structure of a flat PBR in their 2D CFD simulated cases which have also shown higher turbulence values at the water-air interface.

Generally, most of the simulated PBR cases revealed a low to medium turbulence intensity in the bubble rising zone while all PBRs revealed medium to high turbulence intensity at the injection zone. Although a direct link between turbulence intensity to growth and death of cells is not strongly established even in literatures, the findings obtained here have further supported the reports of Camacho *et al*. (2000) and Zhong and Yuan (2009) who found out that more cell deaths happen at the water-air interface zones where the bubble raptures. Presented in **Fig. 5-7** is a top view of the contour profiles of the average turbulence intensity obtained in the water-air interface of cases with the low, moderate and high turbulence as a representative example of the simulated cases.

Table 5-8 Average turbulence intensity value of the 32 CFD simulated cases.

Case	Average turbulence intensity (%)		
	Injection zone	Bubble rising zone	Water-air interface
$\mathbf{A_1B_1C_1}$	4.45	0.43	2.68
$\mathbf{A_1B_1C_2}$	2.67	0.88	3.82
$\mathbf{A_1B_2C_1}$	0.57	0.24	0.97
$\mathbf{A_1B_2C_2}$	2.55	2.24	3.86
$\mathbf{A_1B_3C_1}$	8.57	6.64	10.81
$\mathbf{A_1B_3C_2}$	10.02	7.71	11.00
$\mathbf{A_1B_4C_1}$	6.31	5.04	10.21
$\mathbf{A_1B_4C_2}$	7.81	5.57	11.20
$\mathbf{A_2B_1C_1}$	10.05	8.50	10.88
$\mathbf{A_2B_1C_2}$	11.68	9.55	10.89
$\mathbf{A_2B_2C_1}$	1.55	1.22	4.25
$\mathbf{A_2B_2C_2}$	1.61	1.26	4.45
$\mathbf{A_2B_3C_1}$	11.67	9.06	13.61
$\mathbf{A_2B_3C_2}$	12.01	9.80	14.05
$\mathbf{A_2B_4C_1}$	9.02	7.81	11.50
$\mathbf{A_2B_4C_2}$	9.88	8.21	12.01

A: Air flow rates of 0.05, 0.10, 0.15 and 0.20 vvm which corresponds to A_1, A_2, A_3 and A_4, respectively.
B: Nozzle size diameter of 5, 10, 15 and 20 mm which corresponds to B_1, B_2, B_3 and B_4, respectively.
C: PBR geometry design without baffle and with baffle which corresponds to C_1 and C_2, respectively.

Table 5-9 Average turbulence intensity value of the 32 CFD simulated cases (Cont).

Case	Average turbulence intensity (%)		
	Injection zone	Bubble rising zone	Water-air interface
$A_3B_1C_1$	9.91	7.81	11.66
$A_3B_1C_2$	10.51	7.97	12.96
$A_3B_2C_1$	1.77	1.44	3.33
$A_3B_2C_2$	1.79	1.55	3.78
$A_3B_3C_1$	13.58	12.01	16.67
$A_3B_3C_2$	13.66	12.18	16.51
$A_3B_4C_1$	9.51	8.12	12.61
$A_3B_4C_2$	10.12	9.16	13.81
$A_4B_1C_1$	5.95	4.89	7.56
$A_4B_1C_2$	7.98	5.92	8.88
$A_4B_2C_1$	2.12	1.54	3.58
$A_4B_2C_2$	2.22	1.78	4.99
$A_4B_3C_1$	14.52	12.11	18.21
$A_4B_3C_2$	12.31	11.88	17.74
$A_4B_4C_1$	13.04	10.55	14.41
$A_4B_4C_2$	13.88	11.02	15.01

A: Air flow rates of 0.05, 0.10, 0.15 and 0.20 vvm which corresponds to A_1, A_2, A_3 and A_4, respectively.
B: Nozzle size diameter of 5, 10, 15 and 20 mm which corresponds to B_1, B_2, B_3 and B_4, respectively.
C: PBR geometry design without baffle and with baffle which corresponds to C_1 and C_2, respectively.

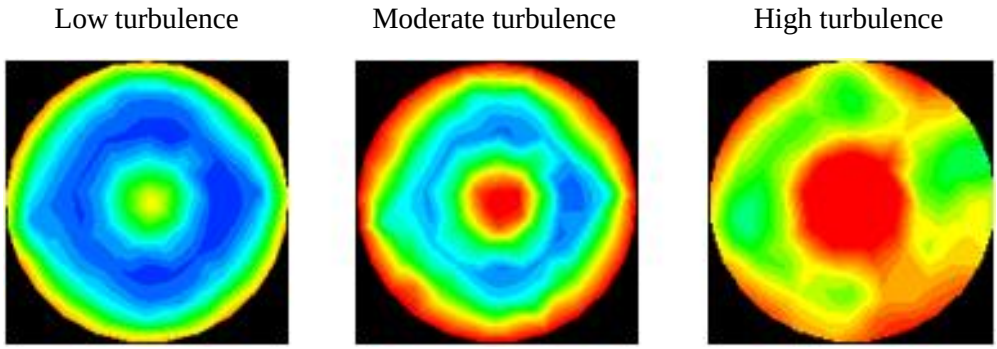

Fig. 5-7 Top view of the contour profiles of the average turbulence obtained in the water-air interface of cases with the low, moderate and high turbulence as a representative example of the results obtained in the simulated cases.

5.3.5. Light intensity in the PBRs

The illumination of the particles can also be estimated based on the distance location of the particles to the walls of the PBRs. From the txt file which saved the location of the particles in the simulation along the X-direction, Y-direction and Z-direction as they travel around the PBR. The light intensity can be estimated using the Lambert-Beer Law presented earlier in (Eq. 5-5) (Lou and Al-Dahhan, 2003). Assuming an external light intensity of 400 μE m^{-2} s^{-1} at the PBR walls and light is available at all sides; an estimate of light intensity is computed. The computed average light intensity is presented in **Table 5-8**. Interestingly, a relationship between the average circulation time and the computed average light intensity can be derived as shown in **Fig. 5-8**. There is a linear relationship between the average circulation time and light intensity ($y = -2.6666x + 389.01$) with R^2 value of 0.073.

Table 5-10 Computed average light intensity of the 32 CFD simulated cases.

Case	Computed average light intensity, μE m^{-2} s^{-1}	Case	Computed average light intensity, μE m^{-2} s^{-1}
$\mathbf{A_1B_1C_1}$	335.48	$\mathbf{A_3B_1C_1}$	339.85
$\mathbf{A_1B_1C_2}$	355.14	$\mathbf{A_3B_1C_2}$	375.66
$\mathbf{A_1B_2C_1}$	341.24	$\mathbf{A_3B_2C_1}$	365.78
$\mathbf{A_1B_2C_2}$	354.12	$\mathbf{A_3B_2C_2}$	369.47
$\mathbf{A_1B_3C_1}$	321.42	$\mathbf{A_3B_3C_1}$	354.71
$\mathbf{A_1B_3C_2}$	325.17	$\mathbf{A_3B_3C_2}$	355.14
$\mathbf{A_1B_4C_1}$	315.14	$\mathbf{A_3B_4C_1}$	332.87
$\mathbf{A_1B_4C_2}$	324.16	$\mathbf{A_3B_4C_2}$	342.65
$\mathbf{A_2B_1C_1}$	349.12	$\mathbf{A_4B_1C_1}$	352.01
$\mathbf{A_2B_1C_2}$	365.16	$\mathbf{A_4B_1C_2}$	368.59
$\mathbf{A_2B_2C_1}$	332.41	$\mathbf{A_4B_2C_1}$	356.42
$\mathbf{A_2B_2C_2}$	364.17	$\mathbf{A_4B_2C_2}$	364.12
$\mathbf{A_2B_3C_1}$	325.47	$\mathbf{A_4B_3C_1}$	344.12
$\mathbf{A_2B_3C_2}$	347.89	$\mathbf{A_4B_3C_2}$	348.14
$\mathbf{A_2B_4C_1}$	348.17	$\mathbf{A_4B_4C_1}$	329.88
$\mathbf{A_2B_4C_2}$	342.27	$\mathbf{A_4B_4C_2}$	354.60

A: Air flow rates of 0.05, 0.10, 0.15 and 0.20 vvm which corresponds to A_1, A_2, A_3 and A_4, respectively.
B: Nozzle size diameter of 5, 10, 15 and 20 mm which corresponds to B_1, B_2, B_3 and B_4, respectively.
C: PBR geometry design without baffle and with baffle which corresponds to C_1 and C_2, respectively.

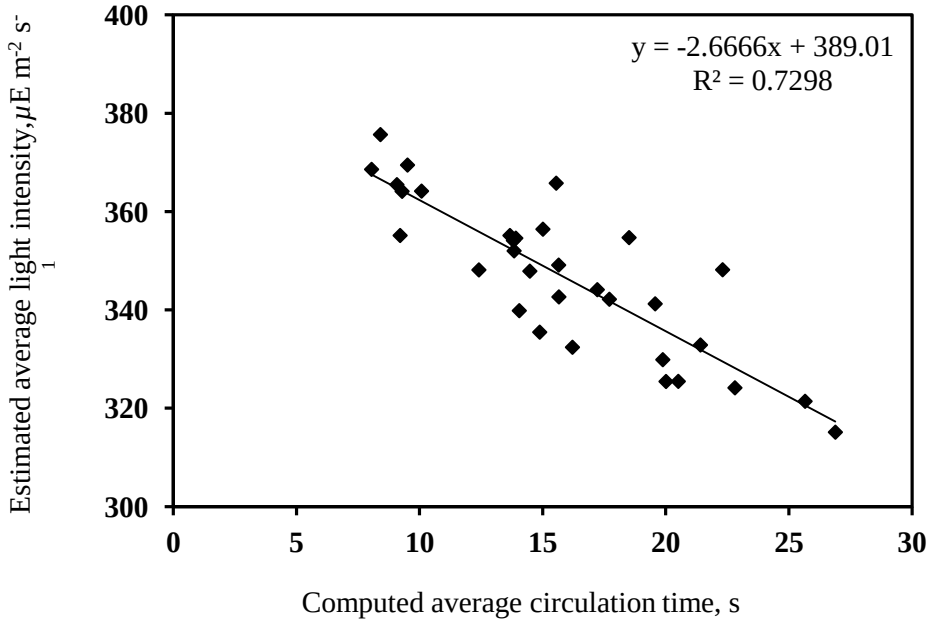

Fig. 5-8 Estimated light intensity with respect to the computed average circulation time obtained from the 32 CFD simulated cases.

5.3.6. Selection of appropriate PBRs combining the three hydrodynamic evaluation parameters and light

Based on the hydrodynamic investigation particularly the percentages of dead zones, average circulation time and turbulence intensity, the most appropriate PBR is chosen and recommended for the actual cultivation of microalgae cells. Applying the hydrodynamic parameters using elimination technique is executed here. There is no available standard in terms of allowable dead zones inside the PBRs, thus the case with the lowest volume percentages of dead zone is preferable if the dead zone is the only criterion. However, this is not the case since circulation time and

turbulence intensity should be considered. The same is true for the average circulation time and turbulence intensity which either cannot be used as the only criterion. Generally, it was also observed that the cases with lower volume percentages of dead zones also displayed shorter circulation time. Considering that this is the first attempt of combining the hydrodynamic parameters to select the appropriate PBR, the following criteria were decided as: Criterion 1 – volume percentages of dead zones shall not be more than 10 %; Criterion 2 – average circulation time shall not exceed 10 s; and Criterion 3 – the turbulence intensity should be within the low to moderate category. Although it is a fact that the growth rates of microalgae increase initially with increasing turbulence, this will decreases sharply with further increase of the gas velocity due to cell damage (Merchuk *et al*., 2000). These criteria were used in choosing which PBR designs are preferable among the 32 simulated cases.

Presented in **Table 5-11** is the result obtained in applying the elimination method based on the set criteria. In the table, cases marked with letter "O" in the respective column with the hydrodynamic evaluation parameter means it passed the set criterion while those with "X" means otherwise. The cases that were highlighted in a rectangular box passed the 3 set criteria and therefore concluded to be the appropriate cases for microalgae cultivation. These cases were further summarized in **Table 5-12.** Observing the said cases, in terms of the PBR design parameters, all the chosen cases are with internal baffle and protruded geometry while two case is under 5 mm nozzle size diameter and the remaining 2 cases are under 10 mm nozzle size. However, considering the construction aspect of the

PBR, it would be very difficult to implement a 5 mm nozzle size diameter especially when the bottom geometry of the PBR is protruded and cone-shaped. Therefore, case $A_1B_1C_2$ and case $A_4B_1C_2$ are removed from the selection list and nozzle size diameter of 10 mm is therefore chosen. In terms of the air flow rate, the selected 2 remaining cases have air flow rates of 0.10 and 0.15 vvm. Considering that air flow rate is an operating parameter, this can be easily adjusted in the actual cultivation. In addition, considering that the air flow rate has an influence in terms of volume percentages of dead zones in the PBRs, it can be recommended that the minimum air flow rate for the PBR under investigation is 0.10 vvm. This can be slightly increase to finally eliminate the dead zones inside the PBR but should not exceed 0.15 vvm air flow rate. The two cases have also displayed higher amount of estimated light intensity which is approximately 364.17 and 369.47 μE m^{-2} s^{-1} for cases $A_2B_2C_2$ and $A_3B_2C_2$, respectively.

Table 5-11 Selection of cases appropriate for microalgae cultivation based on the set hydrodynamic criteria.

Case	Criteria 1, ≤ 10 % dead zone	Criteria 2, ≤ 10 s of circulation time	Criteria 3, low to medium turbulence intensity		
			Injection zone	Bubble rising zone	Water-air interface
$A_1B_1C_1$	O	X	O	O	O
$A_1B_1C_2$	O	O	O	O	O
$A_1B_2C_1$	X	X	O	O	O
$A_1B_2C_2$	X	X	O	O	O
$A_1B_3C_1$	X	X	O	O	X
$A_1B_3C_2$	X	X	X	O	X
$A_1B_4C_1$	X	X	O	O	X
$A_1B_4C_2$	X	X	O	O	X
$A_2B_1C_1$	O	X	X	O	X
$A_2B_1C_2$	O	O	X	O	X
$A_2B_2C_1$	X	X	O	O	O
$A_2B_2C_2$	O	O	O	O	O
$A_2B_3C_1$	X	X	X	O	X
$A_2B_3C_2$	X	X	X	O	X
$A_2B_4C_1$	X	X	X	O	X
$A_2B_4C_2$	X	X	X	O	X
$A_3B_1C_1$	O	X	X	O	X
$A_3B_1C_2$	O	O	X	O	X
$A_3B_2C_1$	O	X	O	O	O
$A_3B_2C_2$	O	O	O	O	O
$A_3B_3C_1$	X	X	X	X	X
$A_3B_3C_2$	O	X	X	X	X
$A_3B_4C_1$	X	X	O	O	X
$A_3B_4C_2$	X	X	X	O	X
$A_4B_1C_1$	O	X	O	O	O
$A_4B_1C_2$	O	O	O	O	O
$A_4B_2C_1$	O	X	O	O	O
$A_4B_2C_2$	O	O	O	O	O
$A_4B_3C_1$	X	X	X	X	X
$A_4B_3C_2$	O	X	X	X	X
$A_4B_4C_1$	X	X	X	X	X
$A_4B_4C_2$	X	X	X	X	X

Table 5-12 The cases that passed the set criteria which are selected for cultivating microalgae.

Case	Air flow rate, vvm	Nozzle size diameter, mm	PBR design
$\mathbf{A_1B_1C_2}$	0.05	5	With baffle
$\mathbf{A_2B_2C_2}$	0.10	10	With baffle
$\mathbf{A_3B_2C_2}$	0.15	10	With baffle
$\mathbf{A_4B_1C_2}$	0.20	5	With baffle

5.4. Conclusions

In engineering perspective, the structural configuration and design of the PBRs have critical role in the flow hydrodynamics inside the reactor which are very significant in providing ideal growth conditions for the microalgae cells. Hence, in this study, CFD was utilized to investigate the flow hydrodynamics inside 30 L PBRs simulating 32 cases. The 32 cases simulated in the study were accounted from four various air flow rates, four nozzle size diameters and two PBR geometry designs. The volume percentage of dead zones, average circulation time and turbulence intensity were used to investigate the performance of the PBRs as a cultivating vessel for microalgae cells. Simulation results have revealed the hydrodynamic advantages of the PBRs designed with internal baffle and protruded bottom cone-shaped geometry. This PBR design can eliminate the dead zones at the same time execute better mixing and mass transfer because of its faster average

circulation time. In addition, a linear relationship was revealed in terms of average circulation time and the computed average light intensity. The faster circulation time, more light intensity is received by the particle cells.

This approach of selecting a PBR operating condition and design combining the three hydrodynamics parameters is a first attempt of its kind and no standard value in each parameter is available in literatures. Thus, a criterion on each parameter was set and elimination technique was executed in the 32 simulated cases until some appropriate PBRs suited for microalgae production were selected.

The volume percentages of dead zones in the typical PBR design without baffle were also found at the bottom and near the PBR walls. Thus, cell coagulation and settling are then highly suspected to happen in these regions. Nevertheless, it was concluded that based on the set criterion, the minimum air flow rate in the investigated PBR is 0.10 vvm. This can be adjusted in actual cultivation to eliminate the volume percentages of dead zones, however, should not exceed 0.15 vvm

The effect of nozzle size diameter has shown to significantly influence the average circulation time. This is in consistent with the expected hydrodynamic flow analysis since the input value of air velocity in the simulation depends on the nozzle diameter especially when the PBRs have the same air flow rates. Results have shown that based on the set criteria in selecting appropriate PBRs, a nozzle size diameter of 10 mm is appropriate.

The regions where cell death is highly suspected because of shear forces were

also investigated in terms of turbulence intensity evaluated as low turbulence (≤ 1 %), moderate turbulence (≥ 1 % ≤ 10 %) and high turbulence (≥ 10 %). Results have shown that turbulence intensities are higher in the water-air interface zones confirming further the results reported by Camacho (2000) and Zhong and Yuan (2009). Moderate to high turbulence were observed in the injection zones while low to moderate turbulence were observed in the bubble rising region. The results were also used in the selection of the appropriate PBR. In terms of turbulent intensity, PBRs with low to moderate range of turbulence is preferable. Thus, based on the hydrodynamic analysis inside the PBRs applying the 3 set criteria, cases $A_2B_2C_2$ and $A_3B_2C_2$ were actually chosen. Both cases have the same nozzle size diameter and PBR geometry which are considered design parameters while they only differ in flow rate of 0.10 and 0.15 vvm which is an operating parameter and can be easily adjusted during the actual cultivation of microalgae. The results obtained in the actual cultivation of microalgae in the 30 L PBRs are reported in the succeeding chapter.

Finally, it can be concluded that the CFD approach have demonstrated its capability in investigating flow hydrodynamics inside the PBRs which can result to better design of efficient and effective PBRs for maximum cultivation of microalgae. The approach can be very promising in doing researches designs of PBRs while reducing significant research time, labor and resources.

6. Cultivation of *Chlorella vulgaris* in 30 L cylindrical bubble column photobioreactors (PBRs)

6.1. Introduction

Microalgae are believed to have the potential as the main energy source in the future. In recent research reviews in Patil *et al*. (2008) and Chisti (2007), microalgae was shown to be the only source of renewable biodiesel capable of meeting the global demand for transport fuels, with the potential to completely displace the use of fossil fuels. Producing alternative oil from microalgae is not new; it dates back in the 70s during the gas supply scare (Barkley *et al*., 1987). However, further research on mass production and oil extraction were temporarily hampered during that time because of high production costs. Currently, amidst the reality of increasing energy demand and rapidly depleting energy sources, finding new alternative energy sources is an imperative and the idea of oil extraction from microalgae is again gaining much attention (Bitog *et al*., 2011).

In the past decades, microalgae have been extensively studied to determine its growth requirements to obtain optimum cell multiplication and growth. Thus, the growth factors such as light intensity, CO_2 and temperature are already known to be the main factors that when their optimal amount is provided to the algae culture, maximum growth can be achieved. The amount needed from these varies depending on the microalgae specie, the type of growing vessel and the volume of culture medium, etc. However, according to Fogg and Thake (1987), there are basically four reasonably well defined phases of microalgae growth particularly in

batch cultures (**Fig. 6-1**). Phase 1 is known as the lag phase which usually could last for a couple of days. This occurs when cultures of algae are transferred to fresh medium under the same light, temperature and salinity conditions. Lag phase also occur when the culture is transferred from one set of growth conditions to another. Phase 2 is the exponential phase where cells are expected to exponentially multiply in number. Thus, it is in this phase where the microalgae growth rate is being measured. Growth rate is one important way of expressing the relative ecological success of a species or strain in adapting to its natural environment or the experimental environment imposed upon it. The duration of exponential phase in cultures depends upon the size of the culture, the growth rate and the capacity of the medium and culturing conditions to support microalgae growth. A declining growth sometimes occurs just after the exponential growth phase. This happens when the requirement for cell division is limiting or something else is inhibiting reproduction. In this time of growth biomass is often very high and exhaustion of a nutrient salt, limiting carbon dioxide or light limitation becomes the primary causes of declining growth. The stationary phase (Phase 3) follows next where the cell net growth is almost zero, and within a matter of hours cells may undergo dramatic biochemical changes and a logarithmic decline of growth rate is expected. Death phase (Phase 4) is the last phase where cell metabolism can no longer be maintained and the death of cells can be generally very rapid, hence the term "culture crash" is often used.

Currently, microalgae are now regularly cultivated for other equally important use such as a healthy food supplement since they are complete in protein with

essential amino acids which are involved in metabolic processes such as energy and enzyme production. They are also utilized as a stabilizing agent particularly in milk products, as fertilizer, as biofilters for wastewater treatment, etc. Microalgae can be cultivated also to produce biomass, which can be burned to produce heat and electricity. Mass cultivation of microalgae can be implemented in outdoor to take advantage of the availability of free sunlight needed for photosynthesis to power the growth and multiplication of cells. However, outdoor cultivation faces complex challenges to maximizing the growth potential of the cells. Thus, indoor cultivation supplied with artificial lights has become an alternative. In addition, indoor cultivation allows full control of providing the microalgae with the main growth factors for maximum cell growth.

Numerous laboratory studies have been published on microalgae where attention is focused on the growth of the algae as influenced by the environmental conditions such as light, temperature, CO_2, nutrient availability, etc (Lee *et al*., 2006; Scragg *et al*., 2002; Park and Lee, 2000; Merchuk *et al*., 1998; Tredici and Zittelli, 1998). The optimum light intensity, CO_2 and temperature to be supplied vary according to specie, culture medium, the type, design and size of the bioreactor, etc. Particularly for *Chlorella vulgaris*, the reported optimum temperature was between 20-35 ^{O}C (Cassidy, 2011; Converti *et al*., 2009; Chinnasamy *et al*., 2009), CO_2 level is under 5-10% (Chinnasamy *et al*., 2009; Mandalam and Palsson, 1988) while light intensity significantly varies between 60 ~100 μmol photons m^{-2} s^{-1} (Seyfabadi *et al*., 2011; Lv *et al*., 2010). However, these reported values are not conclusive especially when considering large scale

production where the size and geometry of the production vessel is significantly scaled up. Furthermore, the cultivation of microalgae under high light intensity close to natural light have not yet been reported in which for practical reasons, should be desired especially when considering to cultivate microalgae under natural light to minimize production cost.

In indoor cultivation, microalgae are commonly cultivated in photobioreactors (PBRs), a growth vessel where light can easily pass through for cells consumption. The most typical PBRs are bubble column cylindrical and rectangular type PBRs. These PBRs are usually simple in design with no moving parts, and very easy to construct and operate (Bitog *et al*., 2011).

At present, cylindrical bubble column photobioreactors (PBRs) have been receiving enormous attention because they are very efficient in growing photosynthetic cells. These PBRs have suitable heat and mass transfer characteristics and have often been thought to achieve the most efficient mixing and the most volumetric gas transfer (Barbosa, 2003; Eriksen, 2008). In addition, they require less operational cost because of low energy input requirements (Bitog *et al*., 2011). The geometry of cylindrical type PBRs also maximized the surface area where the entry of light can be equally distributed for cell consumption especially when light is stalled surrounding the PBR. The operation and management of bubble column types PBRs are also very simple. The gas is usually injected at the bottom purposely to maximize its mixing effect throughout the column at the same time provides more time for mass transfer. The reactant gas itself provides the stirring action that is required to conduct gas-liquid and gas-

liquid-solid interactions and reaction (Rampure *et al*., 2007). However, despite its recognized advantages for mass production, few studies have been conducted. Furthermore most studies on growth and production of microalgae is focused only in small scale cultures. Large scale cultivation of microalgae is still limited and only a few published researches are available. Presented in **Table 6-1** is a summary of some laboratory researches on cylindrical bubble column PBRs. It is obvious that most of the laboratory studies were focused on the hydrodynamic characteristics inside PBRs such as their growth performance as affected by the density of culture, mixing, shear forces, etc. However, maximizing the growth and multiplication of cells in larger scale PBRs is still limited, thus this study.

In Chapter 5, it has been shown that the design geometry of PBRs is one of the most important factors to carefully consider in obtaining higher cell growth rate and maximizing biomass production. Especially for large scale cultivation, the design is very critical because several factors should be considered such as the flow hydrodynamics inside the PBRs. These hydrodynamic factors such as volume percentages of dead zones, average circulation time and turbulence intensity were earlier investigated in 30 L PBRs via numerical simulation and among the simulated cases, some were recommended for the actual cultivation of microalgae.

Therefore, this study was implemented to investigate the growth response of microalgae cells from larger cylindrical bubble column PBRs of 30 L following the recommended PBR design and operating parameters obtained in Chapter 5. The results would further cement the conclusions made based from the numerical investigation conducted in Chapter 5 via computational fluid dynamics.

However, before the final cultivation of microalgae in the 30 L PBRs, initial laboratory scale experiments were conducted in small size PBRs to determine the effect of temperature and CO_2 on the growth of microalgae. The recommended temperature and CO_2 level obtained in the small scale laboratory tests were supplied in the 30 L culture cultivation. Several small scale laboratory studies were already published in terms of the effect of light intensity in microalgae growth, however, the investigated range of light intensity are lower if cultivation of microalgae under free sunlight is one of the objectives. Thus the recommended light intensity range in literatures cannot be used specially in large scale outdoor production. In this study, with the long term goal of growing algae in outdoor and utilizing the free sunlight, artificial light was supplied with higher light intensity attempting to mimic the light intensity under day light condition.

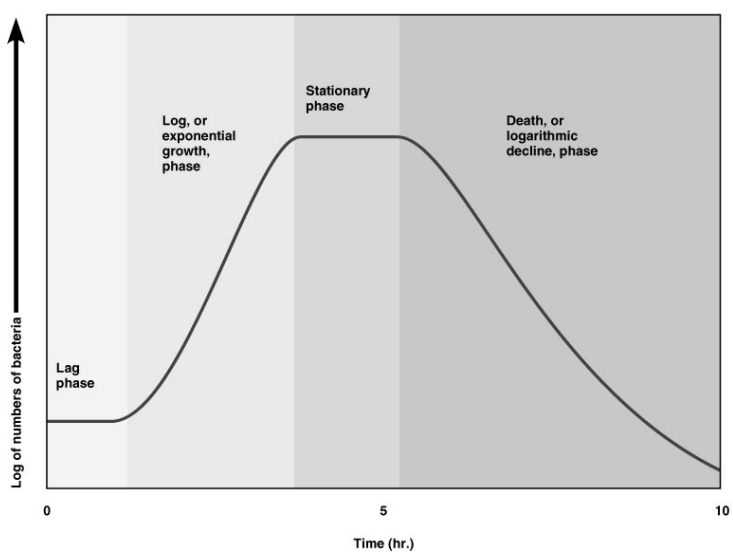

Fig. 6-1 Growth phases of microalgae cells (Source: Pearson Education Inc., publishing as Benjamin Cummings, Copyright 2004).

Table 6-1 Summary list of researches on microalgae cultivated in typical cylindrical bubble column photobioreactors.

PBR characteristics	Approximate culture volume in liters	Focus of the study	Reference/Year
Cylindrical column	21	Mass transfer and shear	Bannari *et al*., 2011
Cylindrical column with centric tube and porous centric tube	4	Laboratory study on flow patterning high-density cultures of microalgae and carbon dioxide removal	Chui et al., 2009
Cylindrical column with centric tube	20	Local characteristics of hydrodynamics in the reactor	Lou and Al-Dahhan, 2008
Cylindrical column	3.6	Photoautotrophic high-density cultivation	Kaewpintong *et al*., 2007
Cylindrical column	2.5	Determining the best specific light uptake rates for the lumostatic cultures	Lee et al., 2006
Cylindrical column	60	Mixing as a new approach to characterize dispersion coefficients	Rubio *et al*., 2004
Cylindrical column	0.75	Shear stress of microalgae in sparged PBRs	Barbosa *et al*., 2004
Cylindrical column	20	Experiment of the stirred tank photobioreactor for biohydrogen production	Ogbonna *et al*., 1998

6.2. Materials and Methods

6.2.1. Microalgae specie

The selection of microalgae specie used in this is study for is based on the following factors such as high lipid productivity, faster growth to support commercial production in the future. A review of microalgae species intended for biodiesel production was presented by Sharma *et al*., 2012 with the several approaches to increase the lipid content of the specie and one promising candidate is *Chlorella vulgaris*.

Chlorella vulgaris was chosen in this study for the actual cultivation considering its great potential as a resource for biodiesel production. Chlorella is a single celled microalga that grows in fresh water ponds and lakes. Its color is a brilliant deep green, due to its high amount of chlorophyll. However, according to Illman *et al*., (2000) and Spolaore *et al*., (2006), the lipids content in *Chlorella vulgaris* under general growth conditions is up to 20 ~ 30% by weight of dry biomass which is still cannot meet the standard industrial requirements. Although the specie has lower oil content of approximately 28 ~ 32 % of dry weight (Chisti, 2007) as compared to other species, *Chlorella vulgaris* is believed to have faster growth and easy cultivation.

6.2.2. Descriptions of the PBRs used in the microalgae cultivation

Determining the growth of microalgae in the 30 L PBR is the main goal of the

study; however, initial small scale experiments were conducted to determine the effect of temperature and CO_2 on cells growth. The result will be used in cultivating the microalgae specie in the 30 L PBRs. To investigate the effect of temperature, a 250 mL flask reactor was used while a 0.4 L column PBR made of glass was utilized for the CO_2 test.

The PBRs used in the large scale cultivation were a typical cylindrical bubble column design and an upgraded type PBR with a 30L culture medium. The upgraded PBR which was recommended in the simulation study was constructed with internal baffle while the geometry of bottom part was protruded and designed to be cone-shaped. As discussed in Chapter 5, the internal baffle is expected to improve the hydrodynamic characteristics inside the PBR suited for microalgae cultivation. For instance, the internal baffle can minimize dead zones and also can provide good mixing inside the PBR and also increase the average circulation time. The bottom part cone-shaped geometry design is supposed eliminate dead zones at the bottom; and prevent cell coagulation and minimize settling of cells to the bottom of the PBRs. The internal baffle is basically an open acrylic cylindrical tube with inner diameter of 85 mm and height of 700 mm. The inner diameter of the typical and upgraded PBRs is 185 mm while the height is 1400 mm and 1550 mm, respectively. The vertical height of the cone-shaped bottom part of the upgraded PBR is 250 mm. The introduction of air and CO_2 for the cells consumption is via bubble from the bottom part of the PBRs. The PBRs were surrounded with 28 kW artificial fluorescent lights where 5 fluorescent lights were equally distributed in each side of the PBRs resulting to supply approximately 560 kW artificial light.

The distance between the PBRs and the fluorescent bulbs is approximately 150 mm. The PBRs were supported with square aluminum frames where the fluorescent bulb lights were also installed. The actual view of the PBRs with light installations is presented in **Fig. 6-2** and a geometry comparison of the typical and upgraded PBR is presented in **Table 6-2**. Both PBRs were subjected with the same amount of light intensity and supplied with equal levels of CO_2 and under the same temperature for the entire duration of the experiment.

(a) **(b)**

Fig. 6-2 The typical bubble column PBR (right) and the upgraded PBR (left) utilized in the two successive experiments, (a) view at the start of the experiment and when the light is OFF and (b) view at the end of the experiment and when light is ON.

Table 6-2 Comparison between the typical and the upgraded PBR where *Cholera vulgaris* cells are cultivated.

Characteristics	Typical PBR	Upgraded PBR
Design geometry	Without Baffle and the bottom part is flat	With Baffle and the bottom part is protruded (cone-shaped)
Nozzle size	10 mm	10 mm
Air flow rate	0.10 vvm	0.10 vvm
Culture medium height	1050 mm	1110 mm
PBR diameter	185 mm	185 mm
Baffle diameter	-	85 mm
Baffle height	-	700 mm
Light intensity	Equally supplied with 20pcs of 28kW Fluorescent light	
Temperature	15 ~ 25 ^{0}C	15 ~ 25 ^{0}C
CO_2	Under 10% level	Under 10% level
Initial cell concentration	Approximately 0.5 g L^{-1} and 2.0 g L^{-1} for Experiments 1 and 2, respectively	

6.2.3. Initial experiments on the effect of temperature and CO_2

The set of experiments to investigate the effect of temperature and CO_2 on the growth of *Chlorella vulgaris* in a 250 mL flask and a 0.4 L bubble PBR, respectively was initially conducted under a Modified Bold's Basal culture medium following Choi *et al*. (2003); Pruvost *et al.* (2009). The temperatures considered

were 10, 15, 20 and 25 ^{0}C for the first test and 30, 35, 40 and 45 ^{0}C for the second test while for the CO_2 experiment, 0.035 (air), under 3, under 7 and under 10 % levels of CO_2 were investigated. Two separate experiments were conducted to determine the effect of temperature from 15 ~ 45 ^{0}C range because the availability of growth chambers is limited only to four units. The growth chambers utilized in the experiment are shaking incubators (Model VS 8480 SF, South Korea) which also provide mixing in the 240 mL flask. Nevertheless, the same experimental procedures were conducted in the two sets of temperature experiment. The temperature inside the growth chambers can be completely maintained from the settings of the unit; however, supply of CO_2 inside the chamber is not possible. Thus, only the sole effect temperature on the growth of microalgae is investigated in this set-up. Artificial light from commercial fluorescent lamp was supplied into the growth chamber of light intensity reading of about 70±1 μE m^{-2} s^{-1}.

The laboratory experiment to determine the effect of CO_2 on growth of microalgae was conducted in a room where the temperature is maintained through an air-condition unit. The recommended temperature environment for microalgae which was determined in the temperature experiments was maintained during the conduct of the experiment. Light was also supplied at both side of the PBR with the same light intensity reading of 70±1 μE m^{-2} s^{-1}. Mixing is realized through bubbles introduced at the bottom part of the PBR under 0.10 vvm flow rate.

The successive experiments on temperature and CO_2 were conducted in the Department of Biological Engineering, Inha University, Incheon, Korea who also provided the chlorella specie used in the test. The initial pH level of the culture

medium was prepared 6.5 ~ 7.0 while the cell diameter was 0.22 μm. The initial cell concentration used in all the experiments is approximately 1.0 x 10^6 mL^{-1}. The growth medium was initially infiltrated to remove bacteria & other unwanted microorganisms of more than 0.22 μm size. The cell number, size and fresh cell weight were measured using an automated cell coulter counter (Beckman Coulter, Z™ Series COULTER COUNTER® Cell and Particle Counter, USA) daily until the experiment is terminated while the growth pH was measured via a portable pH meter (Omega Model PHH-65A, USA). Based on the results, the daily cell concentration and specific growth rate was computed.

The maximum specific growth of the cells is expected to be obtained during the exponential growth phase where the rate of increase in cells per unit time is proportional to the number of cells present in the culture (Wood *et al*., 2005). In simple terms, the population growth of the cells follows Eq. (6-1) where the solution of N is presented in Eq. (6-2). Based on the cell concentration, the specific growth rate of was computed using the standard equation for exponential growth of the cells as shown in Eq. (6-3), which states that the rate of increase in cells per unit time is proportional to the number of cells present at the beginning of any unit of time (Wood *et al*., 2005).

$$\frac{dn}{dt} = rN \qquad (6\text{-}1)$$

$$N_t = N_o e^{rt} \qquad (6\text{-}2)$$

$$r = \frac{\ln\left(N_t / N_o\right)}{\Delta t} = \frac{\ln N_t - \ln N_o}{\Delta t} \qquad (6\text{-}3)$$

6.2.4. Experimental set-up and methodology for the cultivation of microalgae in the 30 L PBR

The culture *Chlorella vulgaris* cultivated in the 30 L PBRs was collected from the laboratory of the Biosystems Research Division of the Korea Research Institute of Bioscience and Biotechnology (KRIBB), Daejeon, South Korea. The algae were initially grown in a tank until a sufficient amount is available to growing algae with approximately 30 L culture medium in each PBR. The experiment was set-up at the basement of the College of Agriculture and Life Sciences (CALS) building at Seoul National University (SNU), Seoul, South Korea. Setting up the experiment entails lot of time particularly the installation of air flow rate meters, CO_2 regulator and making tight connections from the CO_2 tank and air pump to the PBRs. The CO_2 level supply as well as air flow rates were controlled using flow meters installed for each PBRs which were carefully connected using Tygon tubes. Each PBR were installed with two flow meters which regulates the entry of CO_2 and air inside the PBRs. The PBRs were thoroughly inspected for leaks by initially testing it with tap water and the joints where leaks occur were sealed with high strength epoxy. The strength of the PBRs were also tested by pouring sufficient amount of water into the PBR during a span of time and check if it can constantly sustain the pressure exerted by the culture medium for the whole duration of the experiment.

Two sets of laboratory experiments were conducted from September 26 to October 16, 2012. Experiment 1 was conducted in 10 days while Experiment 2 lasted for 8 days. The first experiment started from September 26 to October 05 with an initial biomass concentration of approximately 0.5 g L^{-1}, while the second

experiment started from October 6 to 13 where the initial biomass concentration of approximately 2.0 g L^{-1}. Microalgae were cultivated in N-8 culture medium following Lee and Palsson (1994); Lee and Lee (2001), and included 1.0 g L^{-1} of KNO_3, 0.74 g L^{-1} of KH_2PO_4, 0.21 g L^{-1} of Na_2HPO_4, 0.05 g L^{-1} of $MgSO_47H_2O$, 0.0132 g L^{-1} of $CaCl_22H_2O$, 0.01 g L^{-1} of Fe-Na EDTA. The N8 medium is commonly used for culturing *Chlorella vulgaris* for its capacity to support high-density cultures on the basis of elemental stoichiometric composition of the algae (Mandalam and Palsson, 1998). The medium has also a trace metal solution of 12.98 µg L^{-1} of $MnCl_24H_2O$, 3.2 µg L^{-1} of $ZnSO_47H_2O$, 1.83 µg L^{-1} of $CuSO_45H_2O$ and 1.84 µg L^{-1} of $Al_2(SO_4)_3$.

Samples of approximately 50 mL were collected everyday at the same particular time from the top, middle and bottom parts of the PBRs. The samples were weighed immediately after the sampling and the biomass content of the collected samples was estimated gravimetrically using Total Suspended Solid (TSS) in a 47 mm diameter Whatman GF/C filter paper. The filters used in the test were initially dried overnight in a container with silica gel and weigh before being used to filter the collected samples. The wet weight of the filter paper was determined after allowing water to pass though it using suction pump in a specialized container. Immediately after determining the wet weight of the filter paper, the samples were poured into the container and were forced to pass through the wet filter using the same suction pump. The cells and water content from the samples are then separated where the cells remained into the filter paper where its weight was immediately measured. The difference in weight between the wet filter

paper and the wet filter paper with cells gives an estimate of the biomass content or the fresh cell weight. After measuring the weight, the samples are placed overnight into a container box with silica gel for drying and weigh the next day to obtain an estimate of the dry cell weight. The same procedure was done in all the samples collected from the top, middle and bottom part of each PBR.

6.3. Results and discussion

6.3.1. Effect of temperature on the growth of *Chlorella vulgaris*

The daily cell concentration of *Chlorella vulgaris* obtained under varied temperatures of 10, 15, 20 and 25 ^{0}C is presented in **Fig. 6-3** and under temperatures of 25, 30, 35 and 40 ^{0}C is shown in **Fig. 6-4.** The experiments were terminated when the computed growth rates were observed to be decreasing. After 5 days of cultivation, the cell growth as affected by temperature is very obvious where a temperature of 25 ^{0}C displayed the highest concentration followed by 20 ^{0}C of temperature for the first experiment while temperatures 30 and 35 ^{0}C displayed higher concentrations for the second experiment. Temperatures of 10, 15, 35, 40 ^{0}C obviously displayed lower cell concentrations while the worst was obtained when the temperature was set at 45^{0}C which actually killed the cells, thus a decreasing cell concentration was observed.

The computed specific cell growth rate per day of *Chlorella vulgaris* as affected by the temperature is presented in **Table 6-3**. The highest specific growth was obtained in Day 3 when the temperature was 30 ^{0}C with a value 1.07 day^{-1}.

Under the 5-day of cultivation, the average growth rate under temperatures of 20, 25, 30 and 35 ^{0}C are observed to be comparable which were computed to be 0.54, 0.64, 0.66, and 0.67 day^{-1}, respectively. The results obtained are in consonant with previous studies such as (Cassidy, 2011; Converti *et al*., 2009; Chinnasamy *et al*., 2009) where higher growth of microalgae cells can be obtained in a temperature range between 20 ~ 35 ^{0}C. Thus, considering also the complex the set-up in cultivating *Chlorella vulgaris* especially in larger scale production systems, temperatures within 20 ~ 35 ^{0}C range can be recommended.

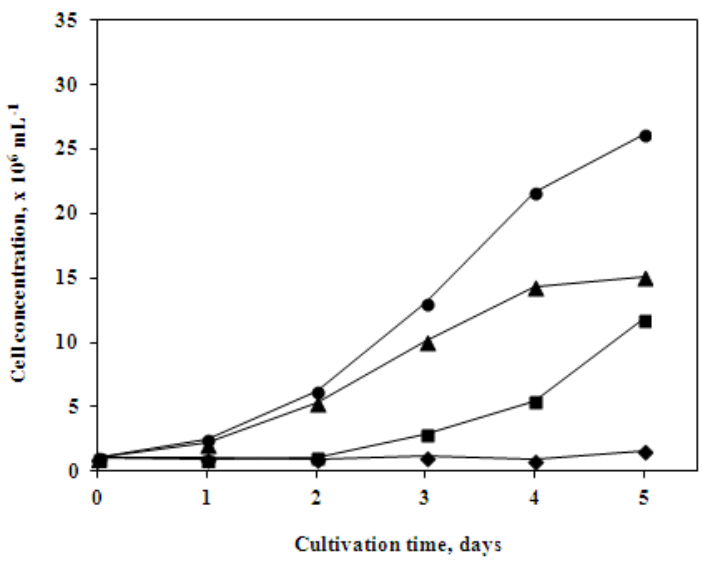

Fig. 6-3 The daily cell concentration of *Chlorella vulgaris* obtained at varied temperatures from 10 – 25 ^{0}C (♦ – 10, ■ – 15, ▲ – 20, ● – 25).

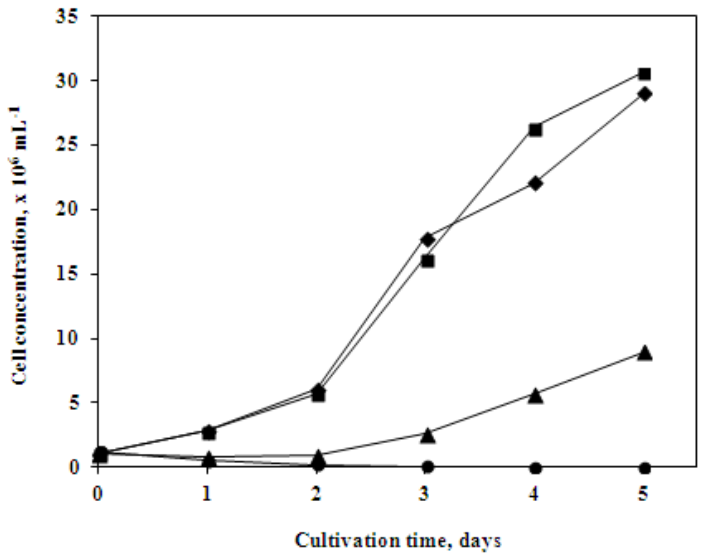

Fig. 6-4 The daily cell concentration of *Chlorella vulgaris* obtained at varied temperatures from 25 – 45 ^{0}C (♦ – 30, ■ – 35, ▲ – 40, ● – 45).

Table 6-3 Computed specific growth rate of *Chlorella vulgaris* at varied temperatures.

Temperature, ^{0}C	**Specific cell growth rate, day^{-1}**					
	Day 1	**Day 2**	**Day 3**	**Day 4**	**Day 5**	**Average**
10	0.03	-0.09	0.21	-0.27	0.57	**0.09**
15	-0.13	0.19	0.99	0.64	0.78	**0.49**
20	0.76	0.90	0.64	0.36	0.05	**0.54**
25	0.85	0.92	0.74	0.51	0.19	**0.64**
30	0.98	0.75	1.07	0.22	0.27	**0.66**
35	0.96	0.71	1.04	0.49	0.15	**0.67**
40	-0.33	0.11	0.68	0.79	0.45	**0.42**
45	-0.81	-0.94	-1.35	-2.55	0.00	**-1.13**

6.3.2. The effect of CO_2 on the growth of *Chlorella vulgaris*

The daily cell concentration of *Chlorella vulgaris* obtained under varied levels of CO_2 and cultivated in a 0.4 L PBR is presented in **Fig. 6-5.** The significant increase of cell concentration is very obvious as the amount of CO_2 supply for the cells is increased. The daily cell concentrations under 10 % level of CO_2 have displayed an exponential growth from day 2 to Day 5. The same observation can be seen under 7 % level of CO_2, however, significantly lower as compared to under 10 % level of CO_2. The daily cell concentrations under 0.035 % (air) and 3 % have consistently displayed significantly lower values and still have not yet encounter the exponential growth stage. The computed specific cell growth rate per day of *Chlorella vulgar* as affected by the amount of CO_2 level supplied in the PBR is presented in **Table 6-4**. The highest specific growth rate was observed in Day 3 under 10 % levels of CO_2 with approximately 1.99 day^{-1}. Day 1 and 2 of the same CO_2 level also posted higher specific growth rate which is approximately 1.62 and 1.82 day^{-1}, respectively. After 8 days of cultivation in the 0.4 L PBR, the average specific growth rates under CO_2 levels on 0.035 % (air), under 3 %, under 7 % and under 10 % were 0.44, 0.51, 0.61, 0.97 day^{-1}, respectively. Aside from the quantitative analysis, visual comparison of the effect of CO_2 on growth of the cells from the start, middle and the last day of the laboratory experiment is hereby presented in **Fig. 6-6**. Comparing the specific daily growth rates obtained for the temperature and CO_2 experiments, the specific growth rates obtained in the CO_2 experiment are significantly higher especially when the amount of CO_2 is increased. This is expected since the recommended temperature for the growth of

cells was provided in the CO_2 experiment while no amount of CO_2 was supplied in the temperature experiment. Since CO_2 supply is one of the main growth factors for microalgae, in the larger scale cultivation in the 30 L PBRs, under 10 % level of CO_2 will be supplied for the cells.

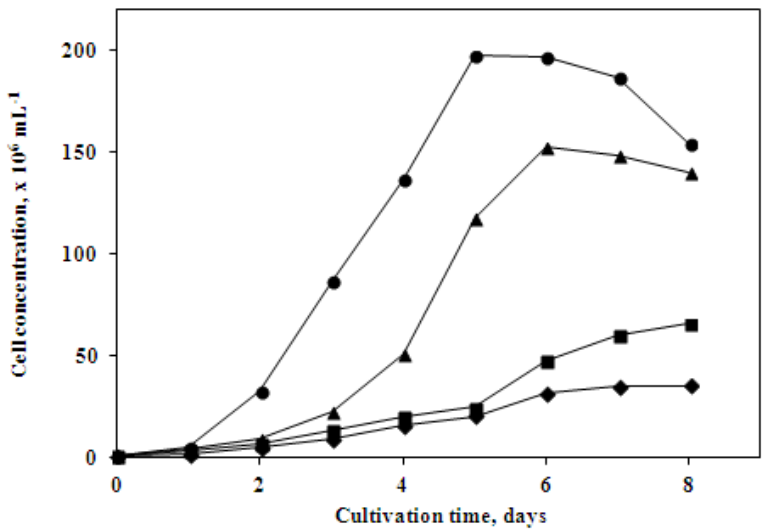

Fig. 6-5 The daily cell concentration of *Chlorella vulgaris* obtained at varied levels of CO_2 (♦ – air, ■ – under 3 %, ▲ – under 7 %, ● – under 10 %).

Table 6-4. The computed growth rate of *Chlorella vulgaris* at varied CO_2 level.

CO_2 level	Specific cell growth rate, day^{-1}								
	Day1	**Day2**	**Day3**	**Day4**	**Day5**	**Day6**	**Day7**	**Day8**	**Ave.**
0.035 %	0.71	0.88	0.64	0.54	0.24	0.44	0.10	0.01	**0.44**
Under 3 %	1.26	0.57	0.72	0.39	0.19	0.66	0.23	0.09	**0.51**
Under 7 %	1.38	0.87	0.85	0.80	0.84	0.26	-0.08	-0.06	**0.61**
Under 10%	1.62	1.82	1.99	1.45	1.36	-0.09	-0.15	-0.25	**0.97**

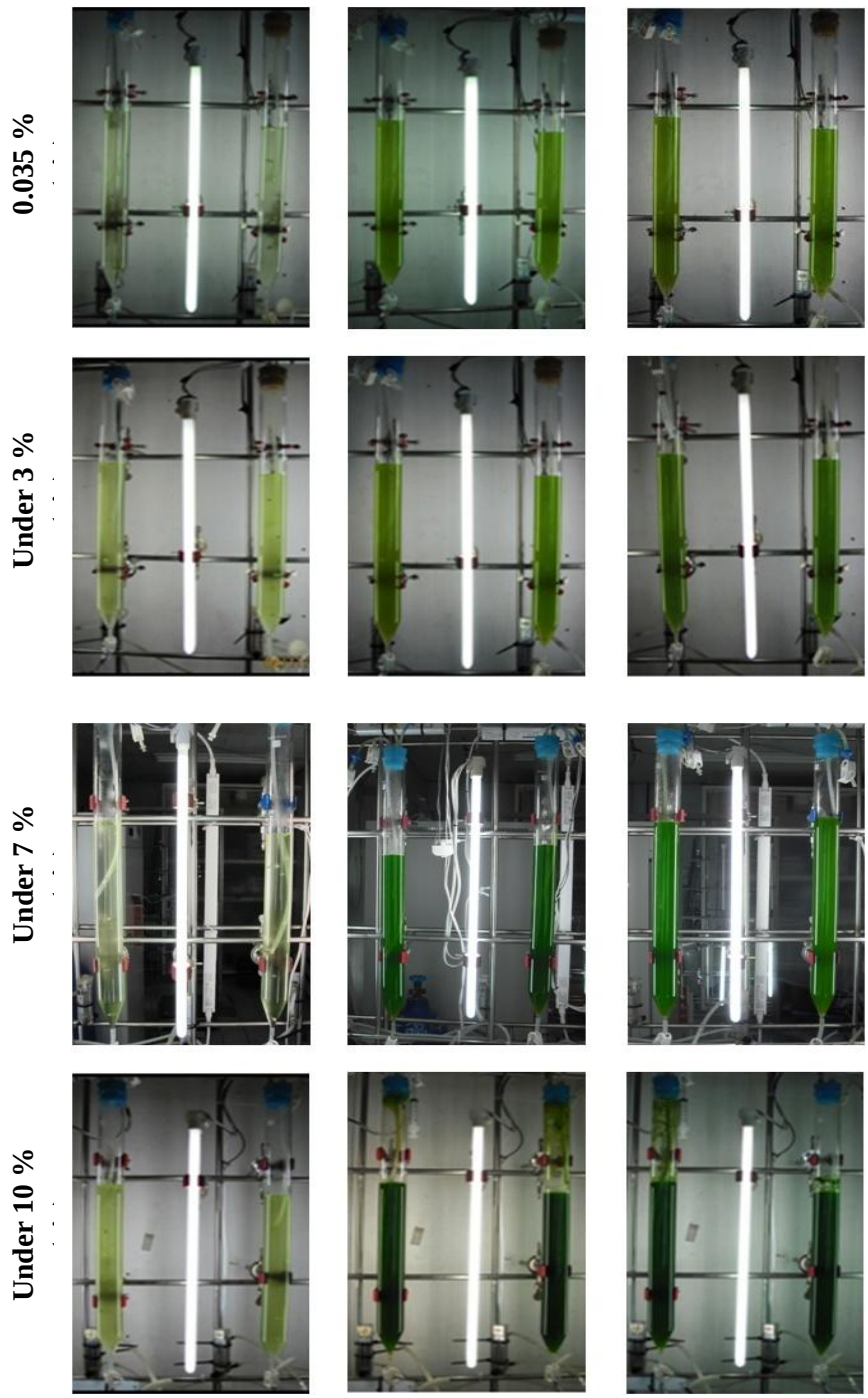

Fig. 6-6 Visual comparison of the growth of *Chlorella vulgaris* from the start, middle and the last day of the experiment at varied levels of CO_2 supply.

6.3.3. Cultivation in 30 L PBRs

The comparison of growth obtained in the actual cultivation of microalgae in the 30 L PBRs is the goal of the study. However, other factors which are also equally important which are can be contributory to obtaining the maximum growth of the cells is initially presented here such as the actual effect of flow rate and mixing which were earlier investigated. The mixing characteristics inside the PBRs were also discussed based on the biomass concentration measured daily during the actual cultivation.

6.3.3.1 Air flow rate in the 30 L PBR

In Chapter 5, hydrodynamic investigations have shown that air flow rate have significant influence in terms of the volume percentages of dead zones in the PBRs. The dead zones are strongly suspected for cells settling and coagulation to occur. To prove this, experiments under varied flow rate can be easily conducted in the actual scenario. This will also initially confirm the minimum air flow rate found out in Chapter 5 which is enough to cause movement of the culture medium at the same time minimizes the settling of the cells to the bottom part of the PBRs. Thus, both PBRs were initially supplied with cells with biomass concentration of approximately 3.0 g L^{-1} and then air was injected at varied air flow rates from 0.05, 0.10, 0.15 and 0.20 vvm which corresponds to 1.5, 3.0, 4.5 and 6.0 L min^{-1}, respectively for a couple of hours in each flow rate. Results have shown that with an air flow rate of 0.05 vvm, significant biomass content of the culture medium

have easily settle down to the bottom while some were attached on the walls of the PBR particularly for the typical design. This observation can be easily seen in **Fig. 6-7** comparing both PBRs. The region where the cells are attached particularly at the bottom and to the walls is highlighted. Most of the cells also settled down to the bottom part of the typical PBR, thus, the upper portion is seen to be more transparent. This is not observed in the upgraded PBR. Based on visual observation, the protruded cone-shaped design of the bottom part of the upgraded PBR has shown to eliminate the dead zones thus no settling of biomass is seen. Increasing the air flow rate to 0.10 vvm have visually shown to stop the settling of the biomass to the bottom and also prevented the biomass to be attached to the walls particularly for the typical PBR. It was also observed that the flow rate is enough to instill fluid movement inside the PBR. Increasing further the air flow rate to 0.15 and 0.20 vvm have shown to significantly cause higher turbulence inside the PBR; however, this as discussed in Chapter 5, this might be carefully suspected to be too much for the cells to contain the shearing effect due to the high turbulence. Therefore, based on results of these initial tests, the two sets of succeeding experiments then utilizes air flow rate of 0.10 vvm in both the typical and upgraded PBR. In the upgraded PBR with an air flow rate of 0.10 vvm and nozzle diameter of 10 vvm, this actually falls to case $A_2B_2C_2$ which is also one of the cases being recommended in Chapter 5.

Typical PBR Upgraded PBR

Fig. 6-7 Effect of air flow rate on the flow characteristics and the settling of cells to the bottom of the PBRs.

6.3.3.2. Mixing analysis in the 30 L PBR

The biomass concentration measured separately from the top, middle and bottom part of the PBRs can be carefully discussed and can be correlated to the mixing characteristics inside the PBRs. Presented in **Figs. 6-8 and 6-9** the estimated biomass concentration measured particularly for the typical and upgraded PBR, respectively for Experiment 1. From the start of the experiment until day 2, the initial biomass concentration measured from the top, middle and bottom part of the PBR posted almost equal amount of biomass concentration for both PBRs. It can therefore be assumed that the biomass content inside the PBRs was equally

distributed. However, the biomass concentrations measured from Day 4 onwards have shown different results. The biomass concentration differs significantly in the typical PBR wherein higher values were obtained in the following order, at the bottom, middle and top part of the PBR. It can therefore be wisely assumed that mixing during this cultivation period for the typical PBR is not sufficient to obtain uniformity inside the typical PBR. In contrast, the biomass concentrations measured from the various location of the upgraded PBR have shown almost equal values throughout the duration of the experiment. Similar results were also found in Experiment 2 where the biomass concentration obtained from the bottom part of the typical PBR posted higher values compared to the biomass concentration obtained in the middle and top of the PBR while no significant differences of biomass concentration were observed in terms of sampling locations for the upgraded PBR. These results could somehow lead us further into the conclusion that mixing in the upgraded PBR is significantly improved compared to the typical PBR which can be attributed with the cone-shaped geometry of the bottom part of the PBR and the installed internal baffle. The flow of the culture medium in the upgraded PBR can be assumed to be more uniform in movement from the bottom going upward to the inner cylinder (baffle) then cycles downward from the top to the outer part of the inner cylinder.

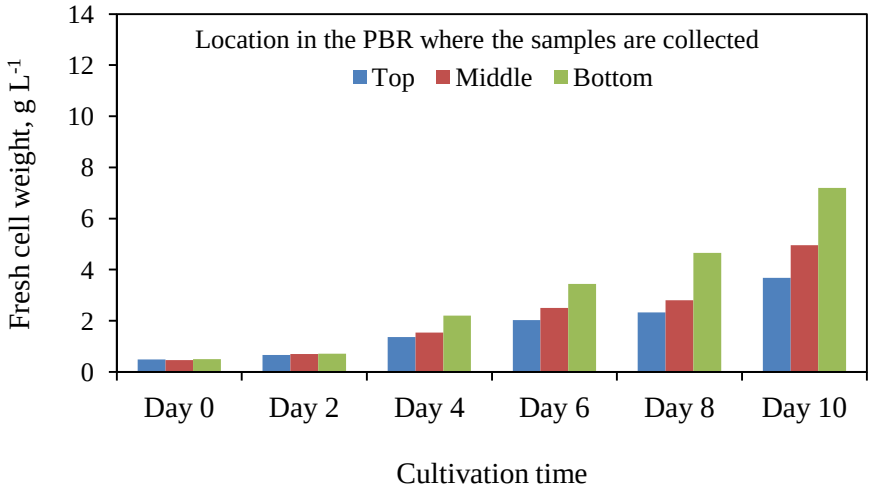

Fig. 6-8 Biomass concentration measured from the top, middle and bottom part of the typical PBR in Experiment 1.

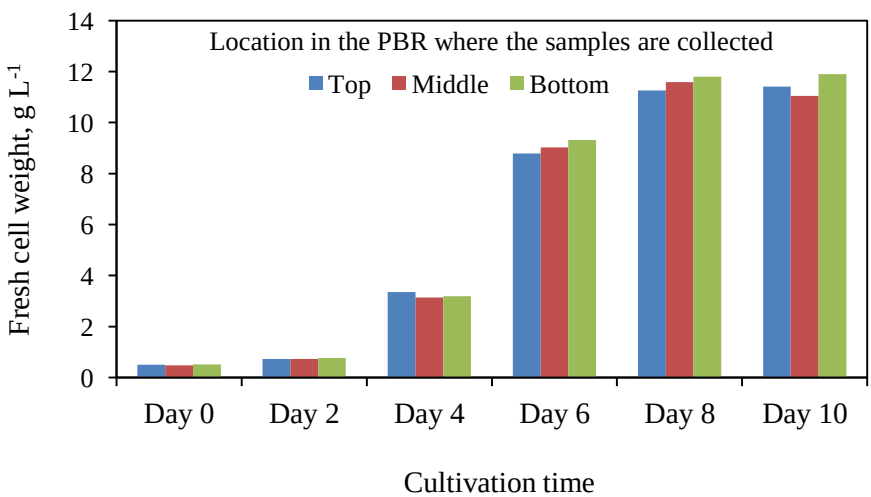

Fig. 6-9 Biomass concentration measured from the top, middle and bottom part of the upgraded PBR in Experiment 2.

6.3.3.3. Fresh cell weight and specific growth rate

The fresh cell weight of *Chlorella vulgaris* measured from the typical and upgraded PBR for Experiment 1 is presented in **Fig. 6-10**. From the figure, higher cell concentrations can be achieved in Days 7, 8, and 9 for the upgraded PBR with values of approximately 11.17, 11.55 and 11.96 g L^{-1}, respectively. The maximum concentration was achieved in Day 10 for the typical PBR with 5.26 g L^{-1}. Computing the average cell concentration for the upgraded PBR where the concentration is divided with the days of cultivation gives values of 1.60, 1.44 and 1.33 g L^{-1} for Day 7, 8 and 9 respectively. Obviously, Day 7 gives the highest average cell concentration which clearly shows that maximum cultivation of microalgae can be achieved three days earlier for the upgraded PBR compared to the typical PBR. The decrease in time duration in obtaining higher cell concentration using the upgraded PBR is very significant. For instance, in one month duration, batch cultivation of microalgae can be implemented four times in the upgraded PBR while only three batch cultivation can be achieved in the typical PBR. Furthermore, the average cell concentration for the typical PBR is only approximately 0.53 g L^{-1} as compared to the upgraded PBR which is 1.60 g L^{-1}. From the start of cultivation up to Day 3, the biomass concentration obtained from both PBRs have shown very minimal increase in growth which can be assumed that the cells are in their adaptation phase. The exponential growth phase of microalgae cultivated in the upgraded PBR was obtained in Day 3 to Day 7, thus delivering higher multiplication of cells. The typical PBR shows slightly increasing growth wherein an exponential type of cell multiplication is not observed.

In terms of their specific growth rates, the maximum specific growth rate for the typical PBR is obtained in Day 4 with approximate value of 2.21 day^{-1}, while approximately 2.58 day^{-1} was achieved in the upgraded PBR in Day 5 (**Table 6.5**). Estimating their maximum productivity, in g L^{-1} day^{-1}, which is computed by multiplying the maximum specific growth rate (day^{-1}) and the average fresh cell weight or density (g L^{-1}) yields a productivity of approximately 1.15 g L^{-1} day^{-1} and 3.43 g L^{-1} day^{-1} for the typical PBR and the upgraded PBR, respectively.

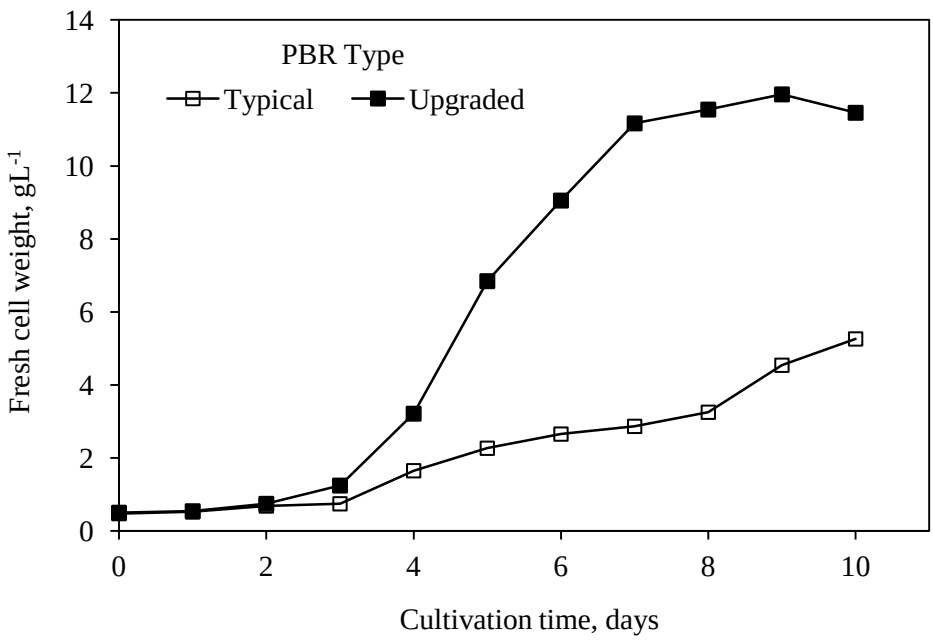

Fig. 6-10 Fresh cell weight of *Chlorella vulgaris* obtained in Experiment 1.

Table 6-5 Computed daily specific growth rate of *Chlorella vulgaris* cultivated in the 30 L PBRs for Experiment 1.

PBR type (Exp. 1)	Specific cell growth rate, day^{-1}									
	Day1	**Day2**	**Day3**	**Day4**	**Day5**	**Day6**	**Day7**	**Day8**	**Day9**	**Day10**
Typical PBR	1.10	1.31	1.09	**2.21**	1.37	1.17	1.08	1.13	1.40	1.16
Upgraded PBR	1.08	1.37	1.67	2.13	**2.58**	1.32	1.23	1.03	1.04	0.96

The results obtained from Experiment 2 displayed similar growth trend despite the higher initial biomass concentration as shown in **Fig. 6-11.** However, higher cell concentrations can be obtained in shorter time by 1 day. The peak cell concentration for the typical PBR is approximately 5.64 g L^{-1} in Day 8 and 11.55 g L^{-1} for the upgraded PBR obtained Day 6. Thus computing the average fresh cell weight concentration for Experiment 2 gives values of approximately 0.71 and 1.93 g L^{-1} for the typical PBR and the upgraded PBR, respectively.

The specific growth rate obtained in Experiment 2 is presented in **Table 6-6**. The maximum specific cell growth rate is obtained in Day 8 of approximately 1.40 day^{-1} for the typical PBR while approximately 1.56 day^{-1} was obtained for the upgraded PBR in Day 3. This further confirms the result obtained in Experiment 1 where maximum fresh cell weights are obtained in the upgraded PBR in shorter time than the typical PBR.

Estimating the maximum productivity of the PBRs applying similar procedure from Experiment 1, yield productivities of approximately 0.99 g L^{-1} day^{-1} and 3.01 g L^{-1} day^{-1} for the typical PBR and upgraded PBR, respectively. Computing the average maximum productivities for the two successive experiments shows values of approximately 1.03 g L^{-1} day^{-1} and 3.23 g L^{-1} day^{-1} for the typical PBR and upgraded PBR, respectively. This posted an increase of productivity of approximately 314 % in utilizing the upgraded PBR.

The biomass productivity obtained particularly from the 30 L upgraded PBR can be compared with productivities reported in literatures. Most literatures reported productivities in dry weight basis where it is generally four times lower than the fresh weight value. Thus, for the 30 L upgraded PBR in this study, the productivity in dry weight basis can be approximately 0.81 g L^{-1} day^{-1}. The value is lower compared to the maximum productivity obtained for *Chlorella sorokinian* which is approximately 1.47 g L^{-1} day^{-1} obtained in an inclined tubular PBR (Ugwu *et al*., 2002). Other reports are also higher such as Fernandez *et al*. (2001) and Hall *et al*., (2003) who estimated the maximum productivity of *Phaeodactrylum tricornutum* to approximately 1.40 and 1.2 g L^{-1} day^{-1} obtained in a helical tubular PBR and an airlift PBR, respectively. Higher biomass productivities are also obtained for other microalgae species such as *Phaeodactylum tricomutum* cultivated in a 200 L airlift design PBR with approximately 1.90 g L^{-1} day^{-1} (Molina *et al*., 2001) and *Arthrospira platensis* with a productivity 2.70 g L^{-1} day^{-1} cultivated in 11 L tubular PBR. However, the productivity obtained in this study was found to be higher compared to other species such as *Haematococcus pluvalis*

and *Nannochloropsis sp.* where the reported productivities were approximately 0.06 and 0.27 g L^{-1} day^{-1} as reported by Olaiza (2000) and Wu *et al.*, (2001), respectively. Nevertheless, it should be noted that the productivity of microalgae depends on many factors such as the type of PBR, the method of cultivation, the microalgae specie, the nutrients supplied, etc.

Visual comparison of the growth of microalgae cells in the 30 L PBRs is also presented in **Fig. 6-12** particularly for Experiment 1. A difference specifically in color of culture medium and the collected samples can be significantly distinguished between the typical and the upgraded PBRs from both experiments.

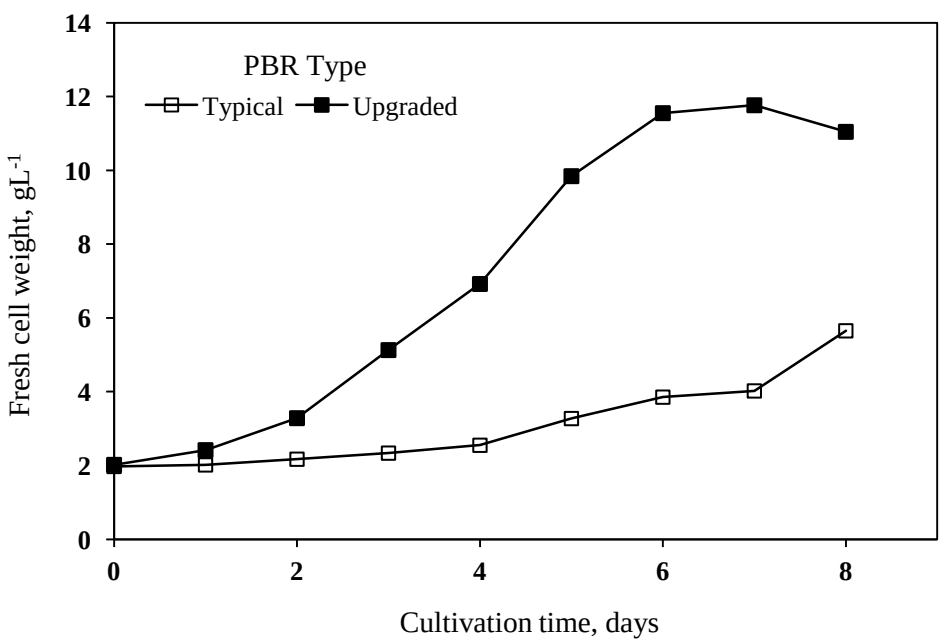

Fig. 6-11 Fresh cell weight of *Chlorella vulgaris* obtained in Experiment 2.

Table 6-6 Computed daily specific growth rate of *Chlorella vulgaris* cultivated in the 30 L PBRs for Experiment 2.

PBR type (Exp. 2)	Specific cell growth rate, day^{-1}							
	Day 1	**Day 2**	**Day 3**	**Day 4**	**Day 5**	**Day 6**	**Day 7**	**Day 8**
Typical PBR	1.02	1.08	1.08	1.09	1.28	1.18	1.04	**1.40**
Upgraded PBR	1.20	1.36	**1.56**	1.35	1.42	1.17	1.02	0.94

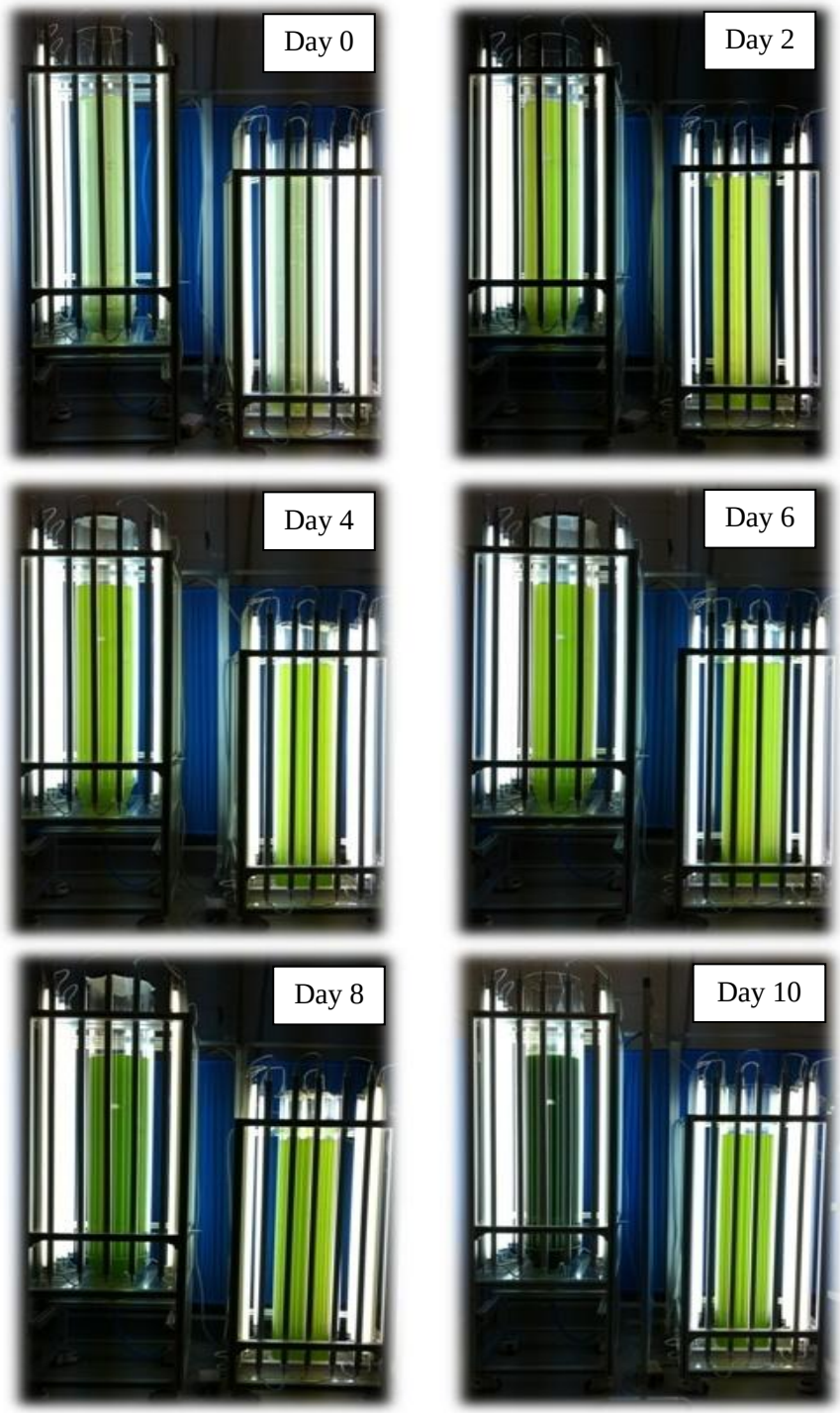

Fig. 6-12 Visualization on the growth of *Cholera vulgaris* cultivated in the PBRs for Experiment 1 (Left side: upgraded PBR; right side: typical PBR).

6.4. Conclusions

In engineering perspective, the structural configuration and design of the PBRs have critical role in the flow hydrodynamics which is also important in providing ideal growth conditions for the cells. Hence, in this study, *Chlorella vulgaris* were cultivated in 30-L culture medium cylindrical bubble column PBRs and investigation was focused on comparing the biomass concentration of the algal cells in a typical PBR design versus an upgraded design recommended from the numerical investigated conducted in Chapter 5.

The upgraded PBR was constructed with internal baffle to improve the circulation of culture medium within the PBR. Likewise, the geometry of the bottom part of the upgraded PBR was protruded and vertical cone-shape design to eliminate the dead zones and in turn prevent settling and coagulation of the cells to the bottom of the PBR. Both PBRs were injected with equal levels of CO_2 and continuously supplied with approximately 560 kW light from 20 pcs of 28-kW fluorescent bulbs which were installed in every side surrounding the PBRs.

Two successive experiments were conducted wherein Experiment 1 was finished in 10 culturing days while Experiment 2, 8 days. The decision to terminate the experiments depended on the biomass concentration when it reached its peak value and the growth rate starts to decline.

The average fresh cell weight of *Chlorella vulgaris* measured from Experiment 1 in the upgraded PBR is approximately 1.60 g L^{-1} as compared to approximately 0.53 g L^{-1}, for the typical PBR. The maximum fresh cell weight in the upgraded

PBR can be achieved in 7 days as compared to the typical PBR which is 10 days. The decrease in time duration in obtaining higher cell concentration using the upgraded PBR is very significant since lesser time for cultivation can result to more production. For instance, in one month duration, batch cultivation of microalgae can be implemented four times in the upgraded PBR while only three batch cultivation can be achieved in the typical PBR. In terms of their specific growth rates, the maximum specific growth rate for the typical PBR is approximately 2.21 day^{-1}, while approximately 2.58 day^{-1} was achieved in the upgraded PBR. Estimating their maximum productivities yields approximately 1.15 g L^{-1} day^{-1} and 3.43 g L^{-1} day^{-1} for the typical PBR and the upgraded PBR, respectively.

The results obtained from Experiment 2 with higher initial cell concentration can lessen the time to achieve maximum cell concentration to about a day. Computing the average fresh cell weight concentration for Experiment 2 gives values of approximately 0.71 and 1.93 g L^{-1} for the typical PBR and the upgraded PBR, respectively. In terms of the specific growth rate, maximum values of 1.28 day^{-1} for the typical PBR is obtained while approximately 1.56 day^{-1} was obtained for the upgraded PBR. Estimating the maximum productivity of the PBRs for Experiment 2, yield productivities of approximately 0.91 g L^{-1} day^{-1} and 3.01 g L^{-1} day^{-1} for the typical PBR and upgraded PBR, respectively. Computing the average maximum productivities for the two successive experiments shows values of approximately 1.03 g L^{-1} day^{-1} and 3.23 g L^{-1} day^{-1} for the typical PBR and upgraded PBR, respectively posting an increase of productivity of approximately 314 % in utilizing the upgraded PBR.

7. General conclusions

The current studies conducted for this dissertation have utilized four main approaches to realize the set objectives of the research study. These approaches include CFD review, particle image velocimetry, computational fluid dynamics simulations and experiment thru practical cultivation of microalgae in photobioreactors.

The review has provided profound understanding on the application of numerical approaches in designing appropriate photobioreactors tailored for maximum cultivation of microalgae. Most numerical approaches have utilized computational fluid dynamics technique in designing photobioreactors which have shown to be very effective while significantly reducing time, labor and cost in the conducting the research. However, the approach must be strongly validated first to establish its reliability and gain confidence in applying the technique. This also ensures that correct results are obtained.

Validation of the CFD approach and technique in the design of photobioreactors can be conducted via laboratory or field experiments. In this study, particle image velocimetry or PIV was conducted with 8 experimental cases. The flow fields particularly the average velocity magnitude obtained inside the photobioreactors using PIV were compared with the CFD results. The CFD approach varied the mesh grid sizes in the design of the photobioreactor and obtains the average velocity magnitude. Results revealed that a mesh grid size of 0.005 m is appropriate in the design which showed a difference of less than 10%

when compared with the PIV computed data. The result is also in consonance with similar numerical studies on photobioreactors where a 0.004 m grid size was recommended (Seo *et al*., 2012). The approach of utilizing the Lagrangian-Eulerian multiphase model and RNG k-ε turbulence model was also validated. The use of the multi-phase model and the RNG k-ε turbulence have become popular since the simulation results obtained as presented in several studies have shown to be closer to the actual phenomenon.

Simulation of PBRs with 32 simulation cases was conducted which is comprised from four varied air flow rates, four varied nozzle size diameters and two photobioreactor geometry design. These photobioreactors were evaluated in terms of the major hydrodynamic parameters such as the volume percentages of dead zones, the average circulation time and turbulence intensity. The selection of which appropriate photobioreactor is appropriate for microalgae cultivation was done by setting a criteria as follows: 1) the volume percentages of dead zones should not exceed 10%; 2) the average circulation time should be within 10 s and the turbulence intensity must fall from low to moderate turbulence category based on Fluent method evaluating turbulence. This elimination technique is considered first of its kind in evaluating the photobioreactors where the three major hydrodynamic parameters were combined in the selection process. Based on the evaluation criteria, the recommended air flow rate was found to be from 0.10 vvm to 0.15 vvm while the nozzle size diameter is 10 mm. The PBR design with internal baffle and protruded bottom part was also found to display better hydrodynamic characteristics thus the design is recommended for microalgae cultivation.

A practical cultivation of microalgae immediately followed where the recommended photobioreactor design and operating parameter was implemented. The cultivation of microalgae was done in a 30L PBR using the typical design and the design recommended based form the simulation study and referred here as the upgraded design. Two successive experiments were conducted and the biomass concentrations and the specific growth rates obtained the typical photobioreactor and the upgraded design was compared. Results have shown that the upgraded design delivered higher fresh cell weight concentration and specific growth rates compared to the typical photobioreactor. Computing the average maximum productivities for the two successive experiments shows values of approximately 1.03 g L^{-1} day^{-1} and 3.23 g L^{-1} day^{-1} for the typical PBR and upgraded PBR, respectively posting an increase of productivity of approximately 314 % in utilizing the upgraded PBR. Therefore, based from the simulation results and supported with experimental proof that was practically conducted, the upgraded design is strongly recommended for microalgae cultivation.

Furthermore, the results have shown the applicability of numerical simulation technique in the design of photobioreactors which can significantly reduce time, labor and cost.

8. References

Ai, W., Guo, S., Qin L, Tang, Y., 2008. Development of a ground-based space micro-algae photo-bioreactor. Advances in Space Research 41: 742-7.

Akhtar, A., Pareek, V., Tade, M., 2007. CFD simulations for continuous flow of bubble through gas-liquid columns: application of VOF method. The Berkeley Electronics Press Vol. 2, Issue 1, Article 9.

Apt, K.A., Behrens, P.W., 1999. Commercial developments in microalgal biotechnology. Journal of Phycology 35: 215-26.

Ayed, H., Chahed, J., Roig, V., 2007. Hydrodynamics and mass transfer in a turbulent buoyant bubbly shear layer. AIChE Journal 53, 2742–53.

Bakker, A., 2002. Applied computational fluid dynamics, Lecture 17: Multiphase flows. Fluent Inc.

Bannari, R., Bannari, A., Selma, B., Proulx, P., 2011. Mass Transfer and shear in an airlift bioreactor: using a mathematical model to improve reactor design and performance. Chemical Engineering Science Vol 66, Issue 10, pp 2057-2067.

Barbosa, M.J., 2003. Microalgal photobioreactors: Scale-up and optimization. Ph.D. Thesis, Wageningen University, Wageningen, The Netherlands.

Barbosa, M.J., Hadiyanto, Wijffels, R.H., 2004. Overcoming shear stress of microalgae cultures in sparged photobioreactors. Biotechnology and Bioengineering 85(1):78-85.

Barkley, W.C.W., Lewin, R.A., Cheng. L., 1987. I*n*: Sadler T, editor. Development of microalgal systems for the production of liquid fuels. Applied Science; Villeneuve d'Ascq, France.

Baten, J.M., Ellenberger, J., Krishna, R., 2003. Hydrodynamics of internal air-lift reactors: experiments versus CFD simulations. Chemical Engineering and Processing 42: 733-42.

Bertola, F., Vanni, M., Baldi, G., 2003. Application of computational fluid dynamics to multiphase flow in bubble columns. International Journal of Chemical Engineering Vol.1, Article A3.

Blazey, M., Glover, C., Generalis, S.C., Markos J., 2004. Gas-liquid simulation of an airlift bubble column reactor. Chemical Engineering and Processing 43: 137-44.

Bitog, J.P., Lee, I.B., Yoo, J.I., Hwang, S.B., Hong, S.W., Seo, I.H., et al., 2009. Development of a large-sized photobioreactor for microalgae production. *In*: Proceedings of the 2009 CIGR International Symposium of the Australian Society for Engineering in Agriculture, Brisbane, Queensland, Australia, Sept. 13-16.

Borowitzka, M.A., 1999. Commercial production of microalgae: ponds, tanks, tubes and fermenters. Journal of Biotechnology 70: 313-21.

Camacho, R.F., Garcıa, C.F., Sevilla. F.J.M., Chisti, Y., Molina, G.E., 2003. Mechanistic model of photosynthesis in microalgae. Biotechnology Bioengineering 81: 459-73.

Carvalho, A.P., Meireles, L.A., Malcata, F.X., 2006. Microalgal reactors: a review of enclosed system designs and performances. Biotechnology Progress 22: 1490-1506.

Cassidy, K.O., 2011. Evaluating algal growth at different temperatures. MS Thesis, College of Engineering, University of Kentucky, U.S.A.

Celik, I., 1993. Numerical uncertainty in fluid flow calculations: needs for future research. ASME Journal of Fluid Engineering 115: 194-95.

Chaumont, D., 1993. Biotechnology of algal biomass production: a review of systems for outdoor mass culture. Journal of Applied Phycology 5: 593-604.

Chen, P., Sanyal, J., Dudukovic, M.P., 2005. Numerical simulation of bubble columns flows: Effect of different breakup and coalescence closures. Chemical Engineering Science 60: 1085-1101.

Chen, C.Y., Durbin, E.G., 1994. Effects of pH on the growth and carbon uptake of marine phytoplankton. Marine Ecology Progress Series Vol. 109: 83-94.

Chinnasamy, S., Ramakrishnan, B., Bhatnagar, A., Das, K.C., 2009. Biomass Production Potential of a Wastewater Alga *Chlorella vulgaris* ARC 1 under Elevated Levels of CO_2 and Temperature. International Journal of Molecular Sciences 10: 518-532.

Chiu, S-Y., Tsai, M-T., Kao, C-Y., Ong, S-C., Lin, C-S., 2009. The air-lift photobioreactors with flow patterning for high-density cultures of microalgae and carbon dioxide removal. Engineering in Life Sciences Vol 9, Issue 3, pp 254–260.

Chisti, Y., 2007. Biodiesel from microalgae. Biotechnology Advances 25: 294-306.

Chisti, Y. 1989. Airlift Bioreactors, Elsevier, London, UK.

Choudhury, D., 1993. Introduction to the Renormalization Group Method and Turbulence Modeling. Fluent Inc. Technical Memorandum TM-107.

Choi, S.L., Suh, I.S., Lee, C.G., 2003. Lumostatic operation of bubble column photobioreactors forHaematococcus pluvialis cultures using a specific light uptake rate as a control parameter. Enzyme and Microbial Technology 33 (4): 403–409.

Conley, S.P., 2006. What is Biodiesel? BioEnergy, Purdue Extension, Department of Agricultural and Biological Engineering, Purdue University, ID 337.

Contreras, A., Garcia, F., Molina, E., Merchuk, J.C., 1998. Interaction between CO_2-mass transfer, light availability, and hydrodynamic stress in the growth of *Phaeodactylum tricornutum* in a concentric tube airlift photobioreactor. Biotechnology and Bioengineering Vol. 60, No. 3.

Converti, A., Casazza, A.A., Ortiz, E.Y., Perego, P., Del Borghi, P., Del Borghi, M., 2009. Effect of temperature and nitrogen concentration on the growth and lipid content of *Nannochloropsis oculata* and *Chlorellavulgaris* for biodiesel production. Chemical Engineering and Processing: Process Intensification Vol 48, Issue 6, pp 1146-1151.

Darzins, A., Pienkos, P., Edye, L., 2010. Current status and potential for algal biofuels production: A report to the IAE Bioenergy Task 39. http://www.task39.org/.

Deckwer, W.D., 1992. Bubble Column Reactors. J. Wiley & Sons LTD, Chichester.

Degen, J., Uebele, A., Retze A., Schmid-Staiger, U., Trosch, W., 2001. A novel airlift photobioreactor with baffles for improved light utilization through the flashing light effect. Journal of Biotechnology 92: 89-94.

Delnoij, E., Kuipers, J.A.M., van Swaaij, W.M., 1999. A three-dimensional CFD model for gas-liquid bubble columns. Chemical Engineering Science 54: 2217-26.

Delnoij, E., Kuipers, J.A.M., van Swaaij, W.M., 1997. Computational fluid dynamics applied to gas-liquid contactors. Chemical Engineering Science 52: 3623-38.

Dhotre, M.T., Smith, B.L., Niceno, B., 2007. CFD simulation of bubbly flows: Random dispersion model, Chemical Engineering Science 62, 7140 –50.

Ekambara, K., Dhotre, M.T., Joshi, J.B., 2005. CFD simulations of bubble column reactors: 1D, 2D and 3D approach. Chemical Engineering Science 60: 6733-46.

Eriksen, N.T., 2008. The technology of microalgal culturing. Biotechnology letters 30(9): 1525-1536.

Fan, L., Zhang, Y., Cheng, L., Zhang, L., Tang, D., Chen, H., 2007. Optimization of carbon dioxide fixation by *Chlorella vulgaris* cultivated in membrane-photobioreactor. Chemical Engineering Technology 30, No. 8. 1094-99.

Fernandes, B.D., Dragoner, G.M., Teixiera, J.A., Vicente, A.A., 2010. Light regime characterization in an airlift photobioreactor for production of microalgae with high starch content. Applied Biochemical Biotechnology 161:218–26. Fluent manual, 2006. Fluent Co., New Hampshire, USA.

Fogg, G.E., Thake, B., 1987. Algal cultures and phytoplankton ecology. University of Wisconsin Press (Madison, Wisconsin, USA, 3rd edition.

Gimbun, J., 2009. Assessment of the turbulence models for modeling of bubble column. The Institution of Engineers Journal, Malaysia Vol. 70, No.4.

Glover, C.G.M., Generalis, S.C., 2004. Gas-liquid-solid flow modeling in a bubble column. Chemical Engineering and Processing 43: 117-26.

Glover, C.G.M., Generalis, S.C., Thomas, N.H., 2000. CFD and bubble column reactors: simulation and experiment. Chem. Papers 54 (6a): 361-69.

Grace, J.R., Taghipour, F., 2004. Verification and validation of CFD models and dynamic similarity for fluidized beds. Powder Technology 139: 99-110.

Gudin, C., Chaumont, D., 1991. Cell fragility-key problem of microalgae mass production on closed photobioreactors. Bioresource Technology 38: 145-151.

Hauck, J.T., Olson, G.J., Scierka, S.J., Perry, M.B., Ataai, M.M., 1996. Effects of simulated flue gas on growth of microalgae. Abstracts of Papers. American Chemical Society, 212 Meeting, Pt.1, Fuel 118. Orlando, FL, 25–29 August 1996.

Hideki, K., Shunsuke, K., Michikata, K., Junichi, S., Osamu, O., 1999. Flow Visualization of Turbulent Co-flowing Air in Vicinity of Jet Diffusion Flames by Using PIV. Vol. 4, pp 387-388.

Hirt, C.W., Nichols, B.D., 1981. Volume of Fluid (VOF) method for the dynamics of free boundaries. Journal of computational physics , Vol. 39, 201-225.

Huang, Q., Yang, C., Yu, G., Mao, Z., 2010. CFD simulation of hydrodynamics and mass transfer in an internal airlift loop reactor using a steady two-fluid model. Chemical Engineering Science 65: 5527–36.

Huilin, L., Yurong, H., Gidaspow, D., 2003. Hydrodynamic modelling of binary mixture in a gas bubbling fluidized bed using the kinetic theory of granular flow. Chemical Engineering Science 58: 1197-205.

Hutmacher, D., Singh, H., 2008. Computational fluid dynamics for improved bioreactor design and 3D culture. Opinion, Cell Press.

Illman, A.M., Scragg, A.H., Shales, S.W., 2000. Increase in Chlorella strains calorific values when grown in low nitrogen medium. Enzyme and Microbial Technolgy 27: 631-635.

Irani, M., Khodagholi, M.A., Investigation of a bubble column hydrodynamics using CFD simulations (2D and 3D) and experimental validation. Petroleum and Coal, ISSN 1337 – 1727.

Jansen, M., Tramper, J., Mur, L.R., Wijffels, R., 2003. Enclosed photo bioreactors: light regime photosynthetic efficiency, scale-up and future prospect. Biotechnology and Bioengineering 81, 2.

Jiang, Y., Khadilkar, M.R., Al-Dahhan, M.H., Dudukovic, M.P., 2002. CFD of Multiphase flow in packed-bed reactors: I. *k*-fluid modeling issues. AIChE Journal Vol. 48, No. 4.

Joshi, J.B., 2001. Computational flow modelling and design of bubble column reactors. Chemical Engineering Science 56: 5893-933.

Kaewpintong, K., Shotipruk, A., Powtongsook, S., Pavasant, P., 2007. Photoautotrophic high-density cultivation of vegetative cells of *Haematococcus pluvialis* in airlift bioreactor. Bioresource Technology Vol 98, Issue 2, pp 288-295.

Kazunori, H., Toyohiko, S., Yoshitaka, O., 2006. Reconstruction of the complex flow with POD method (Application to flows passing across tube banks measured by PIV method). Kashika Joho Gakkai Ronbunshu (Web) Vol. 26, No. 12. pp114-122.

Kchmond ,A., 1988. Spirulina. *In*: Micro-algal Biotechnology. Cambridge University Press, Cambridge, pp 85-121.

Kcmond, A., Lichtenberg, E., Stahl, B.,Vonshak, A., 1990. Quantitative assessment of the major limitations on the productivity of Spialina platensis in open raceways. Journal of Applied Phycology 2: 195-206.

Kirk, J.T.O., 1994. Light and photosynthesis in aquatic systems. Cambridge University Press, Cambridge.

Kitaya, Y., Azuma, H., Kiyota, M., 2005. Effects of temperature, CO2/O2 concentrations and light intensity on cellular multiplication of microalgae, *Euglena gracilis*. Advances in Space Research 35: 1584-88.

Kommareddy, A.R., Anderson, G.A., 2005. Mechanistic modeling of photobioreactor system. ASAE Paper No. 057007. St. Joseph, Michigan: ASAE.

Kommareddy, A.R., Anderson, G.A., 2004. Analysis of currents and mixing in a modified bubble column reactor. ASAE Paper No. 043071. St. Joseph, Mich.: ASAE.

Kommareddy, A.R., Anderson, G.A., 2003. Study of light as a parameter in the growth of algae in a photo-bio reactor (PBR). ASAE Paper No. 034057. St. Joseph, Michigan: ASAE.

Kong, Q., Yu, F., Chen, P., Ruan, R., 2007. High oil content microalgae selection for biodiesel production. ASABE Paper No. 077034. St. Joseph Mich.: ASABE.

Kozic, Ristic, S., Puharic, M., Katavic, B., 2011. Comparison of Euler-Euler and Euler-Lagrange in numerical simulation of multiphase flow in ventilating mill-air mixing duct. Third Serbian Congress on Theoretical and Applied Mechanics, Vlasina lake, Serbia, July 5-8.

Krisna, R., Baten, J.M., 2002. Scaling up bubble column reactors with highly viscous liquid phase. Chemical Engineering Technology 25: 10.

Krishna, R., Baten, J.M., 2001. Scaling up bubble column reactors with the aid of CFD. Trans IChemE Vol 79, Part A.

Krishna, R., Baten, J.M., 1999. Rise characteristics of gas bubbles in 2D rectangular column. VOF simulations vs experiments. International Communications in Heat and Mass Transfer Vol. 26: 4913-20.

Krishna, R., Baten, J.M., Urseanu, M.I., 2000. Three- phase Eulerian simulation of bubble column reactors operating in the churn-turbulent regime: a scale up strategy. Chemical Engineering Science 55: 3275-86.

Launder, B.E., Spalding, D.B., 1972. Lecture on mathematical models of turbulence. Academic Press, London.

Lain, S., Broder, D., Sommerfeld, M., 2001. Numerical simulations of the hydrodynamics in a bubble column: Quantitative comparison with experiments, in: Proceedings of the International Conference on Multiphase Flow, New Orleans, USA, May 27 - June 1, 2001.

Lecuona, A., Nogueira, J.I., Rodriguez, P., A., 1998. Flowfield vorticity calculation

using PIV Data. Journal of the Visualization Society of Japan Vol.1., pp 183-193.

Lee, H. S., Seo, M.W., Kim, Z. H., Lee, C. G., 2006. Determining the best specific light uptake rates for the lumostatic cultures in bubble column photobioreactors. Enzyme and Microbial Technology, 39, 447e452.

Lee, K., Lee, C.G., 2001. Effect of light/dark cycles on wastewaster treatments by microalgae. Biotechnology and Bioprocess Engineering 6 (3): 194-199.

Lee, C.G., Palsson, B.O., 1994. Hig density algal photobioreactors using light-emitting diodes. Biotechnology and Bioengineering Hig h-Density Algal Photobioreactors Using Light-Emitting Diodes Vol 44, No.10.

Lehr, A., Bölcs, A., 2000. Application of a Particle Image Velocimetry (PIV) system to the periodic unsteady flow around an isolated compressor blade. *In* proceedings: 15th Symposium on Measurement Techniques in Transonic and Supersonic Flow in Turbomachines, University of Florence, Sept. 21-22.

Leib, T.M., Pereira, C.J., Villadsen, J., 2001. Bioreactors: a chemical engineering perspective. Chemical Engineering Science 56: 5485-97.

Li, Y., Horsman, M., Wu, N., Lan, C.Q., 2008. Dubois-Calero N. Biocatalysts and bioreactor design. Article, Biotechnology Program 24: 815-20.

Li, Y., Zhang, J., Fan, L.S., 2000. Discrete-phase simulation of single bubble rise behavior at elevated pressures in a bubble column. Chemical Engineering Science 55: 459-69.

Lisec, J., 2004. Cultivation of *Pkezaroch ysis ccaterae* CCMP647 in two different photobioreactors. Diploma Ingenieur fur Allgemeine Biotechnologe. Thesis, Techsche Universitat Berlin 93.

Lorstad, D., Fuchs, L., 2004. High-order surface tension VOF-model for 3D bubble flows with high density ratio. Journal of Computational Physics 200: 153–76.

Lou, H.P., Al-Dahhan, M.H., 2004. Analyzing and modeling of photobioreactors by combining first principles of physiology and hydrodynamics. Biotechnology and Bioengineering Vol. 85, No. 4.

Lou, H-P., Al-Dahhan, M.H., 2008. Local characteristics of hydrodynamics in draft tube airlift bioreactor. Chemical Engineering Science 63: 3057-3068.

Lv, J-M., Cheng, L-H., Xu, X-H., Zhang, L., Chen, H-L., 2010. Enhanced lipid production of Chlorella vulgaris by adjustment of cultivation conditions. Bioresource Technology 101: 6797–6804.

Medvitz, R.B., Reddy, V., Deutsch, S., Manning, K.B., Paterson, E.G., 2009. Validation of a CFD methodology for positive displacement LVAD analysis using PIV data. Journal of Biomechanical Engineering 131(11):111009.

Meier, S.J., Hatton, T.A., Wang, D.I., 1999. Cell death from bursting bubbles: role of cell attachment to rising bubbles in sparged reactors. Biotechnology and Bioengineering 62(4):468-478.

Mehlitz, T.H., 2009. Temperature influence and heat management requirements of microalgae cultivation in photobioreactors. Master Thesis. California Polytechnic State University, USA.

Merchuk, J.C., Gluz, M., Mukmenev, I., 2000. Comparison of photobioreactors for cultivation of the red *Porphyridium sp*. Journal of Chemical Technology and Biotechnology 75: 1119-26.

Merchuk, J.C., Wu, X., 2003. Modeling of photobioreactors: Application to bubble column simulation. Journal of Applied Phycology 15: 163-69.

Merchuk, J.C., Ben-Zvi, S., Niranjan, K., 1994. Why use bubble column bioreactors. TIBTECH, Vol. 12.

Merchuk, J.C., Ronen, M., Giris, S., Arad, S., 1998. Light/dark cycles in the growth of the red microalgae *Porphyridium Sp*. Biotechnology and Bioengineering Vol. 59, No.6.

Metting, F.B., 1996. Biodiversity and application of microalgae. Journal of Industrial Microbiology 17: 477-89.

Michele, V., Hempel, D.C., 2002. Liquid flow and phase holdup-measurement and CFD modeling for two-and three-phase bubble columns. Chemical Engineering Science 57:1899-908.

Miron, S.A., Garcia, M.C., Camacho, G.F., Molina, G.E., Chisti, Y., 2004. Mixing in bubble column and airlift reactors. Chemical Engineering Research and Design 82(A10): 1367-74.

Miron, S.A., Gomez, C.A., Camacho, G.F., Molina, G.E., Chisti, Y., 1999. Comparative evaluation of compact photobioreactors for large-scale monoculture of microalgae. Journal of Biotechnology 70: 249-70.

Miron, S.A., Camacho, G.F., Gomez, C.A., Grima, E.M., Chisti, Y., 2000. Bubble-column and airlift photobioreactors for algal culture. AIChe Journal Vol. 46, No.9.

Molina, G.E., Fernandez., J, Acien, F.G., Chisti, Y., 2001. Tubular photobioreactor design for algal cultures. Journal of Biotechnology 92: 113-31.

Molina, G.E., 1999. Mass culture methods. *In*: Flickinger, M.C., Drew, S.W., (editors). Encyclopedia of bioprocess technology: fermentation, biocatalysis and bioseparation Vol. 3. Wiley: 1753-69.

Molina, G.E., Acien, F.G., Fernandez ,J., Camacho, F., Chisti, Y., 1999. Photobioreactors: light regime, mass transfer and scale up. Journal of Biotechnology 70: 231-47.

Mouza KA, Kazakis NA, Paras SV. Bubble column reactor design using a CFD code. 1st International Conference "From Scientific Computing to Computational Engineering". Athens, September 8-10, 2004.

Naoya, T., Akihiko, K., Takeharu, K., Kazuo, U., 2000. Flow Analyses around Transient Jet through a PIV Technique. Nihon Kikai Gakkai Nenji Taikai Koen Ronbunshu Vo. 4. Pp 97-98.

Negoro, M., Shioji, N., Niyamoto, K., Miura, Y., 1991. Growth of microalgae in high CO2 gas and effects of SO*x*, NO*x* . Applied Biochemistry and Biotechnology 28–29: 877–886.

Negoro, M., Hamasaki, A., Ikuta, Y., Makita, T., Hirayama, K., Suzuki, S., 1993. Carbon dioxide fixation by microalgae photosynthesis using actual flue gas discharged from a boiler. Applied Biochemistry and Biotechnology 39–40: 643–653.

Ogbonna, J.C., Soejima, T., Tanaka, H., 1998. Development of efficient large scale photobioreactors. *In*: Zaborosky, O.R. (Ed.), Biohydrogen. Plenum Press, New York, pp. 329–343.

Olaizola, M., 2003. Commercial development of microalgal biotechnology: from test tube to the marketplace. Biomolecular Engineering 20: 459-66.

Oncel, S., Sukan V.F., 2008. Comparison of two different pneumatically mixed column photobioreactors for the cultivation of *Artrospira platensis (Spirulina platensis).* Bioresource Technology 99: 4755-60.

Oncel, S.S., Akpolat, O., 2006. An integrated photobioreactor system for the production of *Spirulina platensis.* Biotechnology 5 (3): 365-72.

Ono, E., Cuello, J.L., 2003. Selection of optimal species for CO_2 sequestration. Second Annual Conference on Carbon Sequestration. May 5-8, Alexandria, Virginia, USA.

Panda, A.K., Mishra, S., Bisaria, V.S., Bhojwani, S.S., 1989. Plant cell reactors-a perspective. Enzyme Microbiology Technology 11: 386-97.

Park, K.H., Lee, C.G., 2000. Optimization of algal photobioreactors using flashing lights. Biotechnology Bioprocess Engineering 5: 186-190.

Patil, V, Tran, K.Q., Giselrod, H.R., 2008. Towards sustainable production of biofuels from microalgae. International Journal of Molecular Science 9:1188-95.

Pereira, F.A.R., Ataide, C.H., Barrozo, M.A.S., 2010. CFD approach using discrete phase model for annular flows. Latin American Applied Research 40: 53-60.

Perner-Nochta, I., Posten, C.. 2007. Simulations of light intensity variation in photobioreactors. Journal of Biotechnology 131: 276-85.

Perner, I, Posten, C., Broneske, J., 2003. CFD optimization of a plate photobioreactor used for cultivation of microalgae. Engineering Life Sciences 3, 7.

Pfleger, D., Gomes, S., Gilbert, N., Wagner, H.G., 1999. Hydrodynamic simulations of laboratory bubble columns fundamental studies of the Eulerian-eulerian modelling approach. Chemical Engineering Science 54: 5091-99.

Pramparo, L., Pruvost, J., Stuber, F., Font, J., Fortuny, A., Fabregat, A.,. 2008. Mixing and hydrodynamics investigation using CFD in a square-sectioned torus reactor in batch & continuous regime. Chemical Engineering Journal 137: 386-95.

Pruvost, J., Vooren, G.V., Cogne, G., Legrand, J., 2009. Investigation of biomass lipids production with Neochloris oleoabundans in photobioreactors. Bioresource Technology 100: 5988–5995.

Pruvost, J., Pottier, L., Legrand, J., 2006. Numerical investigation of hydrodynamic and mixing conditions in a torus photobioreactor. Chemical Engineering Science 61: 4476-89.

Pulz, O., Gross, W., 2004. Valuable products from biotechnology of microalgae. Applied Microbial Biotechnology 65: 635-48.

Pulz, O., 2001. Photobioreactors: production systems for phototrophic microorganisms. Applied Microbiology and Biotechnology 57 (3), 287-93.

Ramkumar, K., Mandalam, R.K., Palsson, B.O., 1998. Elemental balancing of biomass and medium composition enhances growth capacity in high-density *Chlorella vulgaris* cultures. Biotechnology and Bioengineering Vol 59, No.5.

Radmer, R.J., Parker, B.C., 1994. Commercial applications of microalgae: opportunities and constraints. Journal of Applied Phycology 6: 93-8.

Rampure, M.R., Kulkarni, A.A., Ranade, V.V., 2007. Hydrodynamics of bubble column rectors at high gas velocity: experiments and computational fluid dynamics (CFD) simulations. Industrial and Engineering Chemistry Research, 46: 8431-47.

Ranade, V.V., Tayalia, Y., 2001. Modelling of fluid dynamics and mixing in shallow bubble column reactors: influence of sparger design. Chemical Engineering Science 56: 1667-75.

Ranade, V.V., 2002. Computational flow modeling for chemical reactor engineering, Academic Press, San Diego, USA.

Ranjbar, R., Inoue, R., Katsuda, T., Yamaji, H., Katoh, S., 2008. High efficiency production of astaxanthin in an airlift photobioreactor. Journal of Bioscience and Bioengineering Vol. 106, No. 2: 204-7.

Richardson, J.W., Johnson, M.D., Outlaw, J.L., 2012. Economic comparison of open pond raceways to photo bio-reactors for profitable production of algae for transportation fuels in the Southwest. Algal Research 1: 93–100.

Richmond, A., Boussiba, S., Vonshak, A., Kopel, R., 1993. A new tubular reactor for mass production of microalgae outdoors. Journal of Applied Phycology 5: 327-332.

Roache, P.J., Ghia, K.N., White, F.M., 1986. Editorial policy statement on the control of numerical accuracy. ASME Journal of Fluid Engineering 108: 2.

Rubio, F.C., Miron, A.S., Garcia, C.M., Camacho, F.G., Grima, E.M., Chisti, Y., 2004. Mixing in bubble columns: a new approach for characterizing dispersion coefficients. Chemical Engineering Science Vol 59, Issue 20, pp 4369-4376.

Santos, C.M., Dionisio, R., Cerqueira, H.S., Sousa-Aguilar, E.F., Mori, M., d'Avila, M.A., 2007. Three-dimensional gas-liquid CFD simulations in cylindrical bubble columns. International Journal of Chemical Reactor Engineering Vol. 5, Article A90.

Sanyal, J., Vasquez, S., Roy, S., Dudukovic, M.P., 1999. Numerical simulation of gas-liquid dynamics in cylindrical bubble column reactors. Chemical Engineering Science 54: 5071-83.

Sato, T., Yamada, D., Hirabayashi, S., 2010. Development of virtual photobioreactor for microalgae culture considering turbulent flow and flashing light effect. Energy Conversion and Management 51: 1196–1201.

Sawayama, S., Inoue, S., Yokohama, S., 1994. Continuous culture of hydrocarbon-rich microalgae *Botrycoccus barunii* in secondarily treated sewage. Applied

Microbiology and Biotechnology 41: 729-31.
Scragg, A. H., Illman, A.M., Carden, A., Shales, S.W., 2002. Growth of microalgae with increased calorific values in a tubular bioreactor. Biomass and Bioenergy 23: 67-73.

Schlagermann, P., Gottlicher,G., Dillschneider, R., Sastre,R.R., Posten, C., 2012. Composition of Algal Oil and Its Potential as Biofuel. Journal of Combustion Vol. 2012, Article ID 285185, doi:10.1155/2012/285185.

Seo, I.H., Lee, I.B., Hwang, S.H., Hong, S.W., Bitog, J.P., Kwon, K.S., et al., 2010. Numerical investigation of a bubble-column photo-bioreactor design for biodiesel production from microalgae. *In*: Proceedings of the XVIIth World Congress of the International Commission of Agricultural and Biosystems Engineering, Quebec City, Canada, June 13-17.

Seyfabadi, J., Ramezanpour, Z., Khoeyi, Z.A., 2011. Protein, fatty acid, and pigment content of Chlorella vulgaris under different light regimes. Journal of Applied Phycology 23:721–726.

Sharma, K.K., Schuhmann, H., Schenk, P.M., 2012. High lipid induction in microalgae forb production. Energies 5: 1532-1553.

Sheng, J., Meng, H., Fox, R.O., 1998. Validating of CFD simulations of a stirred tank using particle image velocimetry data. The Canadian Journal of Chemical Engineering Vol. 76.

Shigeya, W., Hiroyuki, K., Zhong, L., Taro, I., Shunji, E., 2005. CFD code validation via particle image velocimetry (PIV). JAXA Special Publication No. 04-012, pp 178-183.

Shinji, I., Yasuo, O., Hitomitsu, K., Masamki, O., Tetsuro, T., Yoshihito, T., 2006. Experimental study on flow and pressure fields over the roof of a cube by PIV measurement. Journal of Wind Engineering No. 108. Pp 435-438.

Sierra, E., Acien, F.G., Fernandez, J.M., Garcia, J.L., Gonzales, C., Molina, E. 2008. Characterization of a flat plate photobioreactor for the production of microalgae Chemical Engineering Journal. 138: 136-47.

Simonnet, M., Gentric, C., Olmos, E., Midoux, N., 2008. CFD simulation of the flow field in a bubble column reactor: Importance of the drag force formulation to describe regime transitions. Chemical Engineering and Processing 47:1726–37.

Singh, S.P., Singh, D., 2010. Biodiesel production through the use of different sources and characterization of oils and their esters as the substitute of diesel: A review. Renewable and Sustainable Energy Reviews 14: 200–216.

Spolaore P., Joannis-Cassan C., Duran E., Isambert A., 2006 Commercial applications of microalgae. Journal of Bioscience and Bioengineering 101: 1389-1723.

Su, Z., Kang, R., Shi, S., Cong, W., Cai, Z., 2010. Study on the destabilization mixing in the flat plate photobioreactor by means of CFD. Biomass and Bioenergy 34: 1879-84.

Sundaresan, S., 2000. Modeling the hydrodynamics of multiphase flow reactors: current status and challenges. AIChE 46, 1102–1105.

Szafran, R.G., Kmiec, A., 2004. Application of CFD modelling technique in engineering calculations of three-phase flow hydrodynamics in a jet-loop reactor. International Journal of Chemical Reactor Engineering Vol. 2, Article A30.

Terry, K.L., Raymond, L.P., 1985. System design for the autotrophic production of microalgae. Enzyme Microbial Technology 7: 474-87.

Thakre, S.S., Joshi, J.B., 1999. CFD simulation of bubble column reactors: importance of drag force formulation. Chemical Engineering Science 54: 5055-60.

Thomas, W.H., Gibson, C.H., 1990. Effect of small scale turbulence on microalgae. Journal of Applied Phycology 2: 71-79.

Tredici, M.R., Materassi, R., 1992. From open ponds to vertical alveolar panels: the Italian experience in the development of rectors for mass cultivation of phototrophic microorganisms. Journal of Applied Phycology 4 (3): 221-31.

Tredici, M.R., Zittelli, G.C., 1998. Efficiency of sunlight utilization: tubular versus flat photobioreactors. Biotechnology and Bioengineering Vol. 57, No. 2.

Tredici, M.R., 1999. Bioreactors, photo. *In*: Flickinger, M.C., Drew, S.W., (editors). Encyclopedia of bioprocess technology: fermentation, biocatalysis and bioseparation, Wiley 394-419.

Trujilio, F.J., Safinski, T., Adesina, A.A., 2007. CFD analysis of the radiation distribution in a new immobilized catalyst bubble column externally illuminated photoreactor. Journal of Solar Energy Engineering Vol. 129: 27-35.

Tzuzuki, M., Ohnuma, E., Sato, N., Takaku, T., Kawaguchi, A., 1990. Effects of CO_2 during growth on fatty acid composition in microalgae. Plant Physiology 93: 851-56.

Ugwu, C.U., Aoyagi, H., Uchiyama, H., 2008. Photobioreactors for mass cultivation of algae. Bioresource Technology 99: 4021-28.

Velarde, R.R., Urbina, E.C., Melchor, J.H., Thalassa, F., Villanueva, R.O.C., 2010. Hydrodynamic and mass transfer characterization of a flat-panel airlift photobioreactor with high light path. Chemical Engineering and Processing 49: 97–103.

van Wachem, B.G., Schouten, J.G., van den Bleek, C.M., Krishna, R., Sinclair, J.L., 2001. Comparative analysis of CFD models of dense gas-solid systems. AIChE Journal 47(5):1035–51.

Wen, Z.Y., Chen, F., 2003. Heterotrophic production of eicosapentaenoic acid by microalgae. Biotechnology Advances 21: 273-94.

Wild, G., Li, H.Z., Poncin, S., Olmos, E., 2003. Some aspects of the hydrodynamics of bubble column. International Journal of Chemical Reactor Engineering 2003; Vol. 1, 1-36.

Yan, L., Yutala, H., Tsutomu, H., 2005. PIV measurements of the flow around a savonius rotor (Effects of overlap on the flow field). Nihon Kikai Gakkai Nenji Taikai Koen Ronbunshu Vol. 2. pp 213-214.

Yoo, J.I., Lee, I.B., Hwang, S.H., Hong, S.W., Seo, I.H., Bitog, J.P., et al., 2009. Utilization of CFD simulation model for a bubble column photobioreactor. Journal of the Korean Society of Agricultural Engineers 51 (5).

Yoo, J.I., Lee, I.B., Hwang, S.H., Hong, S.W., Seo, I.H., Bitog, J.P., et al., 2008. Design of a bubble-column photobioreactor for growing microalgae using CFD simulation. *In*: Proceedings of the International Forum on Bioenvironmental and Bioenergy Engineering (IFBBE), Beijing, China, October 15-17.

Yu, G., Li, Y., Shen, G., Wang, W., Lin, C., Wu, H., Chen, Z., 2009. A novel method using CFD to optimize the inner structure parameters of flat photobioreactors. Journal of Applied Phycology 21:719–727.

Zhang, K., Zhang, J., Zhang, B., 2004. CFD simulation of jet behaviour and void age profile in a gas–solid fluidized bed. International Journal of Energy Research 28:1065–74.

Zhang, K., Kurano, N., Miyachi, S., 2002. Optimized aeration by carbon dioxide gas for microalgal production and mass transfer characterization in a vertical flat-plate photobioreactor. Bioprocess and Biosystems Bioengineering 25: 97–101.

Zuber, N., & Findlay, J. A., 1965. Average volumetric concentration in two-phase flow systems. Journal of Heat Transfer 87(4): 453 – 468.

국문초록

최근, 에너지수요의 증가와 에너지자원의 고갈로 인하여 새로운 대체에너지의 중요성이 대두되고 있다. 이에 따라 향후 화석연료 에너지를 대체할 수 있는 잠재적인 자원으로서 미세조류로부터 오일을 추출하는 방법이 재조명 받고 있다. 본 연구에서는 미세조류를 배양할 수 있는 광생물반응기 (Photobioreactor, PBR)의 유동학적 흐름을 분석하기 위해 전산유체역학 (Computational Fluid Dynamics, CFD)을 활용하였다. 또한 미세조류의 배양 실험을 수행하여 본 연구 과정을 실험적으로 검증하고 CFD 시뮬레이션으로부터 얻어진 결과들을 확인하고자 하였다.

본 연구에서는 먼저 PBR의 설계 과정에서 CFD를 이용한 논문들을 검토하여 미세조류와 미세조류의 생장에 필요한 여러 필수요인들, 예를 들면 광, 이산화탄소, 온도 등을 공학적인 관점에서 이해하고자 하였다. 특히 이러한 요인들에 큰 영향을 주는 PBR 내의 수리역학적 흐름 특성들과 데드존(Dead zone)의 비율, 평균 혼합시간 및 난류 강도 등을 종합적으로 연구하여 PBR의 성능을 분석하고자 하였다.

시뮬레이션 연구에 앞서 시뮬레이션 결과의 신뢰도를 제고하기 위하여 CFD 코드와 모델링 방법들은 입자영상유속계 (PIV)를 이용한 실험 결과로 검증되었다. PBR 내에 테스트 영역을 분할하고 다양한 가스 주입 유량에 대해 실험을 진행하였으며, 이로부터 얻어진 PBR 내의 평균 유속은 시뮬레이션 결과와 비교하여 약 6.77%의 오차를 보여 충분히 타당한 결과를 나타냈다.

공학적인 관점에서 PRB의 구조적 형태와 디자인은 반응기 내에 미세조류 세포를 배양함에 있어 수리 역학적으로 이상적인 환경을 제공하는데 중요한 역할을 한다. 이러한 이유로 32가지 형태의 30L급 PBR의 수리 역학적 흐름은 CFD를 사용하여 분석하였다. 이때 수리 역학적 평가의 요소로는 데드존, 평균 혼합시간, 난류 강도로 구성하였으며, 이를 통한 CFD 시뮬레이션 결과는 PBR을 구성하는 내부 배플과 원뿔형의 바닥 형상에 의한 수리 역학적 장점들을 잘 보여주었다. 하지만 이러한 평가 요소를 활용하여 PBR의 적절한 운영 조건과 설계안을 찾는 것은 기존 연구들에서는 없었던 첫 번째 시도로서 그 기준이나 지표를 설정하는데 많은 어려움이 있었다. 따라서 각 평가 요소마다 적절한 기준을 정하고 32개의 시뮬레이션 케이스 중에 미세조류 생장에 가장 적절한 형태가 선정될 때까지 순차적으로 소거시켜나가는 과정으로 분석을 진행하였다. 이에 따라 최종적으로 A2B2C2 형태와 A3B2C2 형태가 가장 적절한 것으로 평가되었으며, 두 모델 모두 10mm의 노즐 직경과 동일한 PBR 형상을 가지고 있다. 단, 두 모델은 운영 조건 면에서 가스의 주입 유속이 각각 0.10과 0.15 vvm 으로 서로 다른데, 이러한 조건은 실제 미세조류를 배양하는 과정에서 쉽게 변경할 수 있는 조건이다.

최종적으로 선정된 PBR 구조를 사용하여 실제 미세조류 배양 실험을 수행하였다. 앞선 시뮬레이션 연구로부터 결정된 PBR의 구조적 형태와 운영 조건을 적용하여 30L 원통형 PBR에서 미세조류의 생장률을 측정하였다. 실험결과는 앞선 시뮬레이션 결과와 동일하게 개선된 형태의 PBR이 미세조류의 배양에 더 효과적인 것으로 나타났으며, 특히 개선된 구조는 미세조류를 대량생산 할 수 있다는 점에서 보다 효율적으로 활용 될 수 있을 것이다.

마지막으로 전산유체역학을 이용한 접근은 PBR 내부의 유동학적 흐름을 살펴볼 수 있다는 점에서 다양하게 활용될 수 있을 것이며 이는 미세조류의 대량생산을 위한 보다 효율적이며 효과적인 구조 개발에 도움이 될 것이다. 또한 PBR 디자인을 연구하는데 있어 연구시간, 노동력, 자원 등을 상당히 절감 할 수 있을 것으로 판단된다.

주요어 : 난류강도, 데드존(Dead zones),미세조류 생산, 입자영상유속계 (PIV), 전산유체역학 (CFD), 혼합시간, CFD 리뷰

학 번 : 2007-31072

ACKNOWLEDGMENT

Above all, I am always grateful to God almighty, the source of everything which makes things possible. He plans everything for His children with promises of prosperity and gives hope to those who believe in Him. This is God's promise in Jeremiah 29:11. This humble achievement gives glory to God, the living Creator and King.

I am also grateful to my immediate family, to my dad, to my beloved wife and partner for life, Gina, and our daughters, Jessa and her sister who is coming very soon, who serves as my daily inspiration and a source of strength while pursuing my advance studies. This work is also dedicated to them.

Residing in foreign country is like moving away to your comfort zones, but special thank you to Pastor Joseph Choi and Nam-Soo Byun who become our immediate family here in Seoul and to the International Church of Seoul (ICOS) community who embraced and accepted us as part of the community which makes our stay in this country worthwhile and meaningful.

Acknowledgement is accorded to my immediate academic adviser Prof. In-Bok Lee, for all his support, comments and suggestions from the start until the end of the study. I also thank him for giving me and my colleagues in the A3EL Laboratory several opportunities to participate and present our research work in international conferences and forums here in Korea and abroad. Thank you for always reminding us to think and act globally. Thank you for the challenges and the pressures which make us academically prepared to do excellent research works. Thank you for encouraging and supporting us in publishing our work in international and reputable journals. I am personally indebted to you in many ways particularly in my professional career.

To my Dissertation Committee Chair Prof. JeongJae Lee and the Members, Prof. In-Bok Lee, Prof. Hee-Mock Oh, Prof. Song-Bae Kim and Prof. Kyo Suh, thank you very much for your constructive criticisms, comments and suggestions which significantly improved the quality of this research work.

I wish also to thank my colleagues in the Aero-Environmental and Energy Engineering Laboratory (A3EL) namely Hyun-Seob, Se-Woon, Il-Hwan, Kyeong-Seok, Tae-Hwan, Yeong-Hee, Song-Bok, Sang-Hyeon, Jeong-Su, Se-Jun and Yeseul (the only rose among the thorns and who acted as the secretary in the final stages of my dissertation, your assistance is very much appreciated). Let me thank you for always helping me in conducting my research activities and also for making my time in the lab exiting and fruitful. I will never forget the lab meeting we always have every Saturdays, our time in the farms, in the reclaimed lands and in wind tunnels for our field experiments, and our leisure and fun time in different places of the world such as Japan, China, Australia, Canada, France, Spain and US (after our presentations of course). I hope you will also come to the Philippines very soon and experience the fun in my beloved country.

To the Department of Rural Systems Engineering – I will always remember the membership trainings we do every semester where I have so much fun. I had most of my first times during the membership training like water rafting, fishing in the sea and eating the fresh caught, skiing and boarding during winter, etc.

May I also thank my University, The Nueva Vizcaya State University (NVSU) headed by our President, Dr. Florentina S. Dumlao, to Dr. Edwin P. Ramos our Vice President for Academic Affair and to my immediate supervisor and Dean, Engr. Salud A. Mangaccat for the support and approval to the various requests I always asked especially when related to the pursuit of my doctoral degree.

JPPB/07/15/2013